UNIVERSITY OF CALIFORNIA, SAN DIEGO

Plankton community composition and grazing dynamics in upwelling regions of the Pacific Ocean

A dissertation submitted in partial satisfaction

of the requirements for the Degree Doctor of Philosophy

in

Oceanography

by

Alexandra Leigh Freibott

Committee in charge:

Professor Michael R. Landry, Chair
Professor Andrew E. Allen
Professor Katherine A. Barbeau
Professor Brian Palenik
Professor Jonathan B. Shurin

2017

The dissertation of Alexandra Leigh Freibott is approved, and it is acceptable in quality and form for publication on microfilm and electronically:

Chair

University of California, San Diego

2017

DEDICATION

For my Dad, who would be so proud

TABLE OF CONTENTS

LIST OF FIGURES

LIST OF TABLES

ACKNOWLEDGEMENTS

I started grad school fresh out of college and truly feel that I've "grow up" these last six years both as a scientist and a person. There are so many people I have to thank for their knowledge, guidance, and friendship that it's inevitable I will forget someone, so first of all – thank you to everyone who has helped me achieve my goals and offered their support and friendship these last six years. Even if you are not mentioned here by name, you are appreciated more than you know.

First, I would like to thank my advisor, Mike Landry. I have learned so much from him that has made me a better scientist and sea-going oceanographer. He always encouraged me to push myself, think critically about my work and results, and strive to present the best work possible. Most importantly, Mike gave me the space I needed to work independently and think for myself. I am a more confident, self-reliant scientist because of him.

Thanks to all of my committee members, Andy Allen, Brian Palenik, Kathy Barbeau, and Jon Shurin, for their valuable insight and contributions to my research. I looked forward to committee meetings with this group of talented and supportive scientists. A special thanks to Andy Allen for his support and guidance on the molecular analysis used my research. He and his lab, especially Ariel Rabines, Hong Zheng, and John McCrow, were incredibly generous with their time and expertise with regards to the molecular analyses, and really made that research possible.

Next, I want to thank all the past members of the Landry lab for their support, friendship, and advice. In addition to being amazing scientists and willing to sharing their broad scientific and practical knowledge, they have been great friends and mentors

throughout the grad school experience. Ally Pasulka was patient enough to answer all of my (many) questions about the ins and outs of classes, lab procedures, and starting my own research projects. I am grateful to Moira Décima for being a great officemate – her unflappable demeanor often kept me grounded and gave me perspective during stressful times in grad school. Andrew Taylor's quirky, and often dark, sense of humor was a great source of entertainment during meetings and on cruises, and I am grateful for his microscopy expertise and advice that was invaluable to my own thesis work. Thanks to Darcy Taniguchi, Mike Stukel, Lorena Linacre, and Andrés Gutiérrez Rodríguez for their friendship, constructive criticism and valuable scientific discussion, and support on many projects and cruises. Thanks also to Kyra Rashid and Jennifer Beatty, the undergraduates I mentored, for their hard work and valuable contributions to my research. Finally, I want to say a special thank you to Belli Valencia for being an amazing labmate, officemate, and friend. Belli helped me through long work days (and nights on cruises), commiserated over science struggles and life challenges, and laughed with me through the craziness of grad school.

My friends at Scripps have been there through thick and thin, and made this such an unforgettable 6 years. Sara Shen, Elizabeth Sibert, Catherine Nickels, Jenni Brandon, Belli Valencia, Amanda Netburn, Maitreyi Nagarkar, and everyone I can't mention by name because this list would go on and on – I am so thankful to have them in my life. They are all amazing, talented people and I am so happy and proud to call them my friends.

My family always supported my desire to grow up and be a marine biologist, even though we lived in a desert and it started to sound a bit far-fetched when I was still saying

that in college. I never doubted my ability to accomplish my goals because they always supported and encouraged me. I am so blessed to call these smart, determined, caring people my family. Finally, I want to thank my husband, Dr. Mark Reineke, for his constant support and love. We started this graduate adventure together, somehow made it through the stress and crazy work hours, got married along the way, and now we are moving onto the next big adventure together.

My research was supported by many funding sources, including internal Scripps fellowships and NSF support. Much of my molecular analyses was possible through funding from the Scripps Mullin Fellowship and the Graduate Student Excellence Research Award. The majority of my research work, cruise opportunities, and conference travel was made possible through the support of the California Current Ecosystem Long Term Ecological Research (CCE LTER) program. I am incredibly grateful for the many opportunities and financial support I was given through the CCE LTER program, and the amazing collaborations among the scientists involved.

Below is the content of the dissertation, either published or in preparation for submission. I was the primary investigator and author on all manuscripts in this dissertation.

Chapter 2, in full, is a reprint of materials as it appears in Freibott, A., Linacre, L., and Landry, M. R. (2014) Permanent filtration preparation for ciliates preserved in Acid Lugol's. Limnology and Oceanography: Methods 12, 54-62, doi: 10.4319/lom.2014.12.54. The dissertation author was the primary investigator and author of this manuscript.

Chapter 3, in full, is a reprint of materials as it appears in Freibott, A., Taylor, A. G., Selph, K. E., Lui, D., Zhang, W., and Landry, M. R. (2015) Biomass and composition of protist grazers and heterotrophic bacteria in the Costa Rica Dome during June-July 2010. Journal of Plankton Research, 38(2):230-243, doi: 10.1093/plankt/fbv107. The dissertation author was the primary investigator and author of this manuscript.

Chapter 4, in full, is currently being prepared for submission for publication of the material with the following co-authors: Freibott, A., Taylor, A.G., Rabines, A., McCrow, J.P., Beatty, J.L., Selph, K.E., Allen, A.E., Landry, M.R. The dissertation author was the primary investigator and author of this paper.

Chapter 5, in full, is currently being prepared for submission for publication of the material with the following co-authors: Freibott, A., Rabines, A., McCrow, K.E., Allen, A.E., Landry, M.R. The dissertation author was the primary investigator and author of this paper.

VITA

2011 Bachelor of Science, Biology: Ecology and Evolution, Arizona State University

2013 Master of Science, Marine Biology, Scripps Institution of Oceanography at the University of California San Diego

2014 Teaching Assistant in California Current Oceanography, Scripps Institution of Oceanography, University of California San Diego

2014 Teaching Assistant in Introduction to Biological Oceanography, Scripps Institution of Oceanography, University of California, San Diego

2017 Doctor of Philosophy, Oceanography, Scripps Institution of Oceanography at the University of California San Diego

PUBLICATIONS

Freibott, A., Taylor, A. G., Selph, K. E., Lui, D., Zhang, W., and Landry, M. R. (2015) Biomass and composition of protist grazers and heterotrophic bacteria in the Costa Rica Dome during June-July 2010. *Journal of Plankton Research*, 38(2):230-243, doi: 10.1093/plankt/fbv107.

Taylor, A. G., Landry, M. R., **Freibott, A.,** Selph, K. E., and Gutiérrez-Rodríguez, A. (2015) Patterns of microbial community biomass, composition and HPLC diagnostic pigments in the Costa Rica upwelling dome. *Journal of Plankton Research*, 38(2):183-198, doi: 10.1093/plankt/fbv086.

Freibott, A., Linacre, L., and Landry, M. R. (2014) Permanent filtration preparation for ciliates preserved in Acid Lugol's. *Limnology and Oceanography: Methods*, 12:54-62, doi: 10.4319/lom.2014.12.54.

ABSTRACT OF THE DISSERTATION

Plankton community composition and grazing dynamics in upwelling regions of the Pacific Ocean

by

Alexandra Leigh Freibott

Doctor of Philosophy in Oceanography

University of California, San Diego, 2017

Professor Michael R. Landry, Chair

Microzooplankton play a pivotal role as primary consumers and trophic links in the marine food web, affecting the efficiency of energy transfer to higher trophic levels through changes in their community composition and grazing activity. Thus, investigating the diversity and dynamics of microzooplankton communities is of particular importance to understanding how climate changes may impact plankton

communities and energy flow in food webs. In my dissertation I address the following topics regarding microzooplankton composition and grazing activity: What is the range in diversity and grazing rates seen in microzooplankton communities across trophic gradients in the eastern Pacific? How are microzooplankton composition and grazing activities shaped by the plankton communities they feed on? What insights can molecular analyses provide about the taxa-specific grazing impacts of microzooplankton on their phytoplankton prey? To address these questions, I investigate the microbial communities in upwelling regions of the eastern Pacific that exhibit broad environmental gradients on relatively small spatial scales and where climate change could strongly impact the productive marine ecosystem.

I find that in the unique, picoplankton-dominated, upwelling area of the Coast Rica Dome, nano-sized dinoflagellates were the dominant primary consumers. The biomass of heterotrophic protists varied little despite large changes in autotrophic prey biomass, suggesting strong top-down control by mesozooplankton predators and highlighting the important role of microzooplankton as trophic links in this food web.

In the California Current Ecosystem (CCE), I specifically focus on mesoscale frontal features which appear to be increasing in number in this area. I find that the microbial community composition at fronts is distinct from that of other eutrophic locations in the CCE, with implications for the future productivity of the region. I also document the microbial community composition and growth-grazing dynamics during the warm water anomaly known as the Blob in 2014. I find that the community composition was not significantly different compared to normal years in the CCE, but the grazing pressures were elevated. Thus, that the majority of phytoplankton production

was funneled through microzooplankton, decreasing energy transfer efficiency in the food web.

CHAPTER 1.

Introduction

The word plankton comes from the Greek word, *planktos*, which means drifter. Marine plankton, often microscopic, are ocean drifters at the whims of the current, and yet they sustain all marine life. Phytoplankton, autotrophs that include both bacteria and eukaryotes, use photosynthesis to fuel their growth, fixing carbon in the process. Zooplankton, heterotrophs that include single and multicellular organisms, consume phytoplankton to grow and recycle nutrients back into the environment through their excretions and sloppy feeding. The dynamics of these organisms at the base of the marine food web determine the amount of energy ultimately available to larger organisms, such as fish, seabirds, and marine mammals; however, their complex interactions and resultant impacts on the marine food web are often difficult to characterize. In this dissertation, I aim to investigate the interactions between microzooplankton grazers and their phytoplankton prey and further characterize their role in the marine food web in a range of environmental conditions.

Microzooplankton in the food web

The term microzooplankton refers technically to heterotrophic plankton between 20 and 200 µm in length, encompassing a variety of taxa including ciliates (Cil), heterotrophic dinoflagellates (H-Dino), radiolarians, foraminifera, and naupliar copepods (Dussart 1965). Nanozooplankton, primarily heterotrophic nanoflagellates (HNF) that fall in the 2 to 20 µm size fraction, are often included within the general category of microzooplankton although they can act as a separate trophic step in the food web

because they are limited to consumption of smaller picoplankton (0.2-2 μm) and can be preyed upon by microzooplankton. Unless specifically stated, I use the broader definition of microzooplankton in this dissertation to include both nano- and micro-sized grazers, whose combined predatory impact on the phytoplankton community is measured by the dilution technique (Landry and Hassett 1982). These organisms are the dominant grazers in the marine planktonic food web, consuming on average 70% of global daily ocean primary production (Calbet and Landry 2004, Calbet 2008). Furthermore, they play critical roles in nutrient remineralization and the regulation of energy transfer efficiency within food webs (Stoecker and Capuzzo 1990, Sherr and Sherr 2002, Sommer et al. 2002, Calbet and Saiz 2005). Within the variety of taxa that fall into this category, the most common protistan grazers – Cil, H-Dino and HNF (Sherr and Sherr 2007) – also comprise major trophic links between small primary producers and larger mesozooplankton (>200 μm) such as copepods and euphausiids, which are unable to directly graze on small pico- and nanoplankton (Calbet and Saiz, 2005).

As a result of their position as trophic intermediaries, microzooplankton consumption of phytoplankton, as opposed to direct consumption by mesozooplankton, can substantially diminish the overall efficiency of food web energy transfer. Significant energy (50-70%) is lost with each additional trophic step in the food web, and multiple trophic steps can occur within the nano- and microzooplankton size categories (Straile 1997). While organisms typically consume prey smaller than themselves, the interactions between microzooplankton taxa are further complicated by a wide variety of feeding strategies. In addition to intercepting their prey directly, dinoflagellates can utilize pallium or peduncle feeding to prey upon organisms much larger than themselves.

Approximately one-third of marine ciliates and a high proportion of pigmented dinoflagellates exhibit a mixotrophic nutritional mode (i.e., mixed photosynthetic and phagotrophic capabilities), often by appropriating the chloroplasts of their prey (kleptoplastidy) and using them as an energy supplement to enhance growth efficiency (Mitra et al. 2016 and citations therein, Esteban et al. 2010). Due to the variety and complexity of feeding strategies among these grazers, the standard 10:1 size ratio of predator to prey is often inappropriate for consumers in this functional category (Hansen et al. 1994), particularly for dinoflagellates whose optimal ratio is approximately 1:1 (Naustvoll 2000). This complicates the identification of potential phytoplankton consumers based solely on size spectra, which is commonly how size is incorporated into food web models (Moloney and Field 1991).

Taxa-specific grazing pressure on phytoplankton

Microzooplankton are known to exhibit prey preference in laboratory experiments (Stoecker et al. 1980, Verity 1991, Naustvoll 2000), suggesting that they do not consume all available prey equally within a given size range. Furthermore, differences in taxon-specific growth and mortality due to grazing rates have been reported in the field (Waterhouse and Welschmeyer 1995, Landry et al. 2008, 2011, Selph et al. 2015), supporting the laboratory findings that microzooplankton exert differential grazing pressures on available phytoplankton prey. Recent evidence suggests that there is as much as a 4-fold increase in nanoflagellate grazing in the high productivity waters of the California Current Ecosystem (CCE) that is linked to higher production of heterotrophic bacteria (Goericke 2011, Taylor 2014). As discussed by Taylor (2014), this suggests that increased grazing pressures may select for strategies among bacteria and

picophytoplankton that either maximize growth rates or minimize grazing losses (i.e. grazing resistance). Strategies against grazing are documented and include alteration of cell surface hydrophobicity (Monger et al. 1999) and proteins (Strom et al. 2012), or production of chemical deterrents, such as dimethysulfoniopropionate (DMSP, Strom et al. 2003).

Despite the fact that these behaviors are documented, most plankton growth-grazing dynamics are reported as single rates for the entire plankton community, which masks the complex trophic interactions that occur between plankton taxa. When taxa-specific rates are reported, these are usually only available for a handful of taxa using targeted measurements often based on pigment analysis or quantitative polymerase chain reaction (qPCR) measurements (Binder et al. 1996, Worden et al. 2004, Demir et al. 2008). The application of analytical techniques that would allow for broad classification of many taxa at once in growth-grazing experiments, such as 18S and 16S ribosomal DNA (rDNA) metabarcoding, could be extremely useful in addressing this topic. In Chapter 5, I address this by using metabarcoding techniques, along with more traditional microscopy and flow cytometry analyses, to investigate taxa-specific growth and mortality rates of phytoplankton due to microzooplankton grazing.

Climate change and pressures on microzooplankton

The potential number of trophic steps within the microbial portion of the food web is affected not only by the taxonomic and size composition of the microbial community, but also by environmental conditions (e.g. temperature, nutrients), bottom-up factors (e.g. phytoplankton composition and growth rates), and top-down forcing (e.g. mesozooplankton predation). Thus, the warmer temperatures, greater water-column

stratification, and decreased nutrient flux to the surface (Behrenfeld et al. 2006) predicted as a result of climate change (Behrenfeld et al., 2006), could have both direct and indirect impacts on microzooplankton grazing. Warming temperatures have been observed to directly increase the metabolic activity and grazing rates of microzooplankton communities (Rose and Caron 2007), consistent with the metabolic theory of ecology (Brown et al. 2004). This increased activity in response to environmental forcing could alter the ratio of production to grazing, particularly in eutrophic areas (Chen et al. 2012). However, enhanced mesozooplankton predation could suppress increased microzooplankton grazing activity in such situations (Irigoien et al. 2005, Riisgaard et al. 2014). Because of these competing pressures on microzooplankton activity, the effects of altered environmental regimes on the role of microzooplankton may not be straightforward (Caron and Hutchins 2013).

In addition to the potential effects of warmer ocean temperatures on the metabolic activity of small grazers, total microzooplankton grazing on a global scale may be enhanced in the future according to some models that predict larger oligotrophic regions of the ocean (Behrenfeld et al. 2006). Such oligotrophic systems are expected to have a higher number of trophic steps in the microbial part of the food web due to the small mean size of primary producers in these communities and the key role of microzooplankton as grazers and nutrient remineralizers. As a result, a greater fraction of global primary production could pass through the microzooplankton, decreasing overall energy transfer to higher trophic levels.

Other models have predicted, however, that areas such as the CCE may become more productive in the future despite increasing global ocean stratification, potentially

decreasing trophic fluxes through microzooplankton (Rykaczewski and Dunne 2010, Di Lorenzo 2015). In addition, unknown details about population-specific interactions among microzooplankton and their microbial prey may lead to unforeseen effects from altered stratification, temperature, nutrient delivery, and system mesoscale structure on lower levels of the food web. For example, increased temperature could enhance specific grazing rates relative to phytoplankton productivity (Chen et al. 2012), and nutrient, temperature or increased grazing stress could select for less palatable or grazing resistant prey (Strom 2002, Taylor 2014). In Chapters 3 through 5, I investigate microzooplankton communities and their grazing impacts on the food web under a variety of environmental conditions in upwelling regions of the eastern Pacific to increase the understanding of the complex pressures on these grazers.

Plankton food web dynamics in an upwelling ecosystem

In an effort to unravel some of the complexity within this small group of grazers, it is important to characterize the phytoplankton and microzooplankton assemblages and their trophic interactions to identify the factors that influence grazing rates under different environmental conditions. Studies performed in the CCE are appropriate in this regard because this region exhibits broad productivity gradients, from coastal upwelling to oligotrophic open ocean, and high mesoscale variability, allowing for the investigation of diverse microbial assemblages within relatively close proximity. This region is home to multiple commercially important fisheries, such as sardine and squid (Checkley and Barth 2009), that are directly impacted by alterations in food web energy efficiency.

Kahru et al. (2012) has shown that the frequency of fronts, defined by sharp transitions in satellite images of temperature or chlorophyll, has increased significantly in

the CCE over the past three decades. Frontal features have been linked to enhanced production and export (Franks 1992, Claustre et al. 1994, Taylor et al. 2012, Stukel et al. 2017), providing one mechanism by which overall productivity of the region may increase in the future. Furthermore, it has been suggested that the microbial communities and dynamics at fronts are unique from others nearby (Franks et al. 2013). As mentioned previously, models of future CCE conditions suggest that productivity will increase in the future (Rykaczewski and Dunne 2010, Di Lorenzo 2015). That, combined with the documented increase in productive mesoscale fronts in the region (Kahru et al. 2012), highlight the need to better understand the implications of lower-level food-web variability on energy transfer in dynamic upwelling regions. I investigate these dynamics in Chapters 3 through 5, both in the CCE and Costa Rica Dome upwelling regions of the eastern Pacific.

Outline of the dissertation

In this dissertation, I investigate the plankton community composition of microzooplankton and their phytoplankton prey, as well as rates of phytoplankton growth and mortality due to microzooplankton grazing under varying environmental conditions and community assemblages in upwelling regions in the eastern Pacific Ocean. These results add to our understanding of the composition and structure of phytoplankton-microzooplankton communities, further quantify microzooplankton grazing impact on the food web under different conditions, and ultimately provide new insights about trophic interactions in marine microbial communities.

In Chapter 2, I present a new slide preparation technique to quantify ciliates preserved in acid Lugol's fixative. Traditionally, ciliates have been preserved in acid

Lugol's and counted in settling chambers to maintain the integrity of these fragile cells; however, this process is time-consuming and the settled samples cannot be saved for any future analyses. The new method I present allows seawater samples to be filtered on polycarbonate membranes, imaged via transmitted light microscopy on a standard glass slide, and stored long-term for later analysis. I also present length and width corrections to account for the shrinking of ciliate cells due to the addition of formaldehyde. Chapter 2 was published in full in 2014 as Freibott, A., Linacre, L., and Landry, M. R., Permanent filtration preparation for ciliates preserved in Acid Lugol's in Limnology and Oceanography: Methods, issue 12, p. 54-62.

In Chapter 3, I investigate the heterotrophic community in the unique upwelling region of the Costa Rica Dome (CRD). Picophytoplankton are the dominant primary producers in the CRD, suggesting that microzooplankton grazing would be integral to the transfer of energy in this food web. Thus, I hypothesized that predator-prey pairs (i.e., picoplankton consumed by nanozooplankton, and in turn by microzooplankton) would be tightly associated and readily apparent in the biomass size structure of the auto- and heterotrophic plankton communities. I found that nanozooplankton did dominate the grazer biomass and were significantly positively correlated with picophytoplankton biomass. However, heterotrophic protistan biomass was relatively constant across the CRD region despite changes in primary production, and there was no significant correlation between nanoplankton and micrograzer biomass. These findings suggest that mesozooplankton predators exerted significant top-down controls on micrograzers. Chapter 3 was published in full in 2015 as Freibott, A., Taylor, A. G., Selph, K. E., Lui, D., Zhang, W., and Landry, M. R., Biomass and composition of protist grazers and

heterotrophic bacteria in the Costa Rica Dome during June-July 2010 in Journal of Plankton Research, issue 38, vol. 2, p. 230-243.

In Chapter 4, I compare the microbial communities at two fronts in the California Current to address the following questions: Are there specific trends in community composition and biomass that are consistent across frontal features in the CCE? Are the microbial communities at mesoscale fronts distinct from the communities in adjacent eutrophic waters? I hypothesized that large phytoplankton such as diatoms would dominate front communities, making them comparable to communities in adjacent eutrophic, coastal waters of comparable biomass and productivity. Using a combination of microscopy and molecular analyses (18S and 16S rDNA metabarcoding), I was able to determine that two fronts, one in 2008 and one in 2012, had comparable total autotrophic biomass and were both comprised of approximately 70% diatom taxa. Furthermore, Prochlorococcus dominated the oligotrophic sides of both fronts, Synechococcus dominated the eutrophic sides, and there was a sharp transition between the two genera at the front. Results of statistical analyses indicated that the front microbial communities were distinct from communities in nearby eutrophic waters, demonstrating that front microbial communities are unique assemblages.

In Chapter 5, I present the first analysis of the microbial community composition and growth-grazing dynamics during the anomalous conditions of summer 2014 in the southern California Current. The Blob, as this warm water phenomenon came to be called, disrupted typical upwelling conditions in the region, and caused a stratified, low nutrient environment where small phytoplankton and micrograzers could dominate food web dynamics. I hypothesized that picophytoplankton would dominate the microbial

community at all sampled locations and that the grazing pressure of microzooplankton would be significantly higher than compared to previous normal years in the CCE because of these environmental conditions. I found that the microbial community composition was dominated by small chlorophytes, dinoflagellates, and Synechococcus. Although the dominance of chlorophytes at first appeared to be atypical of this upwelling region, which is known for diatoms, when compared to data from previous "normal" years, this pattern was not unprecedented. However, the shift in composition towards dominance by picoplankton did lead to higher microzooplankton grazing rates at the coast. The results of this study highlight the ways in which changes in environmental conditions that are indicative of potential future scenarios can shift the phytoplankton composition towards smaller autotrophs, funneling more primary production through the microzooplankton, and decreasing energy transfer efficiency to larger animals.

In Chapter 6, I synthesize and conclude the results of my previous chapters by summarizing the novel findings of this research and suggesting future directions for better understanding microzooplankton grazing dynamics. Together, these chapters demonstrate the pivotal role that microzooplankton play in the microbial food web, and their particular responses to the increased variability in environmental conditions and phytoplankton community composition in a changing climate.

References

Behrenfeld, M. J. (2006) Climate-driven trends in contemporary ocean productivity. *Nature*, 444:752-755.

Binder, B. J., et al. (1996) Dynamics of picophytoplankton, ultraphytoplankton and bacteria in the central equatorial Pacific. *Deep-Sea Research II,* 43(4-6):907-931.

Brown, J. H., et al. (2004) Toward a metabolic theory of ecology. *Ecology,* 85:1771-1789.

Calbet, A. (2008) The trophic roles of microzooplankton in marine systems. *ICES Journal of Marine Science: Journal du Conseil,* 65:325-331.

Calbet, A., and Landry, M. R. (2004) Phytoplankton growth, microzooplankton grazing, and carbon cycling in marine systems. *Limnology and Oceanography,* 49:51-57.

Calbet, A., and Saiz, E. (2005) The ciliate-copepod link in marine ecosystems. *Aquatic Microbial Ecology*, 38:157-167.

Caron, D. A., and Hutchins, D. A. (2013) The effects of changing climate on microzooplankton grazing and community structure: drivers, predictions and knowledge gaps. *Journal of Plankton Research,* 35:235-252.

Checkley Jr., D. M., and Barth, J. A. (2009) Patterns and processes in the California Current System. *Progress in Oceanography*, 83:49-64.

Chen, B., et al. (2012) Does warming enhance the effect of microzooplankton grazing on marine phytoplankton in the ocean? *Limnology and Oceanography,* 57:519-526.

Claustre, H., et al. (1994) Phytoplankton dynamics associated with a geostrophic front: ecological and biogeochemical implications. *Journal of Marine Research,* 52:711-742.

Demir, E., et al. (2007) Assessment of microzooplankton grazing on *Heterosigma akashiwo* using a species-specific approach combining quantitative real-time PCR (qPCR) and dilution methods. *Microbial Ecology,* 55(4):583-594.

Di Lorenzo, E. (2015) Climate science: The future of coastal ocean upwelling. *Nature,* 518:310-311

Dussart, B. H. (1965) Les différentes catégories de plancton. *Hydrobiologia,* 26**:** 72-74.

Esteban, G. F., Fenchel, T., and Finlay, B. J. (2010) Mixotrophy in ciliates. *Protist,* 161:621-641.

Franks, P. J. (1992) Sink or swim: Accumulation of biomass at fronts. *Marine Ecology Progress Series*, 82:1-12.

Franks, P.J., et al. (2013) Modeling physical-biological responses to climate change in the California Current System. *Oceanography*, 26(3):26-33.

Goericke, R. (2011). The size structure of marine phytoplankton—what are the rules? *CalCOFI Reports*, 52:198-204.

Hansen, B., P. Bjørnsen, K., and Hansen, P. J. (1994) Prey size selection in planktonic zooplankton. *Limnology and Oceanography*, 39:395-403.

Irigoien, X., et al. (2005) Phytoplankton blooms: a 'loophole' in microzooplankton grazing impact? *Journal of Plankton Research*, 27:313-321.

Landry, M. R., et al. (2008) Mesozooplankton biomass and grazing responses to Cyclone *Opal*, a subtropical mesoscale eddy. *Deep Sea Research II*, 55:1378-1388.

Landry, M. R., et al. (2011). Phytoplankton growth, grazing and production balances in the HNLC equatorial Pacific. *Deep-Sea Research II*, 58:524-535.

Kahru, M., et al. (2012) Trends in the surface chlorophyll of the California Current: Merging data from multiple ocean color satellites. *Deep Sea Research II*, **77**:89-98.

Mitra, A., et al. (2016) Defining planktonic protist functional groups on mechanisms for energy and nutrient acquisition: Incorporation of diverse mixotrophic strategies. *Protist*, 167(2):106-120.

Moloney, C. L. and Field, J. G. (1991) The size-based dynamics of plankton food webs. I. A simulation model of carbon and nitrogen flows. *Journal of Plankton Research*, 13:1003-1038.

Monger, B. C., et al. (1999) Feeding selection of heterotrophic marine nanoflagellates based on the surface hydrophobicity of their picoplankton prey. *Limnology and Oceanography*, 44:1917-1927.

Naustvoll, L. J. (2000) Prey size spectra and food preferences in thecate heterotrophic dinoflagellates. *Phycologia*, 39**:** 187-198.

Riisgaard, R., et al. (2013) Trophic role and top-down control of a subarctic protozooplankton community. *Marine Ecology Progress Series*, 500:67-82.

Rose, J. M., and Caron, D. A. (2007) Does low temperature constrain the growth rates of heterotrophic protists? Evidence and implications for algal blooms in cold waters. *Limnology and Oceanography,* 52: 886-895.

Rykaczewski, R. R., and Dunne, J. P. (2010) Enhanced nutrient supply to the California Current Ecosystem with global warming and increased stratification in an earth system model. *Geophysical Research Letters,* 37:1-5.

Selph, K. E., et al. (2011) Spatially-resolved taxon-specific phytoplankton production and grazing dynamics in relation to iron distributions in the Equatorial Pacific between 110 and 140 ºW. *Deep-Sea Research Part II,* 58:358-377.

Sherr, E. B., and Sherr, B. F. (2002) Significance of predation by protists in aquatic microbial food webs. *Antonie van Leeuwenhoek,* 81:293-308.

Sherr. E. B., and Sherr, B. F. (2007) Heterotrophic dinoflagellates: a significant component of microzooplankton biomass and major grazers of diatoms in the sea. *Marine Ecology Progress Series,* 352:187-197.

Sommer, U., et al. (2002) Pelagic food web configurations at different levels of nutrient richness and their implications for the ratio fish production: primary production. In *Sustainable Increase of Marine Harvesting: Fundamental Mechanisms and New Concepts.* Springer, 11-20.

Stoecker, D. K., Guillard, R. R. L., and Kavee, R. M. (1981) Selective predation by *Favella ehrenbergii* (Tintinnia) on and among dinoflagellates. *Biological Bulletin,* 160(1):136-145.

Stoecker, D. K., and Capuzzo, J. M. (1990) Predation on protozoa: its importance to zooplankton. *Journal of Plankton Research,* 12:891-908.

Straile, D. (1997) Gross growth efficiencies of protozoan and metazoan zooplankton and their dependence on food concentration, predator-prey weight ratio, and taxonomic group. *Limnology and Oceanography*, 42:1375-1385.

Strom, S. (2002) Novel interactions between phytoplankton and microzooplankton: their influence on the coupling between growth and grazing rates in the sea. *Hydrobiologia,* 480:41-54.

Strom, S., et al. (2003) Chemical defense in the microplankton II: Inhibition of protist feeding by β–dimethylsulfoniopropionate (DMSP). *Limnology and Oceanography,* 48:230-237.

Strom, S. L., et al. (2012) A giant cell surface protein in *Synechococcus* WH102 inhibits feeding by a dinoflagellate predator. *Environmental Microbiology,* 14:807-816.

Stukel, M. R., et al. (2017) Mesoscale ocean fronts enhance carbon export due to gravitational sinking and subduction. *PNAS*, 114(6):1252-1257.

Taylor, A. G., et al. (2012) Sharp gradients in phytoplankton community structure across a frontal zone in the California Current Ecosystem. *Journal of Plankton Research*, 34: 778-789.

Taylor, A. G. (2014) Biomass structure and environmental relationships for phytoplankton communities in the southern California Current and adjacent ocean ecosystems, PhD dissertation. UC San Diego: Oceanography, b8170131.

Waterhouse, T. Y., and Welschmeyer, N. A. (1995) Taxon-specific analysis of microzooplankton grazing rates and phytoplankton growth rates. *Limnology and Oceanography*, 40(4):827-834.

Worden, A., Z., Nolan, J. K., and Palenik, B. (2004) Assessing the dynamics and ecology of marine picophytoplankton: The importance of the eukaryotic component. *Limnology and Oceanography*, 49(1):168-179.

Verity, P. G. (2003) Measurement and simulation of prey uptake by marine planktonic ciliates fed plastidic and aplastidic nanoplankton. *Limnology and Oceanography*, 36(4):729-750.

CHAPTER 2.

A slide preparation technique for light microscopy analysis of ciliates preserved in acid Lugol's fixative

LIMNOLOGY
and
OCEANOGRAPHY: METHODS

Limnol. Oceanogr.: Methods 12, 2014, 54–62

A slide preparation technique for light microscopy analysis of ciliates preserved in acid Lugol's fixative

Alexandra Freibott[1]*, *Lorena Linacre*[1], *and Michael R. Landry*[1]
[1]Scripps Institution of Oceanography, University of California, San Diego, 9500 Gilman Drive, San Diego, CA 92093-0244, USA

Abstract

A slide preparation method for seawater samples preserved in acid Lugol's is presented here as an alternative to the traditional Utermöhl settling chamber method for microplankton analysis. This preparation maintains the integrity of fragile cells, such as ciliates, resolves issues associated with the transience of samples prepared in settling chambers, and allows the use of automated image acquisition methods. Samples are filtered onto polycarbonate membranes and analyzed with transmitted light microscopy. The visibility of pore outlines is minimized by using mounting oil (Cargille Series A immersion oil, Certified Refractive Index, $n_D^{25°C}$ 1.5840 ± 0.0002) with a refractive index matching that of the membrane material. We assessed the efficacy of this new method by comparing abundance and biomass estimates for ciliates in settled and filtered samples. Acceptable results were found for the most delicate of samples stored long-term in acid Lugol's. Some cell shrinkage occurred during the filtration and brief drying steps. Therefore, corrections for ciliate length and width measurements in filtered samples were determined to counteract this effect on total cell biovolume. Overall, the method provides a simple and stable alternative to settling chamber analysis for ciliates preserved in acid Lugol's.

The Utermöhl settling chamber method is a standard and widely used inverted microscopy procedure for enumerating marine protistan microplankton (Lund et al. 1958; Müller et al. 1991; Sohrin et al. 2010; Utermöhl 1931). Major advantages of the technique are that cells are concentrated by gentle gravitational settling and remain in the liquid medium during analysis. The technique can therefore be used in conjunction with acid Lugol's preservative, which is optimal for delicate groups like ciliates (Leakey et al. 1994; Stoecker et al. 1994) but does not fix their cell walls rigidly. Disadvantages are that it requires a laborious set-up procedure, a long settling time in specialized columns (typically 24-48 h, but see Claessens and Prast [2008]), and does not result in a permanent preparation. In practice, once cells have been concentrated onto a coverslip in the lower chamber and most of the original sample water removed, a skilled technician will scan transects or the full area of the chamber. During this analysis, dimensions of representative organisms are taken with an ocular micrometer for biovolume estimations, data are recorded for abundance, cell shape, and taxa, for all cells of interest, and ultimately the sample is discarded. Besides being a very tedious process, questions that arise later about poorly resolved taxa, unmeasured cell properties, or specific taxa that were not enumerated originally, are difficult or impossible to answer without the original sample or an image record. Additionally, given the effort required for analysis and the transient nature of settling column preparations, samples intended for Utermöhl analysis are generally kept in bottles until they are used. This is not only a practical problem for storage of large numbers of samples, but also may lead to degradation of cells stored in the acidic media over time (Menden-Deuer et al. 2001; Sherr et al. 1993; Stoecker et al. 1994).

For the majority of microbial populations, alternate methods such as epifluorescence microscopy and flow cytometry have become increasingly popular for routine analysis of community abundance and biomass (e.g., Taylor et al. 2011). These techniques are especially suited for distinguishing autotrophic from heterotrophic cells based on chlorophyll *a* (Chl *a*) autofluorescence and for quantifying contributions of functional groups too small to be enumerated effectively in settling chambers. They are also convenient for sample concentration and analysis at sea, and various steps of the analyt-

*Corresponding author: E-mail: afreibott@ucsd.edu

Acknowledgments

We thank Andrew Taylor and John Wokuluk for extensive help in adapting computer programs for use with this new method and for general troubleshooting with the microscopy. Sample collections on CalCOFI cruises were made by Shonna Dovel. This work was funded by the National Science Foundation grants OCE-1260055 and #1026607 (CCE-LTER site) and by postdoctoral fellowship support to L. Linacre from the University of California MEXUS-CONACYT Program.

DOI 10.4319/lom.2014.12.54

ical process can be automated for faster processing. For example, with a fully automated epifluorescence microscope, it is possible to program a prearranged pattern of sampling locations on a prepared slide, section the visual field at precise increments of vertical resolution at each location, acquire separate images at precisely the same slide location (x, y, z) with filters that optimize for different fluorescence signals, reassemble the images into one best-of-focus color image per location with minimal halo effect, resolve and quantify dimensions and fluorescence properties of each image, and capture the data in spreadsheets (e.g., Taylor et al. 2012). It remains later for human technicians to identify and place cells into appropriate functional categories, but the digital imaging can be done immediately after sample preparation, producing a permanent visual record of the slide contents in addition to the spreadsheet information. Such a process is efficient and robust to handle many hundreds of slides per cruise (Taylor et al. 2011, 2012), and accurate enough to resolve production contributions of phytoplankton functional groups from biomass and growth rate estimates (Landry et al. 2011). However, it clearly gives severe underestimates of abundance and biomass for ciliated protists (Taylor et al. 2011), whose fragility makes them vulnerable to significant loss from commonly used aldehyde preservatives and filtration procedures (Choi and Stoecker 1989; Leakey et al. 1994).

In search of a more efficient image-analysis approach for routine enumeration of acid Lugol's preserved marine microplankton, particularly ciliates, we first considered some published protocols for slide mounting: filter-transfer-freeze (Hewes and Holm-Hansen 1983), soluble methacrylic resin (Crumpton 1987), and Steedman's wax (Steedman 1957). The first is inherently nonquantitative, and the resin and wax techniques involve heating, drying, and strong adhesive steps that we found even preserved ciliates could not withstand. We also attempted to analyze standard Utermöhl chambers with automated inverted microscopy. However, the large number of motor-driven movements of the microscope stage caused the fluid-suspended cells to move and precluded reconstruction of focused images from multiple pictures at each location. We also eliminated Cyto-clear slides (Poretics) from consideration due to expense per slide and the fact that the frosted slides are incompatible with phase contrast. Nevertheless, according to their description and results of Logan et al. (1994), these slides should minimize membrane pore visibility in transmitted light microscopy in a similar manner to the method described in this article.

In the present study, we examine the effectiveness of an alternative slide preparation method for transmitted light microscopy that uses mounting oil matching the refractive index of polycarbonate membrane filters (Ocklind 1987). The oil is used to fill the membrane pores and visually reduce their outlines, which otherwise greatly detract from identifying cells on the slide. This simple solution is complicated by the fact that polycarbonate is a birefringent material, with one refractive index at 1.584 and one that varies with the exact chemical composition of the membrane and potential crystallization of the polycarbonate material. For pores to disappear, the refractive index of the mounting oil must match at least one of these two refractive indices. Cargille Immersion Liquid Index A, with refractive index 1.584 ($n_D^{25°C}$ 1.5840 ± 0.0002), is the only available material that has an appropriate refractive index and is stable. However, being an oil-based product, it is immiscible with the seawater remaining in the membrane pores after sample filtration, which must be wicked away before mounting the filter. Here, we describe procedures for making these slides and an assessment based on comparison to standard Utermöhl results, with an emphasis on ciliates.

Materials and procedures

Seawater samples available from different cruises were analyzed as part of the method development. Most samples were collected from 2008 to 2010 during quarterly cruises of the California Cooperative Oceanic Fisheries Investigations (CalCOFI) Program in the southern coastal region of the California Current Ecosystem. We also analyzed older samples collected during 1997-98 cruises of the Antarctic Environment and Southern Ocean Process Study (AESOPS) in the Southern Ocean to assess implications of longer storage on slide preparations with fragile cells (Table 1). Regardless of cruise and date, all samples were originally collected from 10-L Niskin bottles by gentle direct transfer to the sample bottle via a silicone tube, preserved in 5% acid Lugol's, and stored in dark polyethylene bottles.

Slide preparation

Based on preliminary observations, acid Lugol's preserved ciliates could be filtered onto polycarbonate membranes under low vacuum pressure (<50 mmHg) without the massive losses seen for slide preparations of aldehyde-preserved epifluorescence samples, or in the making of permanent slides with mounting resin (Crumpton 1987). To toughen the cell walls further for slide preparations, we added 37% formaldehyde to the 250 mL acid Lugol's samples (2% final concentration) and let them fix overnight before filtration. We used a glass filtration system to filter 100 mL sample onto 25-mm, 8-μm black polycarbonate filters with a 10-μm nylon backing filter (GE Water and Process Technologies) to promote even cell distribution. Filtrations were done under low pressure (<50 mmHg), and the vacuum pump was turned off during the final few milliliters to minimize cell damage from rapid pressure change (Crumpton 1987; Taylor et al. 2011).

After the samples were completely concentrated on the filters, both the backing and polycarbonate filters were placed together on plain paper to briefly wick away the residual water trapped in the pores of the membrane. It is important to remove as much water from the pores as possible to enhance visibility during later microscopy analysis, but at the same time, minimize dehydration of cells from air drying. We found that about 30 seconds or less was optimal for this part of the process.

Table 1. Ciliate and dinoflagellate abundance (cell L^{-1}) of both filtered and settled samples, as well as collection information including cruise, date, location, and depth for each sample. Replicate counts of ciliate abundance were available for samples 1, 2, 3, and 6.

						Ciliate abundance (cell L^{-1})				Dinoflagellate abundance (cell L^{-1})	
Sample	Cruise	Lat (°N)	Long (°W)	Depth (m)	Date	Filter	Replicate filter	Settling chamber	Replicate settling chamber	Filter	Settling chamber
1	AESOPS	−62.00	170.10	5	Jan 98	3239	2337	2903	2233	3553	6699
2	AESOPS	−59.30	170.00	30	Nov 97	1375	1141	1116	2030	5964	2664
3	CalCOFI	34.32	120.80	20	Aug 08	4717	5094	2791	5730	7242	10,658
4	CalCOFI	34.32	120.80	10	Oct 08	4826	—	4019	—	5845	3015
5	CalCOFI	34.27	120.03	20	Jan 10	3255	—	5981	—	2846	665
6	CalCOFI	34.27	120.03	15	Jan 09	2294	4246	5806	6364	2174	5471
7	CalCOFI	34.27	120.03	20	Oct 08	6586	—	7927	—	9185	3349
8	CalCOFI	33.18	118.39	30	Oct 08	3014	—	4354	—	12,107	2121
9	CalCOFI	32.65	119.48	20	Oct 08	2197	—	2568	—	9185	4578

A single drop of Cargille Series A immersion oil (Certified Refractive Index Liquids, $n_D^{25°C}$ 1.5840 ± 0.0002) was spread in a thin, even layer across the slide using the side of a glass pipette. The polycarbonate membrane with the sample was then carefully separated from the backing filter using 2 forceps and placed on top of the layer of oil, with a second drop of oil applied on top of the filtered membrane before adding the cover slip (No. 2 glass). Excess oil was removed from the edges of the coverslip, and it was sealed on all four sides to the glass slide with clear nail polish. An initial coat of quick dry polish followed by a coat of durable, long-lasting polish was most effective at completely sealing the coverslip to the slide, preventing the oil from leaking, which might compromise the slide over time. After a few months of storage, it was noted that the nail polish on a few slides had begun to peel, so a coat of acrylic paint varnish was applied to the edges of the coverslip on these slides as an additional sealant. Sealed slides were stored in slide boxes at –20°C with no apparent negative effect. These were brought to room temperature before microscopic analysis to prevent temperature effects on the refractive index.

Sample imaging and processing

Sample slides were analyzed on a Zeiss Axiovert 200M inverted compound microscope equipped with a fully motorized stage and controlled by Zeiss AxioVision software. Digital images were captured with a Zeiss AxioCam MRm black and white 8-bit CCD camera at 200x magnification using automated image acquisition. We imaged 200 visual fields at random positions on each slide, with 7 z-plane images taken at each position. The z-plane images were combined into a single 8-bit black and white image using an extended depth-of-field algorithm to produce a single, completely focused image (image dimensions 425.77 µm x 319.02 µm). Using a VBA script within the Image Pro software, a series of processing steps were made to the images for semi-automated counting and sizing (length, L, and width, W) of cells. A fast Fourier transform was applied to the images to remove background noise, followed by a Laplace filter to improve the definition of cell edges. Poorly resolved field images were discarded. Each cell in each image was manually outlined and identified, and the cell measurement data were exported for processing (Taylor et al. 2012)

Cells were manually identified and placed into one of 4 categories (ciliates, diatoms, dinoflagellates, and others). All of the 200 field images per sample, equivalent to about 10% of total filtered area, were analyzed for ciliates. The more abundant organisms (diatoms, dinoflagellates, others) were identified in random subsets of 50 images, sufficient to obtain 100 cells or more per category whenever possible. Finally, all cells were binned into three size-categories (10 to 20 µm, 20 to 40 µm, and >40 µm) based on measurement of the longest cell axis.

Settling chamber samples

To compare quantitatively against abundance and biomass estimates from the slide preparations, we analyzed 100 mL aliquots of each sample by the Utermöhl method. These sam-

ples were settled at least 20 hours, more than sufficient settling time according to ciliate sinking rates determined by Claessens and Prast (2008), and cells were enumerated in two transects across the diameter of the settling chamber. The area enumerated (about 9% of the total chamber area) was, therefore, roughly equivalent to the 200 microscope fields in the slide analyses. Unlike the automated image acquisition of the slide analyses, the settling chamber transects were analyzed manually, using fine adjustments to locate cells vertically in the chamber and to optimize image taking. Cell sizes for biovolume calculations and carbon biomass estimates were taken as described above for the slide samples.

Biovolume and carbon biomass estimations

Cell biovolumes for settled and filtered samples were calculated from measured dimensions and general cell shapes, assuming that the unmeasured cell height was equal to measured cell width. Equations for estimates of cell biovolumes (BV) followed Hillebrand et al. (1999), with diatoms, dinoflagellates and some ciliates, approximated as prolate spheroids ($BV = 0.524 \times L \times W \times H$). For ciliates, an additional shape option of a cone plus half-sphere was also used where more appropriate ($BV = 0.262 \times W^2 \times [L+W]$). As discussed further in the "Assessment" section, filtered ciliate cell lengths and widths were corrected for shrinkage according to the equations in Fig. 4(*c*-*d*) before calculating biovolume and biomass.

Carbon biomass per cell was estimated from biovolume calculations using the following equations from Menden-Deuer and Lessard (2000): $C = 0.288 \times BV^{0.811}$ for diatoms and $C = 0.216 \times BV^{0.939}$ for non-diatoms and non-ciliates. We used the formula $C = 0.19 \times BV$ from Putt and Stoecker (1989) for carbon estimates of aloricate ciliates. Carbon biomass (μg C L^{-1}) was calculated from carbon per cell and abundance data for each group.

Assessment

Qualitative visual assessment

Fig. 1 compares the visual quality of images taken manually in the settling chamber (*a*-*b*) to images from slides prepared with Cargille immersion oil Type DF with refractive index 1.515 (*c*-*d*), which is typically used in epifluorescence microscopy (Booth 1993), and to images from slides prepared with the oil proposed in this method, Cargille Series A with refractive index 1.584 (*e*-*h*). As a trade-off to minimizing cell dehydration and subsequent damage, we did not dry the filter membranes completely during slide preparation. Consequently, the Series A oil did not make the membrane pores disappear entirely into the background. Even so, the pores are dramatically less visible using Series A compared with standard Type DF immersion oil, greatly decreasing the distracting pore outlines that can obscure cell shapes and complicate the process of cell identification. It was also noted that Type DF immersion oil often spread unevenly across the slide, creating shadows in the transmitted light images (Fig. 1d). This was not apparent in slides prepared with the Series A oil, which spread evenly over the filters. Whereas the settling chamber still offers the least distracting image background for cell enumeration when manually focused prior to image capture, Series A oil sufficiently diminishes the membrane pores so that high quality images can be rapidly taken using automated microscope systems.

Abundance estimates and replication

Ciliate abundance estimates for filtered samples ranged from 40% to 169% of the corresponding abundance estimates for settling chambers (Table 1). On average, filter abundances were 9% lower than settling chamber estimates, but the results were not statistically different (non-parametric Mann-Whitney test, df = 8, $p = 0.453$). A strong positive relationship ($R^2 = 0.60$) was also found between estimates by the two methods (Fig. 2 inset). Results for dinoflagellates and diatoms are likely biased by insufficient settling times for these slower sinking cells. As determined by Claessens and Prast (2008), the sinking rates of acid Lugol's preserved ciliates in seawater are rapid enough to clear the water in 50 mL settling chambers in less than 3 hours. Thus, overnight settling times of at least 20 hours is sufficient for complete sinking of ciliates in our 100 mL columns, but not necessarily for smaller and less dense dinoflagellates and diatoms. Results for diatoms support this explanation, as diatom cells were significantly more abundant in the filtered samples than the settling chambers (Fig. 2, Mann-Whitney test, df = 8, $p = 0.047$). Dinoflagellate abundances were also notably higher in the filtered preparations, averaging more than double the corresponding estimates in settling chambers. This difference, however, was not statistically significant (Mann-Whitney test, df = 8. $p = 0.145$) for the number of samples enumerated. Clearly, the filter preparations minimize potential artifacts that could arise from large differences in sinking rates of different cells in settling chambers.

Because dinoflagellates and diatoms are believed to have been under-sampled in settling chamber counts, our remaining assessment focuses on ciliates only, which were the initial target group for the method development. For samples in which sufficient sample volumes were available (samples 1, 2, 3, 6), replicate subsamples were processed for ciliates by both the filtration and settling methods to determine the consistency of abundance estimates. Although methodological differences were larger than can be explained by replicate counts in one case (sample 6), error bars broadly overlap in the other three comparisons (Fig. 3). Differences between the ciliate abundance estimates in filtered and settled samples are therefore largely explained by counting variability within and between methods.

Biovolume estimates and shrinkage correction

Direct length and width measurements for ciliate biovolumes were conspicuously lower for filtered compared with settled samples, which prompted a closer look at the measurement distributions for each method (Fig. 4). Acid Lugol's fixative is known to shrink cells (Leakey et al. 1994; Stoecker

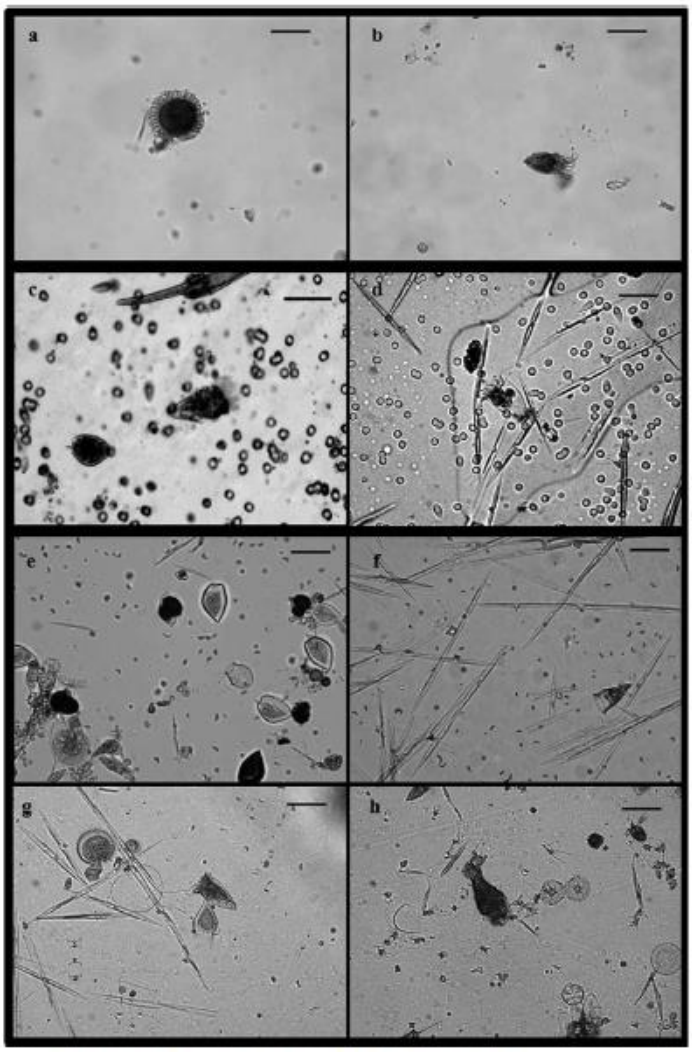

Fig. 1. Representative images of ciliates settled in a settling chamber (*a-b*), mounted on an 8 μm polycarbonate membrane filter with standard epifluorescence immersion oil (*c-d*, Cargille Immersion oil Type DF), and mounted on a filter with the method described in this paper (*e-h*). All images are from samples collected in the southern California Current region and imaged as described in the methods section. All scale bars are 50 μm.

et al. 1994). However, since both filtered and settled subsamples had been stored in this fixative for the same amount of time before sample handling, their cell biovolumes should have been similar in the absence of other effects. We attribute the biovolume discrepancy to cell shrinkage during the filtration and brief drying process.

To quantify the mean measurement differences as rigorously as possible, we compared the size frequency distribu-

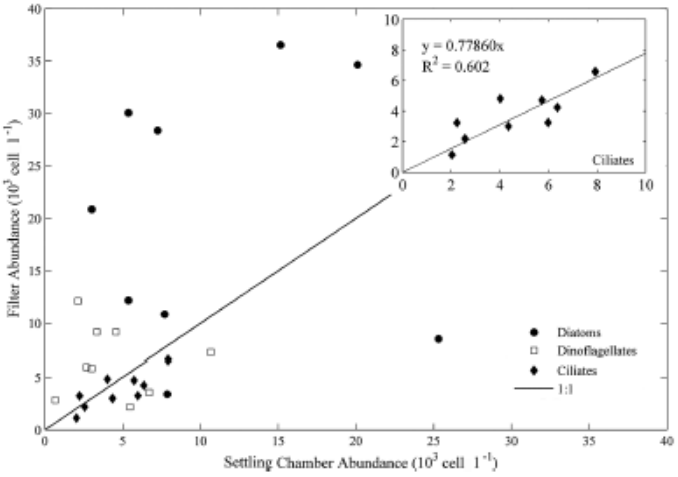

Fig. 2. Abundances (10^3 cell L^{-1}) of diatoms, dinoflagellates, and ciliates in settled versus filtered samples with a 1:1 line for reference. Inset graph is a linear regression for ciliates.

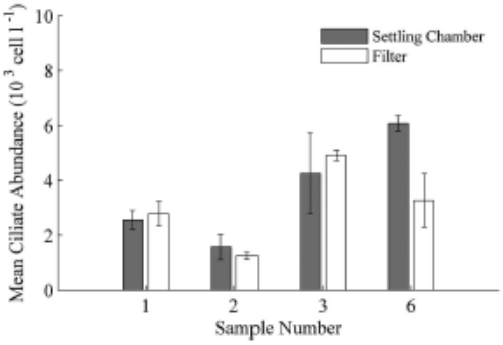

Fig. 3. Mean abundances (10^3 cell L^{-1}) with standard error bars estimated for settled and filtered samples calculated from replicate counts of 100 mL aliquots. Standard error was calculated as standard deviation divided by the square root of the sample size. Information for samples 1, 2, 3, and 6 given in Table 1.

tions of length and width measurements for ciliate cells analyzed by each method (>160 cells). The majority of cells fell into the 10-20 µm length category for both methods, but wider cells were more frequently found in settled (15-35 µm) rather than filtered (5-15 µm) samples (Fig. 4*a*-*b*). To account for the loss of cell volume during slide preparation, we chose randomly an equal number of ciliates from those analyzed by each method, ordered them by size, and then compared their length and width measurements by regression analysis (Fig. 5*c*-*d*). Strong exponential trends could be fit to both length (R^2 = 0.98) and width (R^2 = 0.99) data, and the resulting equations were used as correction factors for cells from the slide preparations. The curvilinear relationships indicate that cell dimensions shrink proportionately less with increasing cell size during slide preparation, perhaps reflecting greater resistance to dessication (reduced surface area to volume ratio) during the brief water-wicking process. Very large cells (>50 µm length, >35 µm width) were, however, very rare in the samples and therefore difficult to compare statistically from analysis by the two techniques. Individual length and width values measured from filtered cells were corrected according to these equations, and recalculated biovolumes were a much better approximation of settled biovolume values (Fig. 5*a*). Additionally, the biovolume corrections more than doubled the total biomass estimates from filtered samples (Fig. 5*b*), resulting in comparable total biomass estimates for settled and filtered samples (Fig. 5*b*-*c*).

Biomass comparisons

Ciliate biomass estimates for the six samples were pooled and compared across methods (Fig. 5*b*). Only six samples had sufficient measurement data from settling chambers to calculate ciliate biomass for comparison with filtered samples. Comparable results for total settling chamber ciliate biomass and filter biomass were found for all samples using the correction factor (Fig. 5*c*). A nonparametric Mann-Whitney test determined no significant difference between settling chamber and corrected filter biomass (df = 5, p = 1.00).

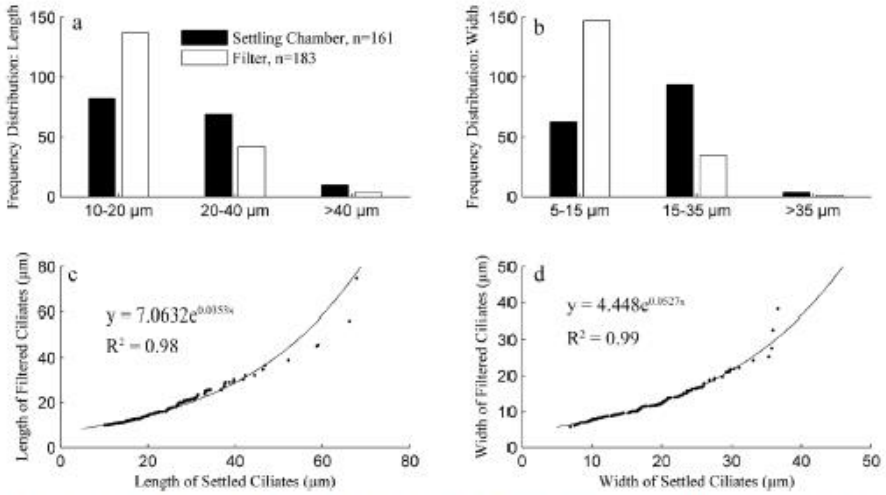

Fig. 4. Frequency distributions for measured lengths (*a*) and widths (*b*) of 161 ciliates in settled samples and 183 ciliates in filtered samples. Exponential regressions for the length ($y = 7.0632e^{0.0353x}$) and width ($y = 4.448e^{0.0527x}$) measurements in each method are shown in the bottom panels (*c-d*). Filtered cells were randomly chosen to create an equal number of measurements in both filtered and settled data sets for regression analysis.

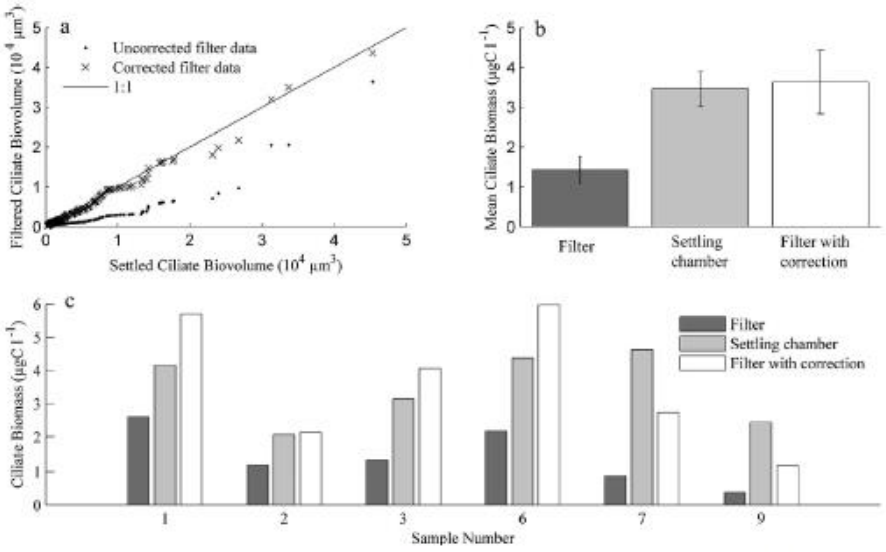

Fig. 5. Corrected and uncorrected biovolume values (10^4 µm³) for 161 representative filtered ciliates compared with settled ciliate biovolumes across samples (*a*). Corrected filter biovolume values better approximate settled ciliate biovolumes than uncorrected values, indicated by a better fit to the 1:1 line. Total mean biomass (µg C L^{-1}) of all samples with standard error bars for filtered, settled, and corrected filter measurements (*b*). Total biomass per sample (µg C L^{-1}) for filter, settling chamber, and corrected filter data (*c*).

Discussion

In this study, we sought to develop a slide preparation procedure that would be an adequate alternative to the Utermöhl method for routine bright-field analyses of microplankton samples by automated image-analysis techniques. We emphasize ciliates in our assessment of this method because they are widely regarded to be the most delicate and fragile of the major microplankton functional groups, and due to incompatible preservation and handling methods, are often grossly underestimated in community assessments based on slides prepared for epifluorescence microscopy. As part of this process, we explored in depth a published resin-based method for permanent slide preparation (Crumpton 1987). While some thecate dinoflagellates fared relatively well with this technique, the heating and drying steps were much too damaging for ciliates. This limited further options for use of existing preparation methods that require similar steps.

In contrast, the slide method developed here is sufficiently gentle to retain these fragile cells on filters, thus allowing them to be readily visualized, counted, and sized by automated techniques that require rigid positioning of cells on an observational plane. Abundance and biomass estimates for ciliates enumerated on prepared slides compared favorably to those from the standard settling chamber method. Our data suggests a slight loss of cells, <10% on average, in the slide-making process, but this is far superior to results achieved in standard slide preparations for epifluorescence microscopy using aldehyde or alkaline Lugol's fixatives, which typically produce ciliate abundance estimates more than an order of magnitude lower than settling chambers (Taylor et al. 2011). Cell shrinkage, however, does need to be accounted for to achieve comparable estimates of size-composition and biomass relative to those for acid Lugol's preserved cells in settling columns alone.

This new slide-making technique is easy enough to be done at sea. It has the advantage that automated image acquisition systems can rapidly capture and retain permanent digital record of the slide contents for later analysis or reference, thereby reducing some of the tedium associated with traditional manual microscopic analysis. It also avoids sample degradation during bottle storage (Menden-Deuer et al. 2001), and reduces space requirements for long-term sample storage.

Comments and recommendations

Based on the present results, our new slide preparation method for seawater samples preserved in acid Lugol's can be an efficient and effective alternative to the traditional Utermöhl method for enumerating ciliates in environmental samples. Whereas this technique has advantages over the traditional approach in terms of preparation speed, automated imaging, shipboard use, and potentially less settling bias, it does not replace Utermöhl settling chambers as the standard for this kind of analysis, just as quantitative protargol stain (QPS) remains a superior alternative for taxonomic analysis and permanent storage (Montagnes and Lynn 1993). The cell volume shrinkage effects that we observed during the preparation process are likely to vary somewhat among locations and taxonomic groups (e.g., diatoms and dinoflagellates), and are especially critical to constrain assessments of biovolumes and biomass. It is therefore recommended that researchers intending to use this method determine appropriate correction factors for their study system and target organisms.

Whereas not tested rigorously, we expect that our method is well suited for dinoflagellates and diatoms, depending on the age and state of the sample being analyzed. Such organisms are typically more robust than ciliates and better able to stand up to filtration pressures and aldehyde fixatives. Menden-Deuer et al. (2001) have observed that dinoflagellates in acid Lugol's preservative can expand and lyse over time, whereas diatoms simply dissolve. If relative abundances of these taxa decline in long-term acid Lugol's storage, slide preparations with fresher samples, and digital image records, may reasonably provide more reliable estimates of plankton community composition and biomass than those from older bottled samples. However, whether the slide preparation stops the negative effects of long-term storage in acid Lugol's, or how long a prepared slide retains its original community composition and integrity cannot be answered here. At the time of this writing, initial slide preparations have been maintained for 9 months at –20°C as described with no detectable deterioration. However, this is a short time relative to the timescales at which samples comparisons may be relevant, for instance, to assess climate changes on decadal or longer timescales.

Advancing technologies, such as flow-through imaging cytometry of living cells (Olson and Sosik 2007), may eventually render community assessments from microscopy unnecessary. However, that is far from what is currently available to researchers around the world to study and compare ocean habitats. Ciliates are an important but frequently missing component in ocean ecosystem studies because they are relatively fragile and inadequately sampled by traditional methods for quantifying phytoplankton or net-collected zooplankton. We hope that the present technique provides a convenient way to include them more often in plankton community analyses.

References

Booth, B. C. 1993. Estimating cell concentration and biomass of autotrophic plankton using microscopy, p. 199-205. *In* P. R. Kemp, B. F. Sherr, E. B. Sherr, and J. J. Cole [eds.], Handbook of methods in aquatic microbial ecology. Lewis Publishers.

Choi, J., and D. Stoecker. 1989. Effects of fixation on cell-volume of marine planktonic protozoa. Appl. Environ. Microbiol. 55:1761-1765.

Claessens, M., and M. Prast. 2008. Concentration of fixed plankton samples via settling: how long is long enough? J.

Plankton Res. 30:57-64 [doi:10.1093/plankt/fbm095].

Crumpton, W. G. 1987. A simple and reliable method for making permanent mounts of phytoplankton for light and fluorescence microscopy. Limnol. Oceanogr. 32:1154-1159 [doi:10.4319/lo.1987.32.5.1154].

Hewes, C. D., and O. Holm-Hansen. 1983. A method for recovering nanoplankton from filters for identification with the microscope: the filter-transfer-freeze (FTF) technique. Limnol. Oceanogr. 28:389-394 [doi:10.4319/lo.1983.28.2.0389].

Hillebrand, H., C. -D. Dürselen, D. Kirschtel, U. Pollingher, and T. Zohary. 1999. Biovolume calculation for pelagic and benthic microalgae. J. Phycol. 35:403-424 [doi:10.1046/j.1529-8817.1999.3520403.x].

Landry, M. R., K. E. Selph, A. G. Taylor, M. Décima, W. M. Balch, and R. R. Bidigare. 2011. Phytoplankton growth, grazing and production balances in the HNLC equatorial Pacific. Deep-Sea Res. II. 58:524-535 [doi:10.1016/j.dsr2.2010.08.011].

Leakey, R. J. G., P. H. Burkill, and M. A. Sleigh. 1994. A comparison of fixatives for the estimation of abundance and biovolume of marine planktonic ciliate populations. J. Plankton Res. 16:375-389 [doi:10.1093/plankt/16.4.375].

Logan, B. E., H. -P. Grossart, and M. Simon. 1994. Direct observation of phytoplankton, TEP, and aggregates on polycarbonate filters using brightfield microscopy. J. Plankton Res. 16:1811-1815 [doi:10.1093/plankt/16.12.1811].

Lund, J. W. G., C. Kipling, and E. D. L. Cren. 1958. The inverted microscope method of estimating algal numbers and the statistical basis of estimations by counting. Hydrobiologia 11:143-170 [doi:10.1007/BF00007865].

Menden-Deuer, S., and E. J. Lessard. 2000. Carbon to volume relationships for dinoflagellates, diatoms, and other protist plankton. Limnol. Oceanogr. 45:569-579 [doi:10.4319/lo.2000.45.3.0569].

———, E. J. Lessard, and J. Satterberg. 2001. Effect of preservation on dinoflagellate and diatom cell volume and consequences for carbon biomass predictions. Mar. Ecol. Prog. Ser. 222:41-50 [doi:10.3354/meps222041].

Montagnes, D. J. S., and D. H. Lynn. 1993. A quantitative protargol stain (QPS) for ciliates and other protists, p. 229-240. *In* P. F. Kemp, B. F. Sherr, E. B. Sherr and J. J. Cole [eds.], Handbook of methods in aquatic microbial ecology. Lewis Publishers.

Müller, H., A. Schöne, R. M. Pinto-Coelho, A. Schweizer, and T. Weisse. 1991. Seasonal succession of ciliates in Lake Constance. Microb. Ecol. 21:119-138 [doi:10.1007/BF02539148].

Ocklind, G. 1987. Optically eliminating the visible outlines of pores in intact polycarbonate (Nucleopore) filters. Acta Cytol. 31:9460949.

Olson, R. J., and H. M. Sosik. 2007. A submersible imaging-in-flow instrument to analyze nano-and microplankton: Imaging FlowCytobot. Limnol. Oceanogr. Methods 5:195-203 [doi:10.4319/lom.2007.5.195].

Putt, M., and D. K. Stoecker. 1989. An experimentally determined carbon: volume ratio for marine "Oligotrichous" ciliates from estuarine and coastal waters. Limnol. Oceanogr. 34:1097-1103 [doi:10.4319/lo.1989.34.6.1097].

Sherr, E. B., D. A. Caron, and B. F. Sherr. 1993. Staining of heterotrophic protists for visualization via epifluorescence microscopy, p. 213-228. *In* P. F. Kemp, B. F. Sherr, E. B. Sherr and J. J. Cole [eds.], Handbook of methods in aquatic microbial ecology. Lewis Publishers.

Sohrin, R., M. Imazawa, H. Fukuda, and Y. Suzuki. 2010. Full-depth profiles of prokaryotes, heterotrophic nanoflagellates, and ciliates along a transect from the equatorial to the subarctic central Pacific Ocean. Deep-Sea Res. II. 57:1537-1550 [doi:10.1016/j.dsr2.2010.02.020].

Steedman, H. F. 1957. Polyester wax: A new ribboning embedding medium for histology. Nature 179:1345 [doi:10.1038/1791345a0].

Stoecker, D. K., D. J. Gifford, and M. Putt. 1994. Preservation of marine planktonic ciliates: losses and cell shrinkage during fixation. Mar. Ecol. Prog. Ser. 110:293-299 [doi:10.3354/meps110293].

Taylor, A. G., M. R. Landry, K. E. Selph, and E. J. Yang. 2011. Biomass, size structure, and depth distributions of the microbial community in the eastern equatorial Pacific. Deep Sea Res. II 58:342-357 [doi:10.1016/j.dsr2.2010.08.017].

———, R. Goericke, M. R. Landry, K. E. Selph, D. A. Wick, and M. J. Roadman. 2012. Sharp gradients in phytoplankton community structure across a frontal zone in the California Current Ecosystem. J. Plankton Res. 34:778-789 [doi:10.1093/plankt/fbs036].

Utermöhl, V. H. 1931. Neue Wege in der quantitativen Erfassung des Planktons. Verh. Int. Verein. Theor. Angew. Limnol. 5:567-596.

Submitted 30 September 2013
Revised 14 November 2013
Accepted 17 December 2013

Chapter 2, in full, is a reprint of materials as it appears in Freibott, A., Linacre, L., and Landry, M. R. (2014) Permanent filtration preparation for ciliates preserved in Acid Lugol's. Limnology and Oceanography: Methods 12, 54-62, doi: 10.4319/lom.2014.12.54. The dissertation author was the primary investigator and author of this manuscript.

CHAPTER 3.

Biomass and composition of protistan grazers and heterotrophic bacteria in the Costa Rica Dome during summer 2010

JPR Advance Access published December 17, 2015

Journal of
Plankton Research

plankt.oxfordjournals.org

J. Plankton Res. (2015) 0(0): 1–14. doi:10.1093/plankt/fbv107

Costa Rica Dome: Flux and Zinc Experiments

Biomass and composition of protistan grazers and heterotrophic bacteria in the Costa Rica Dome during summer 2010

ALEXANDRA FREIBOTT[1]*, ANDREW G. TAYLOR[1], KAREN E. SELPH[2], HONGBIN LIU[3], WUCHANG ZHANG[4] AND MICHAEL R. LANDRY[1]

[1]SCRIPPS INSTITUTION OF OCEANOGRAPHY, UNIVERSITY OF CALIFORNIA AT SAN DIEGO, 9500 GILMAN DR., LA JOLLA, CA, USA, [2]DEPARTMENT OF OCEANOGRAPHY, UNIVERSITY OF HAWAII AT MANOA, HONOLULU, HI, USA, [3]THE HONG KONG UNIVERSITY OF SCIENCE AND TECHNOLOGY, HONG KONG SAR, CHINA AND [4]INSTITUTE OF OCEANOGRAPHY, CHINESE ACADEMY OF SCIENCE, QINGDAO, CHINA

*CORRESPONDING AUTHOR: afreibott@ucsd.edu

Received May 11, 2015; accepted November 19, 2015

Corresponding editor: John Dolan

We investigated biomass and composition of heterotrophic microbes in the Costa Rica Dome during June–July 2010 as part of a broader study of plankton trophic dynamics. Because picophytoplankton (<2 μm) are known to dominate in this unique upwelling region, we hypothesized tight biomass relationships between size-determined predator–prey pairs (i.e. picoplankton–nano-grazers, nanoplankton–micro-grazers) within the microbial community. Integrated biomass of heterotrophic bacteria ranged from 180 to 487 mg C m^{-2} and was significantly correlated with total autotrophic carbon. Heterotrophic protist (H-protist) biomass ranged more narrowly from 488 to 545 mg C m^{-2}, and was comprised of 60% dinoflagellates, 30% other flagellates and 11% ciliates. Nano-sized (<20 μm) protists accounted for the majority (57%) of grazer biomass and were positively correlated with picoplankton, partially supporting our hypothesis, but nanoplankton and micro-grazers (>20 μm) were not significantly correlated. The relative constancy of H-protist biomass among locations despite clear changes in integrated autotrophic biomass, Chl *a*, and primary production suggests that mesozooplankton may exert a tight top-down control on micro-grazers. Biomass-specific consumption rates of phytoplankton by protistan grazers suggest an instantaneous growth rate of 0.52 day^{-1} for H-protists, similar to the growth rate of phytoplankton and consistent with a trophically balanced ecosystem dominated by pico-nanoplankton interactions.

KEYWORDS: heterotrophic protists; microzooplankton; nanozooplankton; community composition

JOURNAL OF PLANKTON RESEARCH | VOLUME 0 | NUMBER 0 | PAGES 1–14 | 2015

INTRODUCTION

The Costa Rica Dome (CRD) is a 300- to 500-km open-ocean upwelling region in the Eastern Tropical Pacific centered around 9°N, 90°W (Wyrtki, 1964; Fiedler, 2002). Shoaling of the thermocline ridge is strongest during summer and results in seasonally high chlorophyll *a* (Chl *a*) concentrations (Fiedler, 2002). Despite a shallow thermocline and enhanced nutrient concentrations in the region, the CRD is distinct from other upwelling areas in the dominance of small picophytoplankton, specifically *Synechococcus* (Li *et al.*, 1983), as opposed to larger phytoplankton such as diatoms. Trace metal experiments suggest that limitation by cobalt, iron or zinc contribute to the dominance of such small primary producers in this otherwise high-nutrient environment by limiting the growth of larger phytoplankton (Franck *et al.*, 2005; Saito *et al.*, 2005; Ahlgren *et al.*, 2014).

Protistan grazers are important consumers in pelagic food webs, responsible for grazing the majority of global primary production (Calbet and Landry, 2004; Calbet, 2008) and playing key roles as nutrient recyclers and trophic links to larger zooplankton (Stoecker and Capuzzo, 1990; Sherr and Sherr, 2002; Sommer *et al.*, 2002; Calbet and Saiz, 2005). Microzooplankton grazers are abundant in both open-ocean (Lessard and Murrell, 1996; Pasulka *et al.*, 2013) and upwelling regions (Chavez *et al.*, 1996; Taylor *et al.*, 2011; Linacre *et al.*, 2012), although taxonomic dominance within the assemblages varies with location and size structure of phytoplankton prey. Heterotrophic dinoflagellates (H-Dino) and ciliates (Cil) generally dominate microzooplankton biomass in eutrophic upwelling regions associated with larger primary producers (Sherr and Sherr, 2007; Calbet, 2008; Linacre *et al.*, 2012), while heterotrophic nanoflagellates (H-Flag) are more important in oligotrophic open-ocean areas associated with small picophytoplankton (Lessard and Murrell, 1996; Calbet, 2008). Because the CRD is a unique upwelling region dominated by small primary producers, small heterotrophs in the microbial loop, including heterotrophic prokaryotes (H-Bact) and eukaryotic nano- (2–20 μm) and microzooplankton (20–200 μm) grazers, are expected to play key roles in mediating trophic interactions in the region. This has important implications for energy transfer efficiencies due to the 50–70% energy loss with each trophic step (Straile, 1997). Characterizing the heterotrophic microbial community of the CRD is therefore integral to understanding trophic interactions and energy flows within the region.

To date, only two studies have reported significant data on the heterotrophic community of the CRD. As part of the EASTROPAC program in the late 1960s, Beers and Stewart (Beers and Stewart, 1971) estimated protistan biovolumes and inferred microzooplankton grazing rates from samples collected in the CRD region. However, their results were limited to Cil and less abundant acantharians because H-Dino and H-Flag were not distinguishable by the techniques of that time. More recently, Olson and Daly (Olson and Daly, 2013) provided a modern and rigorous analysis of heterotrophic protist (H-protist) biomass and a few grazing estimates for a late-autumn CRD cruise, but supporting data were insufficient for assessing structural and rate relationships.

The CRD FLUx and Zinc Experiments (FLUZiE) cruise in June–July 2010 provided an opportunity to examine composition and biomass of the heterotrophic microbial community within the context of a broader food-web study (Landry *et al.*, 2015a) and during summertime, when thermocline shoaling is typically at its maximum. Since picophytoplankton biomass is known to be high in the CRD, we hypothesized that predator–prey pairs would be tightly associated (i.e. picoplankton consumed by nano-grazers, and in turn by micro-grazers) and readily apparent within the biomass size structure of the auto- and heterotrophic microbial community. Using community composition and biomass with experimental rate estimates from companion studies (Selph *et al.*, 2015), we also infer growth rate relationships for H-protist and compare our findings with recent predictions that mixotrophy should dominate as a trophic strategy among protists in open-ocean ecosystems.

METHOD

Study design and sampling

Cruise sampling in the CRD was done on *R/V Melville* from 22 June –27 July 2010 during five multi-day, semi-Lagrangian experiments, referred to as cycles. During each cycle, sampling and daily *in situ* incubation experiments were conducted while following a satellite-tracked drifter with a holey-sock drogue centered at 15 m (Landry *et al.*, 2009, 2015a). Of the five experimental cycles, the first was located close to the Costa Rica coast and outside of the CRD, so only Cycles 2–5 are considered here (Fig. 1). Seawater samples were collected from eight depths within the euphotic zone on each night of the cycles, from 2 m to 80–100 m depending on the fluorescence profiles from the CTD. Seawater was collected from Niskin bottles using silicone tubing and preserved as described below for each analysis.

Microscopic analysis of water-column samples

Seawater samples of 500 mL were preserved for epifluorescence microscopy with 260-μL alkaline Lugol's solution,

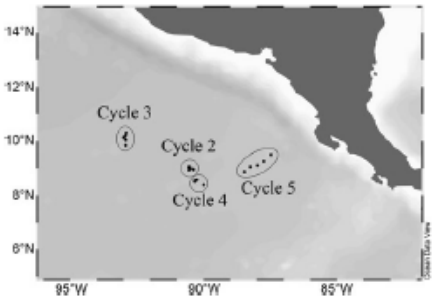

Fig. 1. Map of study region, including cruise sampling locations for Cycles 2–5.

10-mL buffered formalin, 500-mL sodium thiosulfate and 1-mL proflavin (0.033% w/v) (Sherr and Sherr, 1993). Preserved samples were allowed to sit for 1 h in the dark, then stained with 1-mL DAPI (0.01 mg mL^{-1}) before filtration. Aliquots of 50 mL were filtered onto 25-mm, 0.8-μm black polycarbonate membranes for the analysis of small cells, and the remaining 450 mL was filtered onto 25-mm, 8.0-μm black polycarbonate membranes. Membrane filters were mounted on glass slides using Type DF immersion oil, No. 2 glass coverslips, and stored at −80 °C until analysis. Slides were imaged and digitized on a Zeiss AxioVert 200 M inverted epifluorescence microscope with motorized stage. Images were captured with a Zeiss AxioCam MRc black and white camera, utilizing separate filter sets for Chl *a*, DAPI, FITC and phycoerythrin. Slides with 0.8- and 8.0-μm membrane filters were imaged at ×630 and ×200, respectively.

At each image location, 7 z-stack images were taken. The z-stack images were processed and combined using the ImagePro software, and a fast Fourier transform and Laplace filter were applied to reduce the halo effect around cells. Counting and sizing of cells was also done with the ImagePro software. Cells were manually identified and grouped into functional groups: H-Dino and H-Flag discussed in this paper, as well as autotroph populations discussed in Taylor *et al.* (Taylor *et al.*, 2015). H-Dino included cells that could be positively identified as dinoflagellates by the presence of a clear dinokaryon, two flagella and an obvious theca for thecate forms. H-Flag included other heterotrophic cells that were largely flagellated but otherwise unidentifiable. Cells were binned into size categories based on the longest cell axis: <2, 2–5, 5–10, 10–20, 20–40 and >40 μm. Cell biovolumes (μm^3) were calculated using length and width measurements in the formula for a prolate sphere ($BV = 0.524 \times L \times W^2$). Carbon biomass was calculated from biovolumes as: pg C $cell^{-1}$ = $0.216 \times BV^{0.939}$ for non-diatoms and pg C $cell^{-1}$ = $0.288 \times BV^{0.811}$ for diatoms (Menden-Deuer and Lessard, 2000). More detailed information on the epifluorescence methods are in Taylor *et al.* (Taylor *et al.*, 2015). Biomass was depth-integrated according to the trapezoidal rule, averaging community biomass between sampling depths and summing biomass contributions for all depth strata (to the deepest depth sampled for each cycle; Fig. 2).

Seawater samples of 125 mL were also preserved with 5% acid Lugol's solution in amber bottles for the analysis of Cil by transmitted light microscopy. Prior to filtration, 37% formaldehyde was added to the sample (2% final concentration) and allowed to fix for 12 h to solidify cell membranes. Samples were filtered onto 25-mm, 8.0-μm polycarbonate membranes under low pressure (<50 mmHg), and the vacuum pump was shut off during the final few milliliters to allow for gentle gravity filtration. Filters were briefly placed on plain paper to wick away residual moisture, mounted on glass slides using Cargille immersion oil A (Certified Refractive Index Liquids, $n_D^{25°C}$ 1.584 ± 0.0002), and coverslips were sealed with clear nail polish (Freibott *et al.*, 2014). The slides were imaged and processed as described above for epifluorescence microscopy.

Cil were divided into broad taxonomic groups, including aloricate oligotrichs and choreotrichs, tintinnids, scuticociliates, cyclotrichs and other unidentifiable Cil (Agatha, 2004). Large mixotrophic oligotrichs of the genus *Tontonia* were clearly recognizable in the samples and quantified separately. Cells were binned by size based on the longest cell dimension: 8–20, 20–40 and >40 μm. Due to the pore size of the filter used, most nano-sized Cil likely passed through the membrane and are not accounted for here. Length and width measurements from each cell were used to calculate cell biovolume based on the most appropriate cell shape: prolate spheroid ($BV = 0.524 \times L \times W^2$), cone ($BV = 0.262 \times L \times W^2$) or cone plus half sphere [$BV = 0.262 \times W^2 \times (L + W)$]. Carbon biomass was calculated from cell biovolume as pg C = 0.19 × BV (Putt and Stoecker, 1989). Both Cil and dinoflagellates were manually counted in acid Lugol's samples; however, autotrophic and H-Dino are indistinguishable when stained with acid Lugol's fixative, so only epifluorescence estimates of H-Dino abundance and biomass are used in this analysis.

Additionally, at a single station in each cycle, 10–40 L of seawater from six to seven depths was collected for separate analyses of rare tintinnid Cil. Samples were not collected on the same casts or depths as those for microscopy described above, so they are treated here as a separate dataset. Samples were immediately concentrated to 100 mL using a 20-μm mesh and preserved with 2% acid Lugol's. They were then pipetted into Utermöhl (Utermöhl, 1931) settling chambers, settled for 12–24 h, and counted on an

JOURNAL OF PLANKTON RESEARCH | VOLUME 0 | NUMBER 0 | PAGES 1–14 | 2015

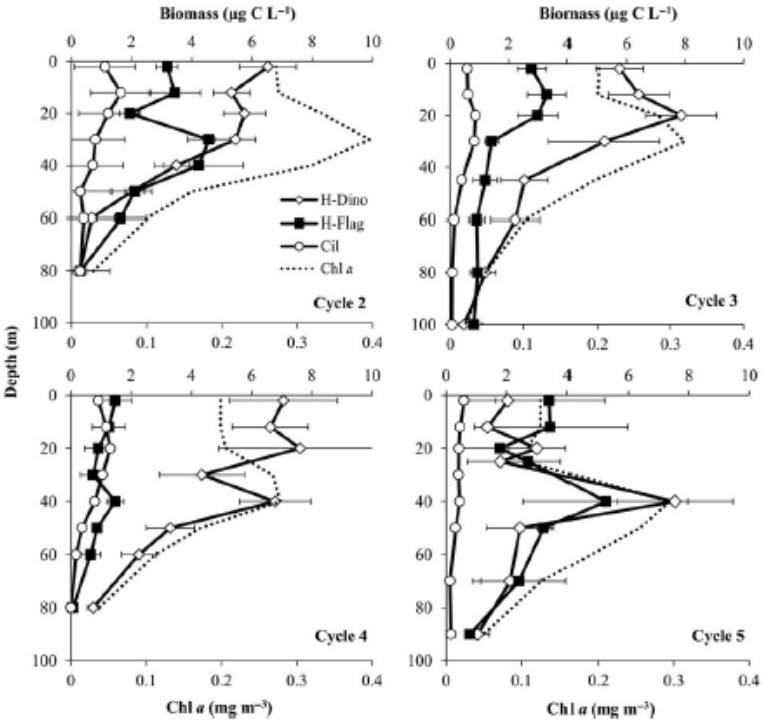

Fig. 2. Depth profiles of mean total biomass (µg C L^{-1}) for all heterotrophic dinoflagellates (H-Dino) and heterotrophic flagellates (H-Flag) from epifluorescence microscopy and ciliate biomass (Cil) from transmitted light microscopy. Dotted line and secondary *x*-axis show mean chlorophyll concentration (mg Chl *a* m^{-3} = µg Chl *a* L^{-1}). Biomass was averaged over the 4-day cycles to obtain mean and standard error bars for each cycle ($n = 5$ for Cycle 2–4; $n = 2$ for Cycle 5).

Olympus IX 71 inverted microscope at ×200 or ×400. Individual cells were photographed, measured and identified to species (Kofoid and Campbell, 1929, 1939; Marshall, 1969; Zhang *et al.*, 2011). All loricae were measured for length and width, and cell biovolumes were calculated and converted to carbon biomass using the equation, pg C = 0.053 × BV (Verity and Langdon, 1984).

Flow cytometry analysis

Seawater samples (1 mL) were preserved with 0.5% paraformaldehyde (v/v, final concentration), flash frozen in liquid nitrogen and stored at −80°C. Prior to analysis, samples were thawed and stained with Hoechst 34 442 (1 µg mL^{-1}) for 1 h in the dark (Monger and Landry, 1993). Aliquots of 100 µL were analyzed using a Beckman-Coulter EPICS Altra flow cytometer with a Harvard Apparatus syringe pump for volumetric sample delivery and two argon lasers tuned to UV (200 mW) and 488 nm (1 W) excitation. Fluorescence signals were collected using filters for Hoechst-bound DNA (blue fluorescence, 450 nm), phycoerythrin (orange fluorescence, 575 nm) and Chl *a* (red fluorescence 680 nm), and normalized to external standards of 0.5 µm yellow-green and 0.5 µm UV polystyrene beads. Cell fluorescence and light-scatter properties were acquired with the Expo32 software and subsequently analyzed with the FlowJo software to define H-Bact populations based on DNA signal (all living cells), absence of photosynthetic pigment and light-scatter signals (forward and 90°light scatter, measures of relative size).

Abundance estimates of H-Bact from flow cytometry analysis were converted to carbon biomass using carbon per cell conversions and depth, using bead-normalized forward angle light scattering (FALS) as a relative measure

of cell biovolume (Linacre *et al.*, 2010, 2012). Estimates of cell carbon content were made using an open-ocean, mixed layer estimate of 10 fg C cell^{-1} as a starting point for H-Bact (Garrison *et al.*, 2000). Then, using the scaling factor FALS$^{0.55}$ (Binder *et al.*, 1996), the carbon:cell content was determined for each depth from the specific mean cell carbon values and the FALS ratio (FALS$_{sample}$:FALS$_{mean}$)$^{0.55}$.

Trophic relationships

We examined potential relationships among autotrophic and heterotrophic size classes using Pearson correlations for biomass values in the upper 45 m, a depth range that includes the mixed layer and chlorophyll maximum on all cycles and accounts for >93% of the primary production (Landry *et al.*, 2015b). Correlations between predator–prey pairs were expected to be negative (e.g. Schmoker and Hernández-León, 2013), indicative of Lotka–Volterra-style oscillations and significant top-down grazer impacts. However, previous studies have also found positive correlations between presumptive predators and prey (Hwang and Heath, 1997; Yang *et al.*, 2008), which may be indicative of strong bottom-up forcing and rapid response of protistan consumers to prey dynamics.

We also used the relationship between the carbon consumed by microzooplankton grazing and H-protist biomass to derive biomass-specific estimates of carbon consumption and growth rate potential of the H-protist assemblages. For these analyses, phytoplankton growth rates and mortality losses to microzooplankton grazing were determined from results of *in situ* incubated dilution experiments (Landry *et al.*, 2015b; Selph *et al.*, 2015). Briefly, during each 4-day experimental cycle, two-treatment dilution experiments were conducted daily at eight depths spanning the euphotic zone, with *in situ* bottle incubations attached to the surface drifter. Experiments were set up with water from the same depths and CTD casts as the samples for community analysis. We used the instantaneous rates of growth and grazing mortality from these experiments along with the corresponding estimates of total autotroph carbon from flow cytometry and microscopy (Taylor *et al.*, 2015) to compute carbon-based grazing rate impacts on the phytoplankton community from the equations in Landry *et al.* (Landry *et al.*, 2000).

RESULTS

Environmental conditions of the sampling sites

Table I gives the dates, locations, euphotic zone depth and mean mixed-layer characteristics for the five experimental cycles conducted on the cruise, and the relative positions of the cycles and daily sampling points are shown in Fig. 1. Physical circulation and hydrographic features of the sampling sites are fully described by Landry *et al.* (Landry *et al.*, 2015a), and detailed presentations of profiled properties are presented elsewhere (Selph *et al.*, 2015; Taylor *et al.*, 2015). Cycle 1, conducted in southward flowing waters close to the Costa Rica coast, is not included in the present analysis. Cycle 2 sampled in the central dome area ~9°N, 91°W, which was located by a transect survey. At the end of Cycle 2, we deployed a satellite-tracked surface drifter with a mixed-layer drogue, and relocated later as the starting point for Cycle 4. In the meanwhile, Cycle 3 was done in waters northwest of the dome. Cycle 5 was conducted east of the dome region in North Equatorial Counter Current (NECC) waters flowing rapidly toward the coast. Several connections can be made among the experiments based on study design and subsequent hydrographic analysis. Cycles 2 and 4 were clearly in the central dome region, and Cycle 3 also fits the criterion for being in the dome region, with the 20°C isotherm at ≤35 m (Fiedler, 2002). Cycle 5 was located out of the dome region, but had T-S properties closely resembling Cycle 4 (Landry *et al.*, 2015a).

Hydrocast profiles for all cycles showed strong stratification of temperature, oxygen and nutrients. The central dome region (Cycles 2 and 4) had the shallowest mixed layers (19 and 21 m, respectively), the lowest mean mixed-layer temperature (25.5–26°C) and the highest concentration of mixed-layer nitrate (5–7 μM, Table I). At all sampling locations, however, temperature decreased sharply by 10°C or more in the upper 50 m, which comprised all or most of the euphotic zone at all locations. Oxygen concentrations declined by almost an order of magnitude and nitrate increased by 25 μM over the same depth range.

Table I: Sampling dates, initial locations, euphotic zone depth (1% surface irradiance) and mean mixed-layer characteristics for experimental Cycles 1–5

					Mixed layer characteristics		
Experiment	Dates	Lat (°N)	Lon (°W)	1% lo (m)	MLD (m)	*T* (°C)	NO_3 (μM)
Cycle 1	23–27 June	9.72	87.00	45.9	23.8	28.4	0.09
Cycle 2	4–8 July	9.04	90.56	44.6	18.7	25.5	6.9
Cycle 3	9–13 July	10.42	92.92	52.1	21.1	27.3	3.1
Cycle 4	15–19 July	8.55	90.40	49.7	20.5	26.0	5.2
Cycle 5	20–24 July	8.88	88.46	56.7	30.9	27.3	2.7

Dates are local time, with daily early morning CTD casts at ~0200. Mixed layer depth (MLD) = depth at which density exceeds 0.05 kg m^{-3} of surface value).

JOURNAL OF PLANKTON RESEARCH | VOLUME 0 | NUMBER 0 | PAGES 1–14 | 2015

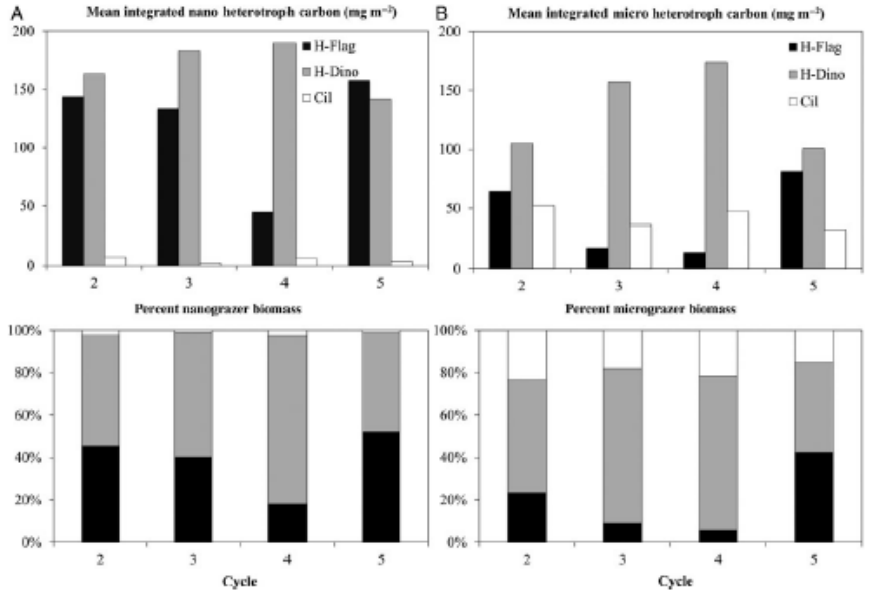

Fig. 3. Mean total integrated grazer biomass (mg C m^{-2}) and percentage of total biomass, including heterotrophic flagellates (H-Flag), heterotrophic dinoflagellates (H-Dino) and ciliates (Cil). Grazers were separated into (**A**) nano (2–20 μm) and (**B**) micro (20–200 μm) size classes, integrated with depth for each day of the experimental cycle and averaged over the 5 sampling days for each cycle.

Heterotrophic dinoflagellates and flagellates

H-Dino and other unidentified flagellates (H-Flag) constituted the majority of micro-grazer biomass in the CRD, averaging 59 and 31%, respectively, across all cycles. Mean H-Dino + H-Flag biomass was greatest at or above the chlorophyll maximum for all cycles (1.5–7.9 μg C L^{-1}) although Cycle 5 exhibited the most pronounced peak at the 40-m chlorophyll maximum (7.5 and 5.3 μg C L^{-1}, respectively). H-Dino biomass generally exceeded H-Flag biomass during Cycles 2–4. However, H-Flag biomass was approximately the same as H-Dino and at times dominated biomass below 30 m in Cycle 2 and throughout the water column in Cycle 5 (Fig. 2).

Across all cycles, integrated H-Flag biomass was comprised of 39% nano-sized cells and 20% micro-sized cells. Cycle 5 had the highest mean integrated biomass of H-Flag (158 and 81 mg C m^{-2} for nano- and micro-sized H-Flag, respectively; Fig. 3). Cycle 4 had the lowest H-Flag biomass (44 and 14 mg C m^{-2} for nano- and micro-sized H-Flag, respectively). H-Dino integrated biomass was evenly distributed between nano- (59%) and micro-grazer (60%) size classes across all cycles. Mean integrated biomass of H-Dino was greatest for Cycle 4 (190 and 174 mg C m^{-2} for nano and micro H-Dino, respectively). Cycle 5 had the lowest H-Dino integrated biomass (142 and 101 mg C m^{-2} for nano and micro H-Dino), illustrating that biomass of H-Dino did not vary as dramatically as H-Flag biomass across cycles. Mean abundances and biomasses of H-Flag, H-Dino, Cil and H-Bact at each sampling depth are given in Supplementary Data, Table SI.

Although the above estimates of H-Dino biomass were obtained from analyses by epifluorescence microscopy, dinoflagellates were also noted in the acid Lugol's preserved samples. The trophic status of these dinoflagellates could not be determined by transmitted light microscopy, so these observations are qualitative rather than quantitative. In these samples, dinoflagellates were dominated by athecate, gymnodinoid forms, such as *Gyrodinium*, which are typically heterotrophic. Other notable dinoflagellate taxa included *Oxytoxum* and *Protoperidinium*, both with known heterotrophic species (Olseng *et al.*, 2002; Mertens *et al.*, 2013; Barton *et al.*, 2013). The composition agrees well with the only other reported data for the region (Olson and Daly, 2013), which found that 26–43% of

total dinoflagellates were heterotrophic gymnodinoids and identified protoperidinoids in a few sampling locations.

Ciliate biomass and taxonomic distribution

Ciliate biomass was highest in Cycles 2 and 4, which were situated closest to the dome center (Landry *et al.*, 2015a). With the exception of Cycle 5, which had the lowest overall ciliate biomass and the least discernable water-column variation, ciliate biomass was highest at or above the chlorophyll maxima (range 0.18−0.48 mg Chl *a* m^{-3}, mean 0.34 mg Chl *a* m^{-3}), which fell between 20 and 40 m in all cycles (Fig. 2).

Mean integrated ciliate biomass was 50.7 mg C m^{-2}, varying considerably from 85 mg C m^{-2} in Cycle 2 to 28.6 mg C m^{-2} in Cycle 5. Despite the cycle differences in total ciliate biomass, taxonomic composition varied little and was dominated by aloricate oligotrichs (mean 75%, range 72−77% of ciliate biomass across cycles). Tintinnids constituted 10−18% of total ciliate biomass (mean = 13%), and Cil categorized as other or unidentifiable averaged 11% of total biomass. The latter category contained a very small number of scuticociliates and cyclotrichs, but the majority were likely aloricate oligotrichs that had been damaged in processing and could not be classified.

A separate analysis of tintinnid species and abundance collected from larger 10−40 L samples yielded further information on ciliate diversity in the CRD. Of the 40 species identified, the three most numerous species were *Asampbelliella armilla*, *Acanthostomella obtusa* and *Dadayiella ganymedes*, which exceeded total abundances of 20 cell L^{-1} and constituted 54% of tintinnids in all samples. For further details on the tintinnid species, see Supplementary Data, Fig. S1. The pattern of tintinnid biomass from this separate sampling method agrees with the acid Lugol's analyses of total ciliate biomass, which found the greatest percentage of integrated tintinnid biomass in Cycles 5 (18%) and 2 (14%), and the lowest in Cycles 3 and 4 (both 10%). Additionally, the mean oral diameters of the cell loricae (Dolan, 2012) suggest that 60−90% of CRD tintinnids should feed most efficiently on nano-sized prey with preferred spherical diameters between 7 and 10 µm, supporting our expectation of a potential predator−prey relationship between Cil and nano-sized prey.

Some groups of Cil displayed specific patterns among cycles. Known ciliate mixotrophs in the genus *Tontonia* were most abundant in Cycle 5. Although this cycle had the lowest total ciliate biomass, it had the highest presence of *Tontonia* on multiple sample days and depths, comprising 96% of total ciliate biomass in one surface sample. *Tontonia* were noted multiple times, but to a lesser extent, in Cycles 3 and 4, and were not present in Cycle 2 samples, closest to the dome center. Scuticociliates, known to be bacterivores, were mainly present in Cycle 2 in small numbers typically comprising less than 10% of total ciliate biomass. Cyclotrichs, such as the mixotrophic *Mesodinium*, were also very rare but present during Cycle 2.

Most Cil (90%) fell into the micro-grazer size category, with only a small number of nano-Cil (Fig. 3). Across all cycles, integrated nano-ciliate biomass averaged only 2% of total nano-grazer biomass, whereas micro-sized Cil averaged 20% of micro-grazer biomass (Fig. 3). It should be noted that Cil smaller than 8−10 µm would have been missed entirely due to the 8-µm pore size of the membrane filter used in this analysis, so numbers of nano-ciliates should be considered underestimates. However, the only previously reported data on Cil in the Eastern Tropical Pacific (Olson and Daly, 2013) indicate that Cil less than 20-µm account for less than 15% of total grazer biomass, and even less (<10%) at stations within the CRD. Thus, the <10-µm Cil missed by our methods likely comprise a very small percentage of the total biomass.

Heterotrophic bacteria

Mean integrated H-Bact biomass was highest in Cycle 2 (487 mg C m^{-2}) and lowest in Cycle 4 (180 mg C m^{-2}; Fig. 4B). Significant linear relationships (Model II linear regression, reduced major axis) were found between H-Bact biomass and total autotrophic carbon biomass (Fig. 4A, $Y = 0.16X - 0.37$, $r^2 = 0.54$, $P < 0.0001$), primary production ($Y = 0.21X + 0.17$, $r^2 = 0.27$, $P < 0.0001$) and Chl *a* ($Y = 28.2X - 1.9$, $r^2 = 0.16$, $P < 0.0001$). However, the goodness of fit between H-Bact biomass and Chl *a* or primary production were substantially lower than between H-Bact and autotroph carbon biomasses.

Size class comparisons and carbon biomass relationships

As seen in Fig. 3, mean integrated biomass of nano-grazers exceeded micro-grazers in all cycles, with highest values in Cycles 3 (319 mg C m^{-2}) and 2 (314 mg C m^{-2}). Micro-grazer biomass was highest in Cycle 4 (235 mg C m^{-2}), which had nearly equal distributions between nano- (240 mg C m^{-2}) and micro-size classes. Total depth-integrated biomass of H-protists (H-Dino, H-Flag and Cil) varied little across cycles, ranging from 536 mg C m^{-2} in Cycle 2 to 488 mg C m^{-2} in Cycle 4 (Fig. 4B). Ratios of total autotrophic carbon (Taylor *et al.*, 2015) to total H-protist carbon varied from 5.1 in Cycle 2−2.7 in Cycle 5.

Depth-integrated H-protist carbon correlates positively with carbon of micro-sized autotrophs (Pearson's correlation, $r = 0.68$, $P < 0.01$), but not with nano- or picoautotrophs. Integrated microheterotroph biomass also positively correlates with microautotroph carbon ($r = 0.58$, $P < 0.05$).

JOURNAL OF PLANKTON RESEARCH | VOLUME 0 | NUMBER 0 | PAGES 1–14 | 2015

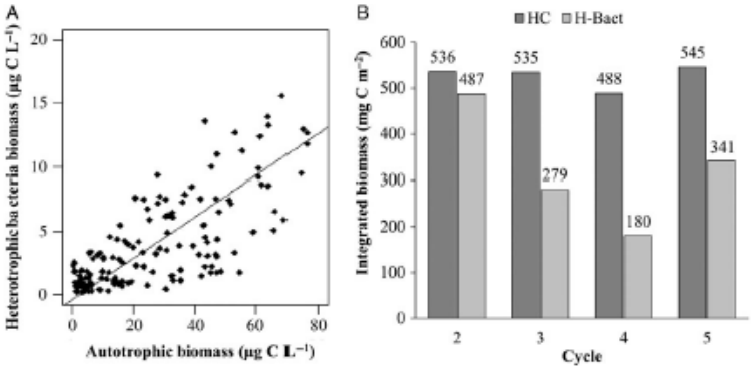

Fig. 4. (**A**) Total biomass (µg C L^{-1}) of all autotrophs determined by epifluorescence microscopy and heterotrophic bacteria (H-Bact) determined by flow cytometry shows a significant linear regressions ($y = 0.16x - 0.37$, $R^2 = 0.54$, $P < 0.0001$). (**B**) Total integrated heterotrophic protist biomass (H-Prot, mg C m^{-2}) including H-Dino, H-Flag and Cil biomass, compared with integrated heterotrophic bacterial biomass (H-Bact, mg C m^{-2}).

Integrated nanoautotroph carbon is positively correlated with H-Flag biomass ($r = 0.68$, $P < 0.01$) and negatively with H-Dino biomass ($r = -0.63$, $P < 0.01$), suggesting grazing by H-Dino on nano-autotrophs.

H-Nanos are significantly correlated with picoplankton ($r = 0.33$, $P < 0.01$), and significant correlations between H-Nanos and both *Synechococcus* ($r = 0.34$, $P < 0.01$) and H-Bact ($r = 0.31$, $P < 0.01$) suggest grazing on these specific pico-sized groups. H-Micros are not significantly correlated with any potential prey size group, suggesting top-down control on this group specifically.

Heterotrophic protist biomass and grazing relationships

The slope of the regression relationship between total H-protist carbon biomass and the carbon consumed by microzooplankton grazing (2.3 µg C µg C L^{-1} day^{-1}; $P < 0.0001$; Fig. 5) provides an estimate of the mean biomass-specific grazing rate of H-protists in the CRD, in this case, 230% body C consumed day^{-1}. This is a conservative estimate of total protistan phagotrophy because it considers only phytoplankton prey and neglects likely feeding on H-Bact and other H-protists (e.g. Cil or H-Dino feeding on nano-heterotrophs) or consumption of detrital particles. Assuming a gross growth efficiency of 30% for H-protists (Straile, 1997; Landry and Calbet, 2004), phytoplankton consumption must therefore support at least a daily mean growth equivalent to 69% of biomass, which translates to an instantaneous growth rate of 0.52 day^{-1}. This computed rate is very similar to the measured integrated instantaneous growth rate of phytoplankton, 0.56 d^{-1}, determined by the dilution experiments conducted on the cruise (Landry *et al.*, 2015b).

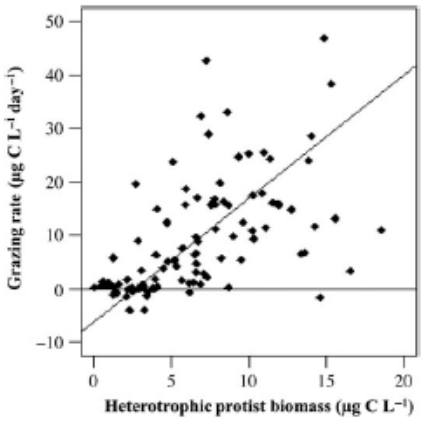

Fig. 5. Linear regression (Model II, reduced major axis) of microzooplankton grazing rates (µg C L^{-1} day^{-1}) determined from dilution experiments as described in Landry *et al.* (Landry *et al.*, 2015b) with heterotrophic protist biomass (µg C L^{-1}) ($y = 2.3x - 6.13$, $R^2 = 0.56$).

DISCUSSION

This study constitutes the first dataset of sufficient sample size and scope to explore the size structure and

composition of the heterotrophic microbial community in the CRD relative to contemporaneous estimates of autotrophic carbon, bacterial carbon and grazing rates. When interpreting results, however, it is important to consider that summer 2010 was not typical of the region. Our cruise was preceded by moderate El Niño physical conditions in winter and spring. Although those conditions had diminished by mid-summer and were even reversing to La Niña-like in the latter half of the year, 2010 still stands out as the only year without a clear mid-summer elevation of surface Chl *a* in a decade of satellite observations from 2004 to 2014 (Landry *et al.*, 2015a). Concentrations of *Synechococcus*, while still high, were almost an order of magnitude lower during our cruise compared with abundances reported previously (Li *et al.*, 1983; Saito *et al.*, 2005). Since normal summertime characteristics of the phytoplankton community in the dome were likely suppressed in 2010, it is reasonable to expect that both the autotroph and heterotroph microbial assemblages would have been sampled at unusually low seasonal levels. Thus, the trophic relationships from this study may be more informative than the absolute magnitudes observed.

CRD protistan grazer composition and comparisons

Nano-sized grazers dominate biomass across the CRD region, specifically small H-Dino. Since picophytoplankton, such as *Synechococcus*, comprised the majority of phytoplankton biomass measured (Landry *et al.*, 2015b; Taylor *et al.*, 2015), it was expected that nano-sized protists would likely dominate as grazers. It is notable, however, that H-Dino are important in CRD waters, where diatoms are scarce (~1% of phytoplankton biomass; Taylor *et al.*, 2015), because H-Dino are often seen in association with diatoms due to their ability to feed on cells as large, or larger, than themselves (Naustvoll, 2000; Sherr and Sherr, 2007). In the CRD, therefore, the importance of H-Dino is indicative of their broader trophic role as consumers, as opposed to diatom specialists.

In comparing our results to previous analyses of H-protists in open-ocean areas of the Eastern Tropical Pacific (Table II), it is clear that flagellate biomass, including H-Dino, usually exceeds that of Cil. The findings of Verity *et al.* (Verity *et al.*, 1996) from US JGOFS studies in the equatorial upwelling region at 140°W stand out as an extreme in this regard, with very low ciliate biomass and dominance of H-Flag over H-Dino. Other studies with data in the same area, however, show a general pattern in which Cil, H-Flag and H-Dino all comprise significant components of the grazer assemblage (Chavez *et al.*, 1996; Taylor *et al.*, 2011). In fact, the overall taxonomic divisions of biomass among H-Dino, H-Flag and Cil in the heterotrophic community studied by Yang *et al.* (Yang *et al.*, 2004) and Olson and Daly (Olson and Daly, 2013) are very similar to that found in this study: H-Dino dominate heterotrophic biomass while H-Flag and Cil make up sizable fractions (10–40%) depending on location and depth.

Our results are most directly comparable with that of Taylor *et al.* (Taylor *et al.*, 2011) based on the same methods used for sample preservation and epifluorescence microscopy, and with that of Olson and Daly (Olson and Daly, 2013) based on the area sampled. In comparison with the former, we found higher absolute and relative contributions of flagellates generally, H-Dino in particular, in the CRD relative to the equatorial upwelling system (Taylor *et al.*, 2011). For Cil, the highest biomass measured in the CRD is similar to the mean euphotic zone values measured in the equatorial upwelling region (3.4 vs. 2.9 μg C L^{-1}, respectively). As noted previously, it is possible, though unlikely, that we missed a large enough biomass of nano-sized Cil by using an 8-μm pore filter in our slide preparation procedure to account for significant system differences, and low Cil concentrations in equatorial upwelling waters have also been reported (Verity *et al.*, 1996). Another explanation for lower mean Cil values in our CRD results is that we analyzed samples taken much deeper in the water column (80–100 m) than the depths of significant primary productivity (93% occurred above 40 m; Landry *et al.*, 2015b). Nonetheless, when results are compared on an areal basis, the differences are clear. The highly stratified and shallow euphotic zone of the CRD had higher integrated biomass of H-protists on average compared with that in the deep euphotic zone of the equatorial upwelling region (525 and 368 mg C m^{-2}, respectively), and the partitioning among H-Flag, H-Dino and Cil groups was substantially different between these studies.

On average, total heterotrophic biomass in the equatorial Pacific study was evenly divided between flagellates, including both H-Flag and H-Dino groups, and Cil (53 and 47%, respectively; Taylor *et al.*, 2011), compared with the clear dominance of flagellates in the CRD (90% H-Dino and H-Flag vs. 11% Cil). Mean mixed-layer Chl *a* concentrations (0.2–0.3 mg m^{-3}) were similar between regions, as were mean estimates of depth-integrated autotrophic biomass (1390 mg C m^{-2} for the CRD and 1385 mg C m^{-2} for the equatorial Pacific; Taylor *et al.*, 2011, 2015). Thus, it appears that seemingly small, but important, differences in phytoplankton community composition can substantially impact the composition of co-occurring H-protists. Picophytoplankton clearly dominated CRD biomass (60 vs. 39% in equatorial Pacific; Taylor *et al.*, 2015), whereas nanoplankton accounted for the most biomass in the equatorial Pacific (Taylor *et al.*, 2011). Closer comparison shows that different taxa were more prominent

JOURNAL OF PLANKTON RESEARCH | VOLUME 0 | NUMBER 0 | PAGES 1–14 | 2015

Table II: Comparison of heterotrophic protist biomass (μg C L^{-1}) reported in multiple studies across the equatorial and eastern Tropical Pacific Ocean

Region and protists	Location	Date	Biomass (μg C L^{-1})	References
Eastern Tropical Pacific	10°N–12°S, 105°W	February–April 1968		Beers and Stewart (1971)
Ciliates			0.13–0.76	
Equatorial Pacific				
Heterotrophic flagellates	10°N–8°S, 110°W	Spring 1992	1.4 ± 0.5	Vors *et al.* (1995)
Choanoflagellates	and 8°S–12°N, 125°W		0.1 ± 0.1	
Heterotrophic dinoflagellates			3.0 ± 1.5	
Ciliates			1.0 ± 0.7	
Equatorial Pacific upwelling				
<20 μm flagellates	0°, 140°W	February–April 1992	6	Verity *et al.* (1996)
Heterotrophic dinoflagellates		August–October 1992	1.3	
Ciliates			0.08	
<20 μm flagellates			5.9	
Heterotrophic dinoflagellates			1.8	
Ciliates			0.16	
Central and Eastern Tropical Pacific				
Heterotrophic flagellates	12°N–10°S, 95°W, 110°W,	Spring 1992	1.7 ± 1.3	Chavez *et al.* (1996)
Heterotrophic dinoflagellates	125°W, 140°W, 170°W	Fall 1992	2.3 ± 2.8	
Aplastic ciliates			1.5 ± 2.0	
Heterotrophic flagellates			1.5 ± 0.7	
Heterotrophic dinoflagellates			3.1 ± 0.5	
Aplastic ciliates			1.3 ± 1.4	
North Equatorial Pacific				
Heterotrophic flagellates	5°N–11°N, 130°30′W	July 1998	0.06–1.1	Yang *et al.* (2004)
Heterotrophic dinoflagellates			0.3–4.0	
Ciliates			0.03–2.9	
Equatorial Pacific upwelling				
Total heterotrophic protists	4°N–4°S,	December 2004,	1.5–8 (3.2)	Taylor *et al.* (2011)
Heterotrophic flagellates	110°W–140°W	September 2005	1.64	
Heterotrophic dinoflagellates			1.54	
Ciliates			1.4–2.9 (2.1)	
Eastern Tropical Pacific and CRD				
Heterotrophic flagellates	9°N–14°N,	October–November 2007	0.5–10.8 (2.1)	Olson and Daly (2013)
Heterotrophic dinoflagellates	90°W–106°W		0.2–14.3 (2.2)	
Ciliates			0.1–18.8 (3.8)	
Costa Rica Dome				
Heterotrophic flagellates	6°N–10°N,	June–July 2010	0.02–9.7 (1.9)	This study
Heterotrophic dinoflagellates	87°W–93°W		0.04–14.1 (4.1)	
Ciliates			0.02–3.4 (0.7)	

Numbers in parentheses are mean values. Ciliate biomass for Beers and Stewart (Beers and Stewart, 1971) was converted from the reported average volume (mm^3 m^{-3}) using the Putt and Stoecker (Putt and Stoecker, 1989) carbon conversion discussed in the Method section. Table was revised and updated from Yang *et al.* (Yang *et al.*, 2004).

in the picophytoplankton communities of the two areas (*Synechococcus* and picoeukaryotes in the CRD and *Prochlorococcus* in the equatorial Pacific). In addition, diatom biomass was an order-of-magnitude greater in the equatorial Pacific (2.9–8.4 mg C m^{-2}) than in the CRD (0.2–0.8 mg C m^{-2}; Taylor *et al.*, 2015). Such differences, notably more nano-sized phytoplankton and more diatoms in the equatorial Pacific, likely provided more of the preferred prey resources for Cil in equatorial waters than were available in the CRD during our study. The similarities in mean Chl *a* and total autotrophic biomass of these two upwelling areas therefore mask significant differences in size-related trophic dynamics and plankton community compositions.

Our results differ in several ways from the previous H-protist analyses in the CRD by Olson and Daly (Olson and Daly, 2013). For example, our estimates of total heterotrophic biomass are lower (535 vs. 686 mg C m^{-2}, respectively), but Olson and Daly (Olson and Daly, 2013) also reported much higher Chl *a* values (mean = 0.8, max = 1.8 μg Chl *a* L^{-1}) than measured during our sampling (mean = 0.2 μg Chl *a* L^{-1}; Taylor *et al.*, 2015). Thus, H-protist biomass during our cruise was lower in absolute terms but disproportionately higher relative to Chl *a* as an indicator of autotroph biomass. Olson and Daly (Olson and Daly, 2013) also reported a higher percentage of Cil than we found (30 vs. 11%, respectively). Although H-Dino accounted for the highest percentages of heterotrophic biomass in both studies (41 and 60%, respectively), H-Flag were less important and Cil much more important in the previous analysis (Olson and Daly, 2013). These compositional differences might also be reasonably attributed to

higher autotrophic biomass on the previous cruise, assuming that higher food concentration and proportionately more large prey would provide a better growth environment for Cil than conditions during our cruise. However, there was no size or compositional analysis of the autotrophic community from the Olson and Daly cruise to evaluate this possibility. Additionally, since Cil are often preferred prey of larger zooplankton, differences in grazing impact of mesozooplankton (top-down control) could be an alternate explanation for the differences in ciliate biomass and heterotroph community composition between the two studies.

Biomass and grazing relationships

H-Bact consumes dissolved organic material produced by autotrophic organisms; thus, it is expected that their biomass should strongly correlate with total autotrophic biomass, Chl *a* and primary production, as noted elsewhere (Azam *et al.*, 1983; Taylor *et al.*, 2011). The significant linear relationship between H-Bact and total autotrophic biomass (Fig. 4A) underlies clear trends among the cycles, where H-Bact biomass tracks variations in autotrophic biomass. In contrast, H-protist biomass did not display clear patterns across cycles. Biomass of nano-grazers and total picoplankton were positively correlated, suggesting a potential predator–prey relationship between these size classes and supporting our hypothesis, but no significant relationship was found between nano-sized protists and microheterotrophs (H-Micros). These relationships suggest that bottom-up forcing has a strong influence on bacteria and picoplankton and their H-Nano consumers, whereas other factors, potentially top-down predation by mesozooplankton, may more strongly influence the micro-heterotroph assemblage.

The relatively constant depth-integrated biomass of H-protists among all sampling locations (488–545 mg C m^{-2}; Fig. 4B) despite clear changes in the integrated autotrophic biomass (1089–1858 mg C m^{-2}; Taylor *et al.*, 2015), integrated H-Bact biomass (180–487 mg C m^{-2}; Fig. 4B), total Chl *a* (16–31 mg Chl *a* m^{-2}; Taylor *et al.*, 2015) and primary production rates (40–70 mg C m^{-3}; Selph *et al.*, 2015) supports the potential of top-down pressure from mesozooplankton. Temporal or spatial imbalances between growth and grazing of predator and prey could also create such a condition; however, microzooplankton grazing rates closely tracked phytoplankton growth rates in individual dilution experiments and balanced picophytoplankton production for the region as a whole (Gutiérrez-Rodríguez *et al.*, 2015; Landry *et al.*, 2015b). Figure 5 also suggests a reasonable relationship between variations in H-protistan biomass and grazing impact on phytoplankton, although there is clearly much unexplained variability that may reflect compositional variability in consumers and prey. Nonetheless, at least from an experimental perspective, the strong coupling observed between protistan biomass and grazing, and between grazing and phytoplankton growth, would seem to argue that predatory influences of higher trophic levels have a key role in explaining the relative constancy of H-protistan biomass among cycles (Fig. 4B).

This idea is further supported by a separate analysis, which found very uniform mesozooplankton biomass among cycles (4.86–5.37 g m^{-2}) despite substantial differences in size structure, composition, biomass-specific grazing rates and diel vertical migratory behavior (Décima *et al.*, 2015). For instance, copepods were abundant in all cycles, while euphausiids notably dominated during Cycle 2 (Décima *et al.*, 2015), near the dome center, where Cil biomass was highest and diatom production insufficient to support mesozooplankton (Taylor *et al.*, 2015). In fact, Cycle 2 had high productivity, but the highest dominance of picophytoplankton and the lowest direct feeding of mesozooplankton on phytoplankton of all cycles. This suggests particularly high mesozooplankton grazing impact on microzooplankton during this cycle, which could explain its similarity in H-protist biomass to other cycles despite conditions of high productivity and picophytoplankton abundance, which would favor elevated H-protist biomass. The observed prevalence of salps and appendicularians during Cycle 5 (Décima *et al.*, 2015), another area of high productivity, suggests that indirect competition for picophytoplankton prey could also influence standing stocks of H-protists, in addition to direct predatory pressure by mesozooplankton. In this case, the different composition of mesozooplankton in Cycle 5 might be related to the distinctly lower ciliate biomass in that area (Fig. 2), while not having much of an impact on total H-protist biomass. Since top-down pressure from mesozooplankton could reasonably have an important regulatory role in the CRD, the micro-mesozooplankton link would be an interesting and important area of focused future study.

Across all cycles, the instantaneous growth rate of H-protistan grazers computed from measured grazing impact on phytoplankton (0.56 day^{-1}) in dilution experiments is similar to the measured growth rate of phytoplankton (0.52 day^{-1}). Because autotrophs and H-protists are both the potential prey for mesozooplankton, the calculated ability of protistan consumers of phytoplankton to sustain growth rates similar to that of phytoplankton is central to maintaining a balance between production and grazing (Landry *et al.*, 2011). Thus, this agreement supports the idea that the CRD is a trophically balanced ecosystem (Landry *et al.*, 2015b). These growth rates are also consistent with microzooplankton providing a significant carbon flow

to mesozooplankton in the CRD (Décima *et al.*, 2015), where picophytoplankton dominate phytoplankton biomass and two thirds of primary production is consumed by protists (Landry *et al.*, 2015b).

Potential mixotrophic complications

Another factor that could influence trophic relationships in the CRD is mixotrophy, a strategy that is reasonably expected among flagellates competing against dominant picophytoplankton for limiting nutrients or trace elements (Unrein *et al.*, 2014). Although we did not specifically address mixed trophic functionality in this study, mixotrophs are common within prymnesiophyte, ciliate (Esteban *et al.*, 2010) and flagellate groups (Green, 1991; Stoecker, 1999), and a recent model suggests that mixotrophy should be the dominant strategy for nanoflagellates in steady-state oligotrophic systems (Mitra *et al.*, 2014). While the predictions of this model agree well with our data with respect to the very low biomass contribution of diatoms in the CRD (non-motile microautotrophs, Supplementary Data, Fig. S2), they differ in substantially underestimating the prevalence of H-Flag, at least according to our ability to distinguish plastidic from non-plastidic cells by epifluorescence microscopy. As also illustrated in Fig. 5, the measured grazing impact of protistan consumers is well correlated with biomass of non-plastidic cells (H-protists), leading to reasonable estimates of biomass-specific ingestion and growth rates. Thus, mixotrophy does not need be invoked to explain the biomass and rate relationships found in our study, though it may nonetheless be present and important.

As a comparative exercise, we roughly estimated the potential grazing-equivalent biomass of mixotrophs in the CRD based on experimental results from the Equatorial Pacific, which found that biomass-specific rates of phagotrophy among pigmented flagellates (including autotrophic flagellates, dinoflagellates and prymnesiophytes) were half the rates, on average, compared with similarly sized non-pigmented cells (Stukel *et al.*, 2011). If this additional biomass is added to that of H-protists and regressed against grazing impacts as in Fig. 5, the relationship is still significant ($P < 0.0001$), but the slope is lower (1.54 μgC μgC^{-1} day^{-1}), translating to a lower mean consumer growth rate of 0.38 day^{-1} (Fig. 5). This is almost the same as the growth rate computed from the similar analysis of biomass-specific grazing including mixotrophs that was done for the equatorial Pacific upwelling region (Landry *et al.*, 2011). Both analyses are conservative, however, in neglecting additional carbon flows from H-Bact, detritus and intra-guild predation by protistan grazers, and, in the case of mixotrophs, the nutritional supplement from phototrophy. Thus, while mixotrophy was unmeasured and is unnecessary to explain the results of our study (i.e. taking a traditional perspective of distinct autotrophic and heterotrophic functions among protists reveals no obvious discrepancies in biomass and rate relationships), our results would also be consistent with a significant role of mixotrophic protists in the CRD. Like the top-down predatory impact of mesozooplankton, focused studies on mixotrophy may help us to explain signature features of the CRD such as the relatively modest regional variability in H-protist biomass, composition and productivity as well as the general maintenance of balanced production and grazing processes. Such studies are also needed to understand the resource acquisition strategies and trade-offs of nano-sized protists in the picophytoplankton-dominated, trace-element limited waters of the CRD.

SUPPLEMENTARY DATA

Supplementary data can be found online at http://plankt.oxfordjournals.org.

DATA ARCHIVING

Core data from this manuscript (H-protist abundance and biomass) are available through the Biological and Chemical Oceanography Data Management Office (http://www.bco-dmo.org/).

ACKNOWLEDGEMENTS

We thank the captain and crew of the R/V Melville and all cruise participants, particularly Darcy Taniguchi and Alexis Pasulka for collecting acid Lugol's samples and Takafumi Kataoka for collecting tintinnid samples.

FUNDING

The study was supported by US National Science Foundation grant OCE-0826626 to M.R.L.

REFERENCES

Agatha, S. (2004) A cladistic approach for the classification of oligotrichid ciliates (Ciliophora: Spirotricha). *Acta Protozool.*, **43**, 201–217.

Ahlgren, N. A., Noble, A., Patton, A. P., Roache-Johnson, K., Jackson, L., Robinson, D., McKay, C., Moore, L. R. *et al.* (2014) The unique trace metal and mixed layer conditions of the Costa Rica upwelling dome support a distinct and dense community of Synechococcus. *Limnol. Oceanogr.*, **59**, 2166–2184.

Azam, F., Fenchel, T., Field, J. G., Gray, J. G., Meyer-Reil, L. A. and Thingstad, F. (1983) The ecological role of water-column microbes in the sea. *Mar. Ecol. Prog. Ser.*, **10**, 257–263.

Barton, A. D., Finkel, Z. V., Ward, B. A., Johns, D. G. and Follows, M. J. (2013) On the roles of cell size and trophic strategy in North Atlantic diatom and dinoflagellate communities. *Limnol. Oceanogr.*, **58**, 254–266.

Beers, J. R. and Stewart, G. L. (1971) Micro-zooplankters in the plankton communities of the upper waters of the eastern tropical Pacific. *Deep Sea Res. I*, **18**, 861–883.

Binder, B. J., Chisholm, S. W., Olson, R. J., Frankel, S. L. and Worden, A. Z. (1996) Dynamics of picoplankton, ultraphytoplankton and bacteria in the central equatorial Pacific. *Deep Sea Res. II*, **43**, 907–931.

Calbet, A. (2008) The trophic roles of microzooplankton in marine systems. *ICES J. Mar. Sci.*, **65**, 325–331.

Calbet, A. and Landry, M. R. (2004) Phytoplankton growth, microzooplankton grazing, and carbon cycling in marine systems. *Limnol. Oceanogr.*, **49**, 51–57.

Calbet, A. and Saiz, E. (2005) The ciliate-copepod link in marine ecosystems. *Aquat. Microb. Ecol.*, **38**, 157–167.

Chavez, F. P., Buck, K. R., Service, S. K., Newton, J. and Barber, R. T. (1996) Phytoplankton variability in the central and eastern tropical Pacific. *Deep Sea Res. II*, **43**, 835–870.

Décima, M., Landry, M. R., Stukel, M. R., Lopez-Lopez, L. and Krause, J. W. (2015) Mesozooplankton biomass and grazing in the Costa Rica Dome: amplifying variability through the plankton food web. *J. Plankton Res.* (this issue).

Dolan, J. (2012) Morphology and ecology in tintinnid ciliates of the marine plankton: correlates of lorica dimensions. *Acta Protozool.*, **49**, 235–244.

Esteban, G. F., Fenchel, T. and Finlay, B. J. (2010) Mixotrophy in ciliates. *Protist*, **161**, 621–641.

Fiedler, P. C. (2002) The annual cycle and biological effects of the Costa Rica Dome. *Deep Sea Res. I*, **49**, 321–338.

Franck, V. M., Smith, G. J., Bruland, K. W. and Brzezinski, M. A. (2005) Comparison of size-dependent carbon, nitrate, and silicic acid uptake rates in high- and low-iron waters. *Limnol. Oceanogr.*, **50**, 825–838.

Freibott, A., Linacre, L. and Landry, M. R. (2014) A slide preparation technique for light microscopy analysis of ciliates preserved in acid Lugol's fixative. *Limnol. Oceanogr. Meth.*, **12**, 54–62.

Garrison, D. L., Gowing, M. M., Hughes, M. P., Campbell, L., Caron, D. A., Dennett, M. R., Shalapyonok, A., Olson, R. J. *et al.* (2000) Microbial food web structure in the Arabian Sea: a US JGOFS study. *Deep Sea Res. II*, **47**, 1387–1422.

Green, J. C. (1991) Phagotrophy in prymnesiophyte flagellates. In Patterson, D. J. and Larsen, J. (eds.), *The Biology of Free-living Heterotrophic Flagellates*. Vol. 45. Claredon Press, Oxford, pp. 401–414.

Gutiérrez-Rodríguez, A., Selph, K. E. and Landry, M. R. (2015) Phytoplankton growth and microzooplankton grazing dynamics across vertical environmental gradients determined by transplant *in situ* dilution experiments. *J. Plankton Res.* (this issue).

Hwang, S. and Heath, R. T. (1997) The distribution of protozoa across a trophic gradient, factors controlling their abundance and importance in the plankton food web. *J. Plankton Res.*, **19**, 491–518.

Kofoid, C. A. and Campbell, A. S. (1929) A conspectus of the marine and freshwater Ciliata belonging to the suborder Tintinnoinea, with descriptions of new species, principally from the Agassiz Expedition to the eastern tropical Pacific, 1904–1905. *Univ. Calif. Publ. Zool.*, **4**, 1–403.

Kofoid, C. A. and Campbell, A. S. (1939) Reports on the scientific results of the expedition to the Eastern Tropical Pacific, in charge of Alexander Agassiz, by the US Fish Commission steamer *Albatross*, from Oct. 1904 to Mar. 1905, Lieut.-Cdr. L.M Garrett, USN, commanding. *Bull. Mus. Comp. Zool.*, **84**, 1–473.

Landry, M. R. and Calbet, A. (2004) Microzooplankton production in the oceans. *ICES J. Mar. Sci.*, **61**, 501–507.

Landry, M. R., Constantinou, J., Latasa, M., Brown, S. L., Bidigare, R. R. and Ondrusek, M. E. (2000) Biological response to iron fertilization in the eastern equatorial Pacific (IronEx II). III. Dynamics of phytoplankton growth and microzooplankton grazing. *Mar. Ecol. Prog. Ser.*, **57**, 57–72.

Landry, M. R., De Verneil, A., Goes, J. I. and Moffett, J. W. (2015a) Plankton dynamics and biogeochemical fluxes in the Costa Rica Dome: introduction to the CRD flux and zinc experiments. *J. Plankton Res.* (this issue).

Landry, M. R., Ohman, M. D., Goericke, R., Stukel, M. R. and Tsyrklevich, K. (2009) Lagrangian studies of phytoplankton growth and grazing relationships in a coastal upwelling ecosystem off Southern California. *Prog. Oceanogr.*, **83**, 208–216.

Landry, M. R., Selph, K. E., Décima, M., Gutiérrez-Rodríguez, A., Stukel, M. R., Taylor, A. G. and Pasulka, A. L. (2015b) Phytoplankton production and grazing balances in the Costa Rica Dome. *J. Plankton Res.* (this issue).

Landry, M. R., Selph, K. E., Taylor, A. G., Décima, M., Balch, W. M. and Bidigare, R. R. (2011) Phytoplankton growth, grazing, and production balances in the HNLC equatorial Pacific. *Deep Sea Res. II*, **58**, 524–535.

Lessard, E. J. and Murrell, M. C. (1996) Distribution, abundance and size composition of heterotrophic dinoflagellates and ciliates in the Sargasso Sea near Bermuda. *Deep Sea Res. I*, **43**, 1045–1065.

Li, W. K. W., Rao, S., Harrison, W. G., Smith, J. C., Cullen, J. J., Irwin, B. and Platt, T. (1983) Autotrophic picoplankton in the tropical ocean. *Science*, **219**, 292–295.

Linacre, L., Landry, M. R., Cajal-Medrano, R., Lara-Lara, J. R., Hernández-Ayón, J. M., Mouriño-Pérez, R. R., García-Mendoza, E. and Bazán-Guzmán, C. (2012) Temporal dynamics of carbon flow through the microbial plankton community in a coastal upwelling system off northern Baja California, Mexico. *Mar. Ecol. Prog. Ser.*, **461**, 31–46.

Linacre, L., Landry, M. R., Lara-Lara, J. R., Hernández-Ayón, J. M. and Bazán-Guzmán, C. (2010) Picoplankton dynamics during contrasting seasonal oceanographic conditions at a coastal upwelling station of Northern Baja California, Mexico. *J. Plankton Res.*, **32**, 539–557.

Marshall, S. M. (1969) Protozoa: Order tintinnida, zooplankton sheets 117–127. In Fraser, J. H. and Hensen, V. Kr. (eds.), *Fiches d'identification du zooplancton*. Cons. Perm. Int. Explor. Mer, Charlottenlund.

Menden-Deuer, S. and Lessard, E. J. (2000) Carbon to volume relationships for dinoflagellates, diatoms, and other protist plankton. *Limnol. Oceanogr.*, **45**, 569–579.

Mertens, K. N., Yamaguchi, A., Yoshihito, T., Pospelova, V., Head, M. J., Radi, T., Pienkowski, A. J., de Vernal, A. *et al.* (2013) A new heterotrophic dinoflagellate from the north-eastern Pacific, Protoperidinium fukuyoi: cyst-theca relationship, phylogeny, distribution and ecology. *J. Eukaryot. Microbiol.*, **60**, 545–563.

Mitra, A., Flynn, J., Burkholder, J. M., Berge, T., Calbet, A., Raven, J. A., Granéli, E., Glibert, P. M. *et al.* (2014) The role of mixotrophic protists in the biological carbon pump. *Biogeosci.*, **11**, 995–1005.

Monger, B. C. and Landry, M. R. (1993) Flow cytometric analysis of marine bacteria with Hoechst 33342. *Appl. Environ. Microbiol.*, **59**, 905–911.

Naustvoll, L. J. (2000) Prey size spectra and food preferences in thecate heterotrophic dinoflagellates. *Phycologia*, **39**, 187–198.

Olseng, C. D., Naustvoll, L.J. and Eystein, P. (2002) Grazing by the heterotrophic dinoflagellate Protoperidinium steinii on a Ceratium bloom. *Mar. Ecol. Prog. Ser.*, **225**, 161–167.

Olson, M. B. and Daly, K. L. (2013) Micro-grazer biomass, composition and distribution across prey resource and dissolved oxygen gradients in the far eastern tropical north Pacific Ocean. *Deep-Sea Res. I*, **75**, 28–38.

Pasulka, A. L., Landry, M. R., Taniguchi, D. A. A., Taylor, A. G. and Church, M. J. (2013) Temporal dynamics of phytoplankton and heterotrophic protists at station ALOHA. *Deep-Sea Res. II*, **93**, 44–57.

Putt, M. and Stoecker, D. K. (1989) An experimentally determined carbon: volume ratio for marine "oligotrichous" ciliates from estuarine and coastal waters. *Limnol. Oceanogr.*, **34**, 1097–1103.

Saito, M. A., Rocap, G. and Moffett, J. W. (2005) Production of cobalt binding ligands in a *Synechococcus* feature at the Costa Rica upwelling dome. *Limnol. Oceanogr.*, **50**, 279–290.

Schmoker, C. and Hernández-León, S. (2013) Stratification effects on the plankton of the subtropical Canary Current. *Prog. Oceanogr.*, **119**, 24–31.

Selph, K. E., Landry, M. R., Taylor, A. G., Gutiérrez-Rodríguez, A., Stukel, M. R., Wokuluk, J. and Pasulka, A. L. (2015) Phytoplankton production and taxon-specific growth rates in the Costa Rica Dome. *J. Plankton Res.* (this issue).

Sherr, E. B. and Sherr, B. F. (1993) Preservation and storage of samples for enumeration of heterotrophic protists. In Kemp, P. K. (ed.), *Handbook of Methods in Aquatic Microbial Ecology*. CRC Press, Boca Raton, Florida, pp. 207–212.

Sherr, E. B. and Sherr, B. F. (2002) Significance of predation by protists in aquatic microbial food webs. *Antonie van Leeuwenhoek*, **81**, 293–308.

Sherr, E. B. and Sherr, B. F. (2007) Heterotrophic dinoflagellates: a significant component of microzooplankton biomass and major grazers of diatoms in the sea. *Mar. Ecol. Prog. Ser.*, **352**, 187–197.

Sommer, U., Stibor, H., Katechakis, A., Sommer, F. and Hansen, T. (2002) Pelagic food web configurations at different levels of nutrient richness and their implications for the ratio fish production:primary production. *Hydrobiologia*, **484**, 11–20.

Stoecker, D. K. (1999) Mixotrophy among dinoflagellates. *J. Eukaryot. Microbiol.*, **46**, 396–401.

Stoecker, D. K. and Capuzzo, J. M. (1990) Predation on protozoa: its importance to zooplankton. *J. Plankton Res.*, **12**, 891–908.

Straile, D. (1997) Gross growth efficiencies of protozoan and metazoan zooplankton and their dependence on food concentration, predator-prey weight ratio, and taxonomic group. *Limnol. Oceanogr.*, **42**, 1375–1385.

Stukel, M. R., Landry, M. R. and Selph, K. E. (2011) Nanoplankton mixotrophy in the eastern equatorial Pacific. *Deep Sea Res. II*, **58**, 378–386.

Taylor, A. G., Landry, M. R., Freibott, A., Selph, K. E. and Gutiérrez-Rodríguez, A. (2015) Patterns of microbial community biomass, composition and HPLC diagnostic pigments in the Costa Rica upwelling dome. *J. Plankton Res.* (this issue).

Taylor, A. G., Landry, M. R., Selph, K. E. and Yang, E. J. (2011) Biomass, size structure and depth distributions of the microbial community in the eastern equatorial Pacific. *Deep Sea Res. II*, **58**, 342–357.

Unrein, F., Gasol, J. M., Not, F., Forn, I. and Massana, R. (2014) Mixotrophic haptophytes are key bacterial grazers in oligotrophic coastal waters. *ISME J.*, **8**, 164–176.

Utermöhl, V. H. (1931) Neue Wege in der quantitativen Erfassung des Planktons. *Verh. Int. Verein. Theor. Angew. Limnol.*, **5**, 567–596.

Verity, P. G. and Langdon, C. (1984) Relationships between lorica volume, carbon, nitrogen, and ATP content of tintinnids in Narragansett Bay. *J. Plankton Res.*, **6**, 859–868.

Verity, P. G., Stoecker, D. K., Sieracki, M. E. and Nelson, J. R. (1996) Microzooplankton grazing of primary production at 140 W in the equatorial Pacific. *Deep Sea Res. II*, **43**, 1227–1255.

Vørs, N., Buck, K. R., Chavez, F. P., Eikrem, W., Hansen, L. E., Østergaard, J. B. and Thomsen, H. A. (1995) Nanoplankton of the equatorial Pacific with emphasis on the heterotrophic protists. *Deep Sea Res. II*, **42**, 585–602.

Wyrtki, K. (1964) Upwelling in the Costa Rica dome. *Fish. Bull.*, **63**, 355–372.

Yang, E. J., Choi, J. K. and Hyun, J. -H. (2004) Distribution and structure of heterotrophic protist communities in the northeast equatorial Pacific Ocean. *Mar. Biol.*, **146**, 1–15.

Yang, E. J., Choi, J. K. and Hyun, J-H. (2008) Seasonal variation in the community and size structure of nano- and microzooplankton in Gyeonggi Bay, Yellow Sea. *Estuar. Coast Shelf. S.*, **77**, 320–330.

Zhang, W., Feng, M., Yu, Y., Zhang, C., Sun, J. and Xiao, T. (2011) Species checklist of contemporary tintinnids (Ciliophora, Spirotrichea, Choreotrichia, Tintinnida) in the world. *Biodiv. Sci.*, **19**, 655–660.

Chapter 3, in full, is a reprint of materials as it appears in Freibott, A., Taylor, A. G., Selph, K. E., Lui, D., Zhang, W., and Landry, M. R. (2015) Biomass and composition of protist grazers and heterotrophic bacteria in the Costa Rica Dome during June-July 2010. Journal of Plankton Research, 38(2):230-243, doi: 10.1093/plankt/fbv107. The dissertation author was the primary investigator and author of this manuscript.

CHAPTER 4.

Distinct microbial communities at mesoscale fronts in the southern California Current

Abstract

We investigated microbial communities at two oceanic fronts in the southern California Current during October 2008 and August 2012 as part of the California Current Ecosystem Long-Term Ecological Research (CCE LTER) program. Combining analyses by microscopy and molecular techniques, we assessed and compared the trends in microbial community biomass and taxonomic composition across fronts and adjacent oligotrophic and eutrophic regions. Both fronts exhibited elevated euphotic zone integrated levels of autotrophic (2008: 2830 mg C m^{-2}, 2012: 3820 mg C m^{-2}) and heterotrophic microbial biomass (2008: 290 mg C m^{-2}, 2012: 1659 mg C m^{-2}). Diatoms dominated, comprising approximately 70% of autotrophic biomass at the front stations in both years. *Prochlorococcus* and *Synechococcus* exhibited opposing patterns across the fronts, with *Prochlorococcus* most abundant on the oligotrophic sides and *Synechococcus* most abundant on the eutrophic sides. Dinoflagellates comprised most of the heterotrophic protistan biomass in all samples but decreased slightly at the fronts, and heterotrophic bacteria were dominated by flavobacteria at all locations. Statistical analyses of the 18S rDNA data indicated that the frontal communities were distinct from those at nearby coastal eutrophic stations largely due to the contributions of operational

taxonomic units (OTUs) representing < 1% of the community, or the 'rare biosphere.' The similarities and differences between the two fronts suggest that subtle changes in community composition could have important implications for food web energy efficiency and carbon cycling at fronts.

Introduction

Oceanic fronts are often regions of elevated primary productivity (Venrick et al. 2000, Landry et al. 2012), biomass (Franks 1992a, Taylor et al. 2012) and carbon export (Fielding et al. 2001, Allen et al. 2005, Stukel et al. 2017) due to increased nutrient uptake, increased phytoplankton growth, and physical accumulation mechanisms at the frontal interfaces (Franks 1992a). Although most fronts are temporary mesoscale features (10-100s km), they can have a disproportionate impact on productivity, community composition and food web structure relative to the mean background characteristics for a region (Laubscher et al. 1993, Li et al. 2012). Mechanisms that form fronts can also impact the types of plankton that dominate. For example, fronts formed by wind-driven upwelling are typically associated with subsurface blooms of diatoms and dinoflagellates (Franks 1992b).

Due to their ephemeral nature, mesoscale fronts can be difficult to locate and study at sea. However, dynamic regions, such as the California Current Ecosystem (CCE), that are rich in mesoscale fronts and eddies, can be ideal systems to study such features. Kahru et al. (2012) has shown that the frequency of fronts, as defined by sharp transitions in satellite images of temperature or chlorophyll, has increased significantly in the California Current over the past three decades due to broad increases in cross-shelf

gradients of sea surface temperature and the local enhancement of coastal upwelling winds. Such a trend suggests that the overall primary productivity of the region, as well as the mean characteristics of its communities and food webs, may be strongly influenced by fronts and change with time. If localized in relatively small, temporary frontal features instead of spread evenly in the coastal upwelling zone, for example, increased primary production in the CCE could increase the total energy available to commercially important fisheries (Checkley and Barth 2009). Recent modeling of long-term data from the CCE has further suggested that the biological communities and trophic interactions that occur at fronts may be distinct from those that would otherwise exist in the vicinity (Franks et al. 2013).

In the present study, we assess the composition of microbial communities sampled across two CCE fronts on cruises in October 2008 (A-Front) and August 2012 (E-Front). Combining microscopy and molecular analyses, we address the following questions: Are there specific trends in community composition and biomass that are consistent across frontal features in the CCE? Are the microbial communities at mesoscale fronts distinct from the communities in adjacent eutrophic waters? Previous studies (Franks 1992a, Laubscher et al. 1993, Taylor et al. 2012) have suggested that the general characteristics of communities that develop at fronts, such as the dominance of larger phytoplankton and diatoms in particular, are similar to those in eutrophic, coastal waters of comparable biomass and productivity. Thus, we hypothesized that the microbial community composition at the fronts would be similar to that of eutrophic, coastal regions. The use of molecular techniques in the present analyses allows a more detailed assessment of community composition in CCE fronts than has been previously

done, and thus, a more rigorous basis for evaluating the distinctions between fronts and adjacent waters.

Materials and Methods

CCE LTER P1208 (E-Front) and P0810 (A-Front) general site information

The CCE LTER conducted two cruises to study the biological and physical characteristics of frontal features in September 30 - October 29, 2008, and July 28 - August 26, 2012. A single front was investigated on each cruise, with rate measurement and experiments conducted on either side of both features (2012: Cycles 2-5, 2008: Cycles 5-6), and on the feature in 2012 (Cycle 1, Figure 1). Overnight transects were conducted across both fronts for detailed sections of each measured variable (Fig. 1). The 2012 E-Front was oriented in a north-south direction and formed between a warm, anticyclonic eddy to the east and a cold, cyclonic eddy to the west. Eutrophic waters were located to the east and oligotrophic waters to the west. The 2008 A-Front was an east-west-oriented front near Point Conception formed between coastal upwelling waters and well-mixed California Current and subtropical waters (Landry et al. 2012). Eutrophic waters were located north of this front, while oligotrophic waters were south of the front.

The cross-front transects were initiated in the water mass adjacent to the front. Samples were collected at stations set approximately 2-4 km apart while crossing the frontal feature, and transect sampling ended when it was apparent from hydrographic information that we had reached the water mass on the other side of the front (9 transect stations in 2008, 13 transect stations in 2012). Samples for chlorophyll, nutrients,

microscopy, and flow cytometry analysis were collected from 8 depths at each transect station. Additionally, semi-Lagrangian style experiments were conducted on and around the fronts using a satellite-tracked drifter with a mixed layer drogue to track water masses over a 3-day period (cycle tracks depicted with lines in Fig. 1).

Microscopic analysis of plankton communities

Epifluorescence microscopy. Seawater samples of 500 mL were preserved for epifluorescence microscopy with 260 µl alkaline Lugol's solution, 10 mL buffered formaldehyde, 500 µl sodium thiosulfate, and 1 mL proflavin (0.033% w/v) (Sherr and Sherr, 1993). Preserved samples rested for an hour in the dark before being stained with 1 mL DAPI (0.01 mg mL^{-1}) and filtered. Aliquots of 50 mL were filtered onto 25 mm, 0.8 µm black polycarbonate membranes for the analysis of small cells, and the remaining 450 mL of preserved sample was filtered onto 25 mm, 8.0 µm black polycarbonate membranes. Membrane filters were mounted on glass slides using Type DF immersion oil, No. 2 glass coverslips, and stored at -80 °C until analysis.

Slides were imaged on a Zeiss AxioVert 200 M inverted epifluorescence microscope with a motorized stage and images were captured with a Zeiss AxioCam MRc black and white camera using separate filter sets for Chl a, DAPI, FITC and phycoerythrin. Slides with 0.8 µm membrane filters were imaged at 630X magnification, and 8.0 µm membrane filters were imaged at 200X magnification. Seven z-stack images were taken at each random image location. The z-stack images were processed and combined using ImagePro software, and a fast Fourier transform and Laplace filter were applied to reduce the halo effect around cells. Cells were counted and sized using the ImagePro software before being manually identified and grouped into functional groups:

diatom, autotrophic dinoflagellate (A-Dino), prymnesiophyte (Prym), cryptophyte (Cryp), autotrophic others (A-Other), heterotrophic dinoflagellate (H-Dino), heterotrophic others (H-Other), and ciliates (Cil). When possible, separate acid Lugol's preserved samples were analyzed for ciliates (Choi and Stoecker 1989, Leakey et al. 1994). Such samples were not available for the A-Front ciliates, which were estimated by epifluorescence microscopy only. Autotrophic cells were identified by the presence of chlorophyll *a*, which fluoresces red under blue light excitation. A-Other included cells that could not be positively identified into one of the other autotrophic categories. H-Dino included cells that could be positively identified as dinoflagellates by the presence of a clear dinokaryon, two flagella and an obvious theca for thecate forms, while H-Other included other heterotrophic cells that were mostly flagellated but otherwise unidentifiable. Cells were binned into size categories based on the longest cell axis: 0.2-2, 2-5, 5-10, 10-20, 20-40 and >40 µm. Cell biovolumes (μm^3) were calculated using length (L) and width (W) measurements in the formula for a prolate sphere, $BV = 0.524*L*W^2$. Carbon biomass was calculated from the biovolumes as: $pgC\ cell^{-1} = 0.216*BV^{0.939}$ for non-diatoms and $pgC\ cell^{-1} = 0.288*BV^{0.811}$ for diatoms (Menden-Deuer and Lessard 2000). More detailed information on the epifluorescence methods used are available in Taylor et al. (2012).

Transmitted light microscopy. Seawater samples of 125 mL were preserved with 5% acid Lugol's solution in amber bottles for the analysis of Cil by transmitted light microscopy. Prior to filtration, 37% formaldehyde was added to the sample (2% final concentration) and allowed to rest for 12 h to solidify cell membranes. Samples were filtered onto 25 mm, 8.0 µm polycarbonate membranes under low pressure (>50 mmHg),

and the vacuum pump was shut off during the final few milliliters to allow for gentle gravity filtration. Filters were briefly placed onto paper to wick away residual moisture, mounted on glass slides using Cargille immersion oil A (Certified Refractive Index Liquids, nD 258C 1.584+0.0002), and coverslips were sealed with clear nail polish (Freibott et al. 2014). The slides were imaged under transmitted light at 200X magnification and images were processed as described above for epifluorescence microscopy. Cil were divided into broad taxonomic groups, including aloricate oligotrichs and choreotrichs, tintinnids, scuticociliates, cyclotrichs and other unidentifiable Cil. Cells were binned by size based on the longest cell dimension: 8-20, 20-40 and >40 µm. Due to the pore size of the filter used, many nano-sized Cil likely passed through the membrane and are not accounted for here. Length and width measurements from each cell were used to calculate cell biovolume based on the most appropriate cell shape: prolate spheroid ($BV = 0.524*L*W^2$), cone ($BV = 0.262*L*W^2$) or cone plus half sphere ($BV = 0.262*W^2*(L+W^2)$). Carbon biomass was calculated from cell biovolume as $pgC = 0.19*BV$ (Putt and Stoecker 1989). Biomass for all microscopy data was depth-integrated according to the trapezoidal rule, averaging community biomass between sampling depths and summing biomass contributions for all depth strata (to the deepest depth sampled for each cycle).

Flow cytometry analysis of bacterial communities

Seawater samples of 1 mL were preserved with 0.5% paraformaldehyde (v/v, final concentration), flash frozen in liquid nitrogen and stored at -80 °C. Prior to analysis, samples were thawed and stained with Hoechst 34442 (1 mg mL^{-1}) for 1 h in the dark (Monger and Landry 1993). Aliquots of 100 mL were analyzed using a Beckman

Coulter EPICS Altra flow cytometer with a Harvard Apparatus syringe pump for volumetric sample delivery and two argon lasers tuned to UV (200 mW) and 488 nm (1 W) excitation. Fluorescence signals were collected using filters for Hoechst-bound DNA (blue fluorescence, 450 nm), phycoerythrin (orange fluorescence, 575 nm) and Chl a (red fluorescence 680 nm), and normalized to external standards of 0.5 mm yellow-green and 0.5 mm UV polystyrene beads. Cell fluorescence and light-scatter properties were acquired with Expo32 software and subsequently analyzed with FlowJo software to define heterotrophic bacterial (H-Bact) populations based on DNA signal (all living cells), absence of photosynthetic pigment and light-scatter signals (forward and 90° light scatter, measures of relative size).

Abundance estimates of HB from flow cytometry analysis were converted to carbon biomass using depth-specific carbon per cell conversions, with bead-normalized forward angle light scattering (FALS) as a relative measure. Estimates of cell carbon content were made using an open-ocean, mixed layer estimate of 10 fg C $cell^{-1}$ as a starting point for H-Bact (Garrison et al. 2000). Then, using the scaling factor $FALS^{0.55}$ (Binder et al. 1996), the carbon:cell content was determined for each depth from the specific mean cell carbon values and the FALS ratio $(FALS_{sample}:FALS_{mean})^{0.55}$.

Statistical analyses of microscopy and FCM data

Samples were categorized as oligotrophic or eutrophic based on integrated fluorometric chlorophyll (mg m^{-2}), where locations with <1 mg m^{-2} integrated chlorophyll were considered oligotrophic. Of the 31 sampled locations, eight were categorized as oligotrophic, 18 were eutrophic, and five were considered front sites based on their locations relative to outcropping of density surfaces and extremely high total biomass.

These included one station on each front transect, station 5 in P0810 and station 10 in P1208, and each day of Cycle 1 in P1208. Integrated carbon biomass from microscopy and FCM analyses (Supplementary Table 1) for each of the sites were converted to a matrix of Bray-Curtis similarity values and visualized using a non-metric multidimensional scaling plot with the vegan package in R (Oksanen et al. 2016). Ciliate data was normalized by the mean ciliate biomass of each category to account for differences in the microscopy methods.

Molecular analysis of planktonic communities

Extraction and amplification. Whole seawater samples of 250 mL were collected from the mixed layer (12-20 m) on the first day of each cycle conducted on either side of the two fronts, and on the 2012 E-Front (Cycle 1, Fig. 1) for molecular analysis. Seawater was filtered onto 0.2 µm Supor filters, before being flash-frozen in liquid nitrogen and stored at -80 °C until analysis. Filtered samples were extracted using the NucleoMag 96 Plant kit and amplified using polymerase chain reaction (PCR). Eukaryotes were amplified by targeting 18S rDNA in the hypervariable V9 (1389F-TTGTACACACCGCCC, 1510R-CCTTCYGCAGGTTCACCTAC) and V4 regions (F-CCAGCASCYGCGGTAATTCC, R-ACTTTCGTTCTTGATYR) and prokaryotes by targeting the V3-V4 regions of 16S rDNA (F-GTGYCAGCMGCCGCGGTAA, R-CCGYCAATTCMTTTRAGT). Amplified DNA was purified using the AMPure XP kit and all samples were pooled at concentrations of no more than 1 ng DNA before sequencing on an Illumina MiSeq.

Sequence processing and phylogenetic assignments. Illumina MiSeq paired sequencing reads from 18S V9 amplicons were quality trimmed to Phred score 30 (Q30,

minimum average, in sliding window of size 2 bp). Paired reads were aligned using PEAR (Zhang et al. 2014) and then filtered to remove possible chimeras using USEARCH (Edgar 2010), and a minimum length of 50 bp. Reads from 16S and 18S V4 were quality trimmed to Q20 due to the lower maximum quality scores of these sequences. Paired reads from 18S V4 were not aligned due to the poor quality of read 2, so only read 1 was used. Quality control measures resulted in a total of 665,944 reads (mean 47,567 ± 4,354 per sample) for 18S V9 samples (n = 14), 86,198 reads (mean 9,577 ± 628 per sample) for 18S V4 samples (n = 9), 296,418 reads (mean 21,172 ± 1,324 per sample) for 16S samples (n = 14), and 13,509 reads (mean 965 ± 1,018 per sample) from plastids (n = 14) from both cruises. All metazoan sequences were removed from both 18S datasets to limit the impact of multicellular organisms, leaving a total of 370,923 (mean 26,495 ± 2,700 per sample) in the V9 dataset and 82,610 (9,179 ± 602 per sample) V4 dataset for both cruises.

Reads from all three amplicons were clustered into operational taxonomic units (OTUs) using SWARM (Mahé et al. 2014), and custom python scripts were used to aggregate library specific OTU read counts (https://github.com/allenlab/rRNA_pipeline). Rarefaction curves for OTUs from all samples are available in Supp. Fig. 1. All operational taxonomic units (OTUs) from each sample were converted to Bray Curtis distances and visualized on an nMDS created using the vegan package in R (Oksanen et al. 2016) to assess community similarity. OTUs were classified by the best hit using FASTA36 GLSEARCH (Pearson and Libman 1988) against the appropriate database. For 16S, the SILVA v111 database was used (Quast et al. 2013), and any OTUs that were classified as potential plastid sequences were separated and re-classified using the

PhtyoRef database (Decelle et al. 2015). For 18S, the PR2 database was used, with taxonomic updates from the Tara Oceans W2 (de Vargas et al. 2015). A total of 7,308 OTUS were identified in the 18S V9 samples, 11,915 in the 18S V4 samples, and 9,780 OTUs in the 16S samples.

Results

Biomass and community composition at the 2012 E-Front

E-Front Overview. The E-Front was identified by the shoaling of the 24.5 kg m^{-3} isopycnal (Fig. 2c), located between stations 9 and 10 on the front transect and associated with 16 °C water at the surface. There was a sharp increase in subsurface chlorophyll concentrations just to the east of the front (Stn. 11, 30 m; Fig. 2d), on the more eutrophic, coastal side. Overall, integrated autotrophic biomass increased 1.7 fold over the 3-km distance between stations at the front. The highest biomass was located at Stns. 10 and 11, 3,775 mg C m^{-2} on average compared to 2,287 mg C m^{-2} at Stn. 9 (Fig. 3c). A similar pattern was seen for heterotrophs, which increased 1.8 fold across the front, from 905 mg C m^{-2} at Stn. 9 to 1,659 mg C m^{-2} at Stn. 10 (Fig. 4c).

Autotrophic community composition. Based on microscopic analyses, diatoms dominated the subsurface chlorophyll maximum at Stn. 11 (Fig. 3c-d) and comprised 60% and 70% of integrated autotrophic biomass at Stns. 9 and 10, respectively (Fig. 3d). The communities at either end of the transect differed in total integrated biomass and percent composition. Stations 1 and 2 were characteristic of oligotrophic waters, with low integrated autotrophic biomass (881 mg C m^{-2} and 910 mg C m^{-2}) and a phytoplankton community composed of *Prochlorococcus* (39% biomass), autotrophic

dinoflagellates (24%), and prymnesiophytes (20%). Similarly, heterotrophic biomass at Stns. 1 and 2 was also low (365 mg C m^{-2} and 605 mg C m^{-2}). The eutrophic end of the front transect had higher integrated autotrophic and heterotrophic biomass (2009 mg C m^{-2} and 1016 mg C m^{-2} at Stn. 13), but lower total biomass than at the front itself. The community composition at Stn. 13 differed from those at either the front or Stns. 1 and 2, with *Synechococcus* (50%) and A-Dinos (29%) dominating and very few diatoms (1%).

Results of the 18S V9 analyses supported the patterns observed from microscopy while revealing deeper details of the taxonomic composition of the front community. Dinoflagellate sequences were the most numerous in all samples, but presumably due to their high and variable 18S rDNA copy number and not necessarily their true numericalcontribution to community composition. Diatoms (Subphylum Bacillariophyta) comprised the next highest portion (14-22%) of total OTUs. 18S V4 results (Supp. Fig. 2) indicated that these were mostly unidentified species of *Brockmanniella* (a genus of polar-centric Mediophyceae, 40-44%), raphid-pennates (26-28%), radial-centric basal Coscinodiscophyceae (an order of polar-centric Mediophyceae, 5-13%), and polar-centric *Thalassiosira* (a genus of polar-centric Mediophyceae, 6-15%). On the oligotrophic side of the front, *Brockmanniella* (0-4%) decreased dramatically, and *Rhizosolenia* (a genus of radial-centric basal Coscinodisophyceae, 7-26%), *Thalassiosira* (9-26%), *Stephanodiscus* (a genus of polar-centric Mediophyceae, up to 28%), araphid-pennate *Thalassiothrix* (a genus of Fragilariophycidae, up to 18%), and polar-centric Coscinodiscophyceae (up to 12%) increased.

For other eukaryotic taxa in the phytoplankton community, 18S V9 data (Fig. 5) identified higher contributions of chlorophytes (up to 10%) and haptophytes (up to 3.6%)

in oligotrophic waters compared to the front. More specifically, haptophytes such as *Emiliania* (11-17%), *Chrysochromulina* (18-23%), and other Prymnesiophyceae (12-22%) were abundant on the oligotrophic side of the front, along with chlorophytes in the Mammielles (up to 16%) and prasino-clades (up to 17%) (Supp. Fig. 2). Pelagophytes were found in higher percentages at the front (10-15%) than at the more oligotrophic stations (2-8%).

Trends in phytoplankton taxa across the front were even clearer in the plastid data from the 16S dataset (Supp. Fig. 4). While this dataset was more limited in scope and total number of reads, the trends in phytoplankton taxa were more readily apparent because dinoflagellates and non-phytoplankton were not part of this dataset (Decelle et al. 2015. Again, Prymnesiophyceae dominated on the oligotrophic side of the front, but to a much greater extent (45-75%) than in the 18S V4 dataset. Other Bacillariophyta, the majority unidentified, dominated the front (50-84%) and eutrophic sites (28-63%). Interestingly, Bacillariophyta and Prymnesiophyceae switched in relative importance between the eutrophic and oligotrophic stations, similar to the change from *Synechococcus* to *Prochlorococcus* across the front discussed below, which was not apparent in the 18S datasets. Further, while Pelagophyceae occurred at the higher percentages at fronts in the 18S data, they were most abundant at oligotrophic sites (7.2-20%) in the plastid data, which is more in line with expectations based on their ecology.

In addition to the elevated diatom biomass at the front, opposing trends in *Prochlorococcus* and *Synechococcus* biomass were evident across the frontal transect. *Prochlorococcus* dominated the offshore community (340 mg C m^2 at Stn. 1), but decreased sharply across the front (13 mg C m^2 at Stn. 13). *Synechococcus* biomass

exhibited the opposite pattern, increasing approximately 20x from Stns. 1 to 13 (140 mg C m^2 at Stn. 1, 998 mg C m^2 at Stn. 13). 16S molecular data (Fig. 6) confirmed this observation, showing abundant *Synechococcus* at the front (up to 14%), on the eutrophic side of the front (14-21%), and downstream of the front in eutrophic waters (up to 53%), but decreasing sharply on the oligotrophic side of the front (<1%). *Prochlorococcus* was barely measurable at the front (approximately 0.02%) and very low in eutrophic waters near the front (6.4-8.3%), but increased sharply on the oligotrophic side of the front (22-13%).

Heterotrophic community composition: Total integrated biomass of heterotrophs was elevated at the E-Front (Fig, 4c), although the increase was less pronounced (1.2 x increase of 754 mg C m^{-2} from Stns. 9 to 10) than that for autotrophs (1,511 mg C m^{-2} or 1.7x, Fig. 3c). H-Dinos dominated the protistan heterotrophs at all stations on the front transect, comprising 65-88% (mean 79%) of their biomass. However, H-Dinos did not show an obvious increase at front Stns. 8-10. In fact, their relative percent contribution (Fig. 4d) to heterotrophic community biomass decreased at the front to 65-67% at Stns. 8-10, while ciliates and other heterotrophs increased in importance (~25% at Stns. 8-10 for Cils, and 8% at Stns. 8-10 for H-Other). Biomass of heterotrophic bacteria also increased at the front, from 1207 mg C m^{-2} at Stn. 9 to 1904 mg C m^{-2} at Stn. 10 (Supp. Table 1).

According to V4 data, most dinoflagellates in all samples were uncultured Dinophyceae (63-99%, mean 92%), with unknown trophic modes. However, a small percentage of gymnodinoids (max 16%, mean 4%), which are often heterotrophic, were identified. Ciliate OTUs were relatively rare in the front samples, despite visual evidence of their presence in the microscopic analyses. Non-front samples were dominated by

aloricate Choreotrichia and Oligotrichia (mean 60%). 18S V9 data also identified heterotrophs that were not seen via microscopy, including a small percentage of radiolarian OTUs (Fig. 6) at the front (3.4% at 12 m) and MAST OTUs in the oligotrophic samples (max 1.8%).

Heterotrophic bacteria from 16S analyses (Fig. 6) were dominated by flavobacteria (9.4-48%, mean 35%). The alphaproteobacteria of the Order Rhodobacterales were common across all samples (4-20%, mean 11%), but especially abundant at the front (19-20%) and in oligotrophic samples (13-19%). Verrucomicrobia had a similar distribution, abundant at the front (12-21%) and in oligotrophic samples (18% at 60m). SAR11 was notably more abundant on the oligotrophic side of the front (24-30%).

Comparisons with the 2008 A-Front

A-Front Overview. The 2008 A-Front was an east-west front that was also characterized by the shoaling of the 24.5 kg m^{-3} isopycnal and the presence of 16 °C water at the surface, which occurred at Stns. 4 and 5 on the front transect for that cruise (Landry et al. 2012). There was a subsurface chlorophyll maximum on the cooler northern side of the front, with the highest integrated autotrophic biomass reaching 2930 mg C m^{-2} at front Stn. 5 (Taylor et al. 2012). Autotrophic carbon biomass increased approximately 2x from Stns. 3 to 4 on the front, roughly 2.2 km apart. Integrated heterotrophic biomass was highest on the northern side of the front, averaging 420 mg C m^{-2} across Stns. 6-10 (Taylor et al. 2012). Diatoms and H-Dinos dominated the auto- and heterotrophic front communities, respectively (Taylor et al. 2012).

Similarities in autotrophic community composition across fronts. Both the A- and E-Fronts were characterized by high autotrophic biomass dominated by diatoms (Fig. 3b, d). The maximum diatom biomass (Fig. 3a, c) at the E-Front (2,669 mg C m^{-2} at Stn. 10) was just slightly higher than at A-Front (2,010 mg C m^{-2} at Stn. 5). Percentage contributions of A-Dinos, Pryms, and A-Others to total autotrophic biomass decreased at both fronts due to the predominance of diatoms. Both fronts also exhibited a clear switch between *Prochlorococcus* and *Synechococcus* at the fronts (Fig. 4a, c). In the 16S data (Fig. 6), *Synechoccocus* showed similar relative abundances of 17-20% in the 2008 front-like samples and 14-21% in the 2012 eutrophic-front samples. Although *Prochlorococcus* was more important at oligotrophic stations in both studies, their contributions to the community varied between years (2008: 4.2-20%; 2012: 22-31%).

While no samples were collected for molecular analysis directly on the A-Front, 18S V9 data from a location close to the front (2008 Cycle 5, referred to as "front-like" in Figs. 5 and 6) showed similarities in diatom relative abundances to E-Front samples (2008: 13-20%; 2012: 14-22%). V9 data from both fronts were dominated by dinoflagellate OTUs (2008: 59-69%; 2012: 70-75%), reflective of both their abundance at fronts, confirmed via microscopy (Supp. Table 1), as well as the high gene copy number of dinoflagellates. Pelagophytes were most common on the oligotrophic sides of both fronts (2008: 4.5-21%; 2012: 3.4-5.2%), as were haptophytes (2008: 5-6.8%; 2012: 3.1-3.6%). Chlorophytes were notably higher in the 2008 front-like samples (11-13%) compared to the 2012 front samples (approximately 0%). This could be due to the fact that the front-like 2008 samples were not directly on the front, since chlorophytes were

found on both the eutrophic (2.2-3.4%) and oligotrophic (8.6-10%) sides of the 2012 front.

Although the 18S V4 analysis for the 2008 front-like samples was unsuccessful, limiting detailed comparisons between years (Supp. Figs. 1-2), some conclusions can be drawn from the 16S plastid analyses (Supp. Fig. 4). Prymnesiophyceae were comparably important on the oligotrophic sides of both fronts (2008: mean 45%; 2012: mean 48%), while Bacillariophyta dominated at the fronts (2008: mean 41%, 2012: mean 67%) and in eutrophic waters (2012: mean 49%). Pelagophytes were present in low numbers at the fronts and eutrophic sites (2008: 7.5% mean; 2012: mean 5%) but increased in relative importance at oligotrophic sites (2008: mean 22%; 2012: 14.3%). In general, samples from 2008 had higher percentages of Mamiellophyceae (2008: mean 4%; 2012: mean 2.7%) and Prasinophyceae (2008: mean 12%; 2012: mean 1.3%) across all sites.

Similarities in heterotrophic community composition across fronts. H-Dinos dominated the biomass of protistan heterotrophs at all stations across the front transects (mean 69% in 2008 and 79% in 2012; Fig. 4). However, they comprised slightly lower percentages at and near the fronts (Fig. 4b, d), where H-Others and Cils increased in relative importance. Cils from the A-Front were enumerated by epifluorescence microscopy and are therefore likely underestimated, leading to lower Cil biomass in 2008 versus 2012. Nonetheless, the trends across the two fronts were similar, with Cils increasing slightly in total biomass and percent contribution at the fronts (max 17% at 2008 Stn. 5 and 24% at 2012 Stn. 10, Fig. 5). H-Others, largely composed of heterotrophic nanoflagellates, increased on the eutrophic sides (max 40% at 2008 Stn. 7 and 9% at 2012 Stn. 12). Cercozoans were abundant (12%) in the V9 analyses of the

2012 mixed-layer front sample (12 m, Fig. 5) but not present in notable amounts in other samples.

Heterotrophic bacteria had elevated biomass near the front stations on both transects (Supp. Table 1). In 2008, peak biomass occurred on the eutrophic side (700 mg C m^{-2} at Stns. 4 and 5, but 1200 mg C m^{-2} at Stn. 6), while the peak was slightly closer to the front at Stn. 10 in 2012 (1904 mg C m^{-2}). Flavobacteria dominated the 16S dataset in all samples (2008: 47%; 2012: 44-46%). SAR11 was most abundant in oligotrophic waters (2008: 15-18%; 2012: 24-30%). The alphaproteobacteria Rhodobacterales was relatively more abundant at the 2012 front than in 2008 front-like samples (2008: 11%; 2012: 19-20%). However, their abundances were very similar on the eutrophic (2008: 11%; 2012: 11-12%) and oligotrophic sides (2008: 7.6-8%; 2012: 6-6.2%) of both transects. Verrucomicrobia were most abundant in the 2012 front samples (12-21%), but they were otherwise found at similarly low levels in front-like samples from 2008 (1%), eutrophic-side samples from 2012 (~1%), and oligotrophic stations on both transects (2008: 1.3-2.1%; 2012: 1.1-1.4%). The similarities and differences in 16S patterns suggest that the 2008 front-like samples closely approximate the front community, but may not be an exact representation.

A distinct front microbial community

To determine if the front communities were distinctly different from the adjacent eutrophic coastal communities with high primary productivity and planktonic biomass, microscopy and molecular data were converted to Bray-Curtis dissimilarities and visualized on an nMDS plot with 95% confidence intervals around the weighted means for eutrophic, oligotrophic and front samples. Using data from both fronts, the biomass

of all taxa identified by microscopy and flow cytometry were analyzed first (n = 29 samples), revealing a distinct separation between the oligotrophic and eutrophic samples, but no clear difference between eutrophic and front samples (Fig. 7a). However, a similar but more detailed analysis based on the 16S and 18S V9 OTUs from both 2008 and 2012 revealed distinct differences between the eutrophic and front communities (Fig. 7b).

To explore this difference further, the analysis was conducted separately with 16S and 18S V9 data. The 16S results did not show any clear differences between front and eutrophic samples, or even between oligotrophic and eutrophic extremes. The 18S V9 data, however, showed clear separations among the oligotrophic, eutrophic, and front communities, suggesting that the eukaryotic taxa largely explained the differences between these communities. Furthermore, when only the top 99% of all OTUs in both 16S and 18S V9 data were analyzed together, oligotrophic and eutrophic samples were different, but eutrophic and front samples showed a slight overlap. This suggests that the rare biosphere (OTUs <1% of the sample) contributed most to the differences between eutrophic and front communities.

Discussion

The increased microbial biomass observed at both the A- and E-Fronts is consistent with expectations based on other front studies (Franks 1992a, Laubscher et al. 1993, Moore and Abbott 2002). The comparable magnitude of total autotrophic biomass at each front (2012: 3820 mg C m^{-2}, 2008: 2830 mg C m^{-2}), despite the different years and seasons, suggests that there may be an upper boundary to the total autotrophic

biomass at CCE fronts. This could be the result of bottom-up effects such as trace-nutrient limitation, which can occur at times in the CCE (Bruland et al. 2001, King and Barbeau 2007), or self-shading. Top-down effects from grazing pressure may also play a role in setting an upper limit for autotrophic biomass at the fronts, where the high biomass concentrations of mesozooplankton were found on both the 2008 (Ohman et al. 2012) and 2012 (Stukel et al. 2017) front transects.

The combination of both microscopy and molecular data to analyze the front communities is unique and gives us novel insights into the details of frontal communities. Diatom dominance at the fronts is consistent with previous observations (Lauhscher et al. 1993, Claustre et al. 1994, Moore and Abbott 2002, Taylor et al. 2012), but the fact that they comprised approximately 70% of autotrophic biomass at both fronts demonstrates surprising consistency. Upon closer inspection, however, the dominant taxa are notably different. At the E-Front, penates were the most apparent types in microscopical analyses, while the molecular data confirmed the presence of both pennate and centric taxa. While molecular data were not available for the A-Front samples, microscopical analysis revealed more centric chain-forming taxa and fewer pennates. This suggests that different diatom taxa can fill the same ecological niche at fronts.

Another unique feature of the front microbial community was the abrupt switch between *Prochlorococcus* and *Synechococcus* at CCE fronts that mirrors the onshore-offshore trend that is typically seen for these cyanobacteria (Partensky and Vaulot 1999, Johnson et al. 2006, Dupont et al. 2015). However, the transition from *Synechococcus* in the coastal California Current to *Prochlorococcus* further offshore has not been documented to be as abrupt as observed at the fronts (Taylor et al. 2012, Sudek et al.

2015). The abrupt compositional switch at the fronts highlights the distinct ecological niches that these two cyanobacteria occupy, and the sharp discontinuity in environmental conditions at ocean fronts.

Among heterotrophic bacteria, flavobacteria were ubiquitous, with no clear enhancement at the front. This finding corresponds with evidence that flavobacteria are among the most dominant free-living heterotrophic marine bacteria in coastal ocean regions (Kirchman 2002, Alonso 2007). Particle-associated flavobacteria (Kirchman 2002, Abell 2005b) may also have an advantage at fronts where large amounts of particulate organic matter are formed because they are among the few heterotrophic bacteria that can utilize the high molecular weight dissolved organic matter produced during phytoplankton blooms (Cottrell 2000, Abell 2005a).

Notable differences among the two front communities highlight broader issues of food web dynamics at fronts. Of particular interest are the patterns in heterotrophic biomass, the predominance of diatoms, and the role of the rare biosphere in shaping the front communities. First, heterotrophic protist biomass was much lower at the A-Front compared to the E-Front (Fig. 4a, c). This dramatic difference in biomass can be only partially explained by the underestimation of ciliate biomass in the 2008 sampling. This pattern suggests that heterotrophic protists are not as closely tied to the bottom-up drivers at fronts as are the autotrophs. A possible explanation is that their prey – largely in the pico (0.2-2 μm) and nano (2-20 μm) size ranges – are not as strongly enhanced the fronts as the larger phytoplankton. Picophytoplankton biomass decreased slightly at the E-Front (365 and 277 mg C m^{-2} at Stns. 9 and 10, respectively) and between Stns. 4 and 5 at the A-Front (Taylor et al. 2012), while nanophytoplankton was only slightly elevated at the

fronts. In addition to modest variations in small phytoplankton as a food resource at the fronts, greater top-down predation pressures from mesozooplankton at the fronts might also contribute to suppressing more dramatic responses of protistan consumers at the fronts (Landry 1981, Nejstgaard et al. 2001). The differing relationships between heterotrophic protists and larger mesozooplankton grazers at the two fronts could have implications for the length of the planktonic food web, and thus, the energy transfer efficiency of front food webs.

The dominance of different diatom taxa at the two fronts highlights the fact that while enhanced nutrient flux at the front appears to generally select for rapidly-responsive phytoplankton such as diatoms, any r-selected species could dominate these communities. Such differences would have direct implications for the functional roles of the dominant phytoplankton taxa at fronts. One potential difference is in sedimentation rates and carbon export at fronts, which can be significantly higher at diatom-dominated fronts than in adjacent areas (Stukel et al. 2017). Larger chain-forming species or more silicified diatoms, for example, may have faster sinking rates (Brzezinski et al. 2015) and other qualities (e.g., aggregation, consumption by large grazers) that lead to higher carbon export at fronts.

Finally, taxa representing the rare biosphere, here defined as less than 1% of the reads in 16S and 18S V9 data, were largely responsible for the distinct community compositions between front and adjacent coastal, eutrophic stations in our data. The importance of the rare biosphere has been recognized (Caron and Countway 2009, Reeder and Knight 2009, Lynch and Neufeld 2015), but its true ecological role is not yet clear. For example, the rare biosphere hypothetically acts as a source of ecological

redundancy from which dormant taxa can be drawn as environmental conditions change (Caron and Countway 2009). The rare biosphere of front communities could therefore represent a unique pool of microbial potential that differs from that in nearby coastal communities.

Although dinoflagellates dominated the 18S data, their patterns were not examined in detail here due to the issue of their highly variable 18S gene copy number and the fact that they were composed largely of uncultured taxa. However, the high biomass of both autotrophic and heterotrophic dinoflagellates in the microscopy analyses is at least partially supportive of the high number of dinoflagellate OTUs identified here. Future work is needed to untangle the complexities of interpreting 18S Dinophyta data in light of their variable copy numbers and vast pool of unreferenced species, which made up the majority of dinoflagellate OTUs in the present study.

Conclusions

Globally, fronts are characterized by high productivity and biomass, but there is no a priori reason to expect that the microbial composition of frontal communities should be as similar as found in this study. The striking similarities between two temporally and spatially separated fronts in the California Current highlight what are likely the distinguishing characteristics of mesoscale fronts in coastal upwelling regions. The fronts exhibited comparable total phytoplankton biomass and very similar taxonomic composition, suggesting they experienced similar pressures from nutrient resources and/or grazers. Molecular analyses further demonstrated that the microbial community at fronts was distinct from communities in adjacent productive waters.

The present findings have important implications for the CCE region, where fronts have been found to enhance carbon export and sedimentation rates (Stukel et al. 2017) and are expected to increase in the future (Kahru et al. 2012). The observed CCE trends may also apply to other coastal upwelling or western boundary current regions. While enhanced phytoplankton biomass, productivity, and diatom prevalence were consistent across the fronts in this study, these features cannot be viewed as static or predetermined. Subtle changes in diatom taxa at the fronts, hinted at in this study, and the potential for rare biosphere taxa to respond favorably to environmental changes in the future, could have significant impacts on microbial community composition at fronts, impacting marine food web function and carbon export. To understand the range of variability and potential for change, more detailed information is needed from molecular analysis of front communities and the bottom-up and top-down mechanisms that regulate the outcomes of frontal community dynamics.

Acknowledgements

Thank you to the captain and crew of the *R/V Melville* on both cruises. Special thanks to Darcy Taniguchi and Alexis Pasulka who collected the samples on the 2008 cruise, to Karen Beeri for her expertise during the preparation of samples for sequencing, and to Maitreyi Nagarkar for her advice during the analyses of molecular data. The A-Front and E-Front cruises were supported by the U.S. National Science Foundation grants OCE 04-17616 and 10-26607, respectively, to the CCE LTER Program. Molecular sample analysis was supported by the Mullin Fellowship through the Scripps Institution of Oceanography to A. Freibott.

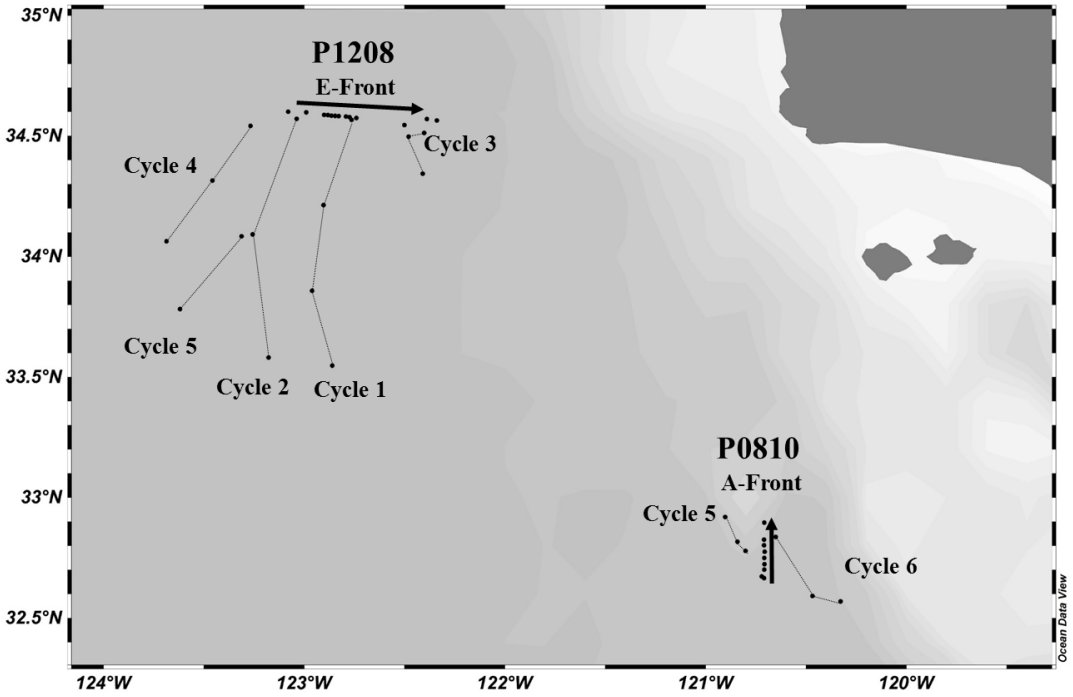

Figure 4.1 Map of CCE LTER sample locations in 2008 and 2012 used in this study.

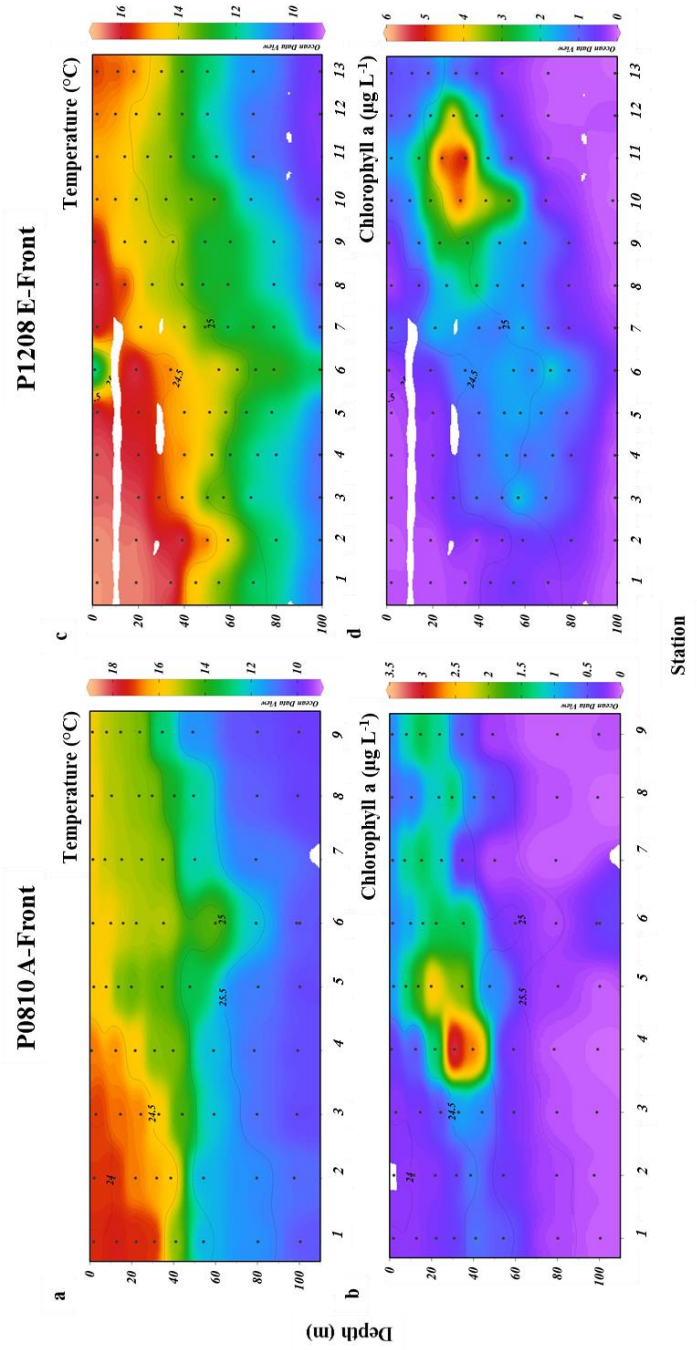

Figure 4.2 Temperature (°C) and fluorometric chlorophyll a (µg L^{-1}) measurements from the front transect stations in (a-b) P0810 A-Front and (c-d) P1208 E-Front. Contour lines on all panels indicate isopycnals.

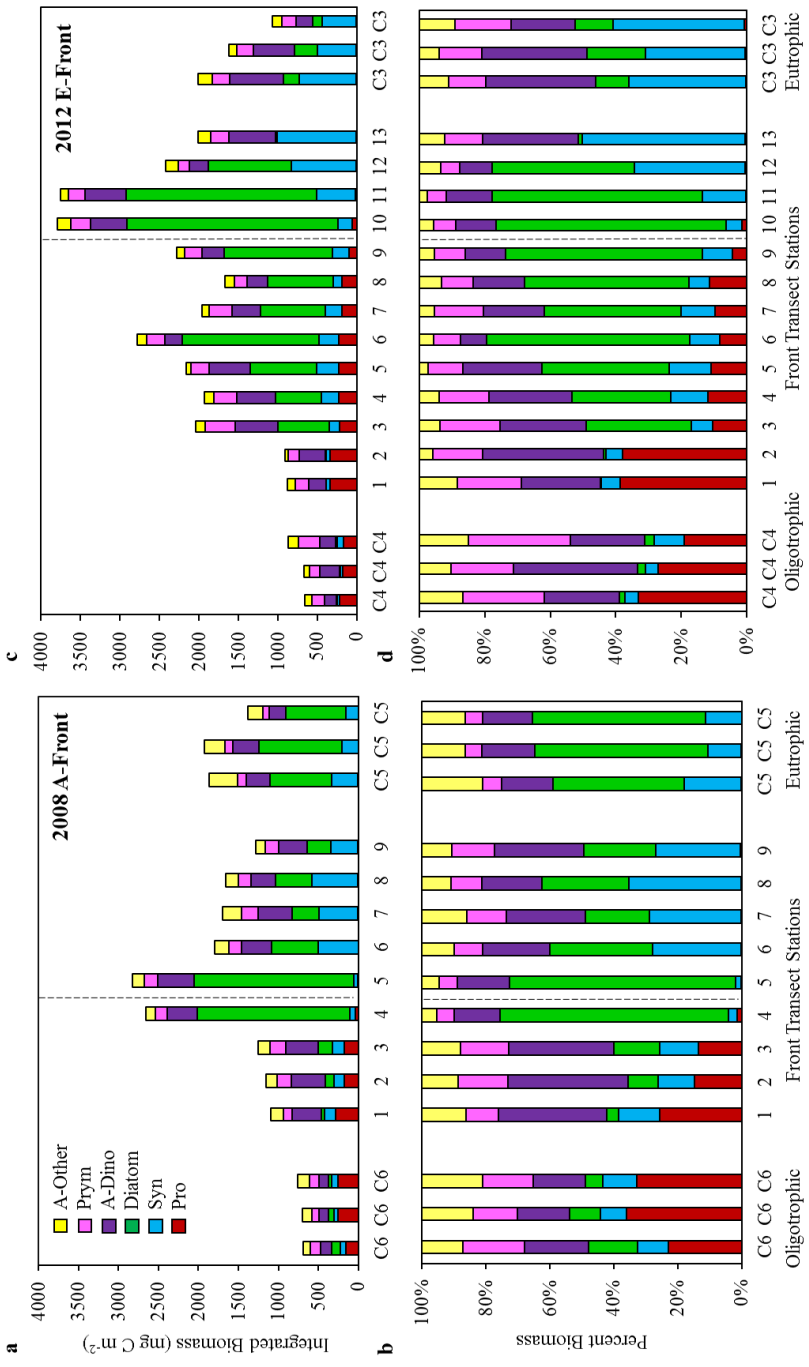

Figure 4.3 A-Front (a) autotrophic depth-integrated biomass (mg C m^{-2}) and (b) percent biomass by type for the front transect stations and cycles on either side of the front (C5 and C6). The same is shown in panels (c) and (d), respectively, for the E-Front transect stations and cycles on either side of that front (C3 and C4). Dashed lines indicate the location of the fronts along the transects.

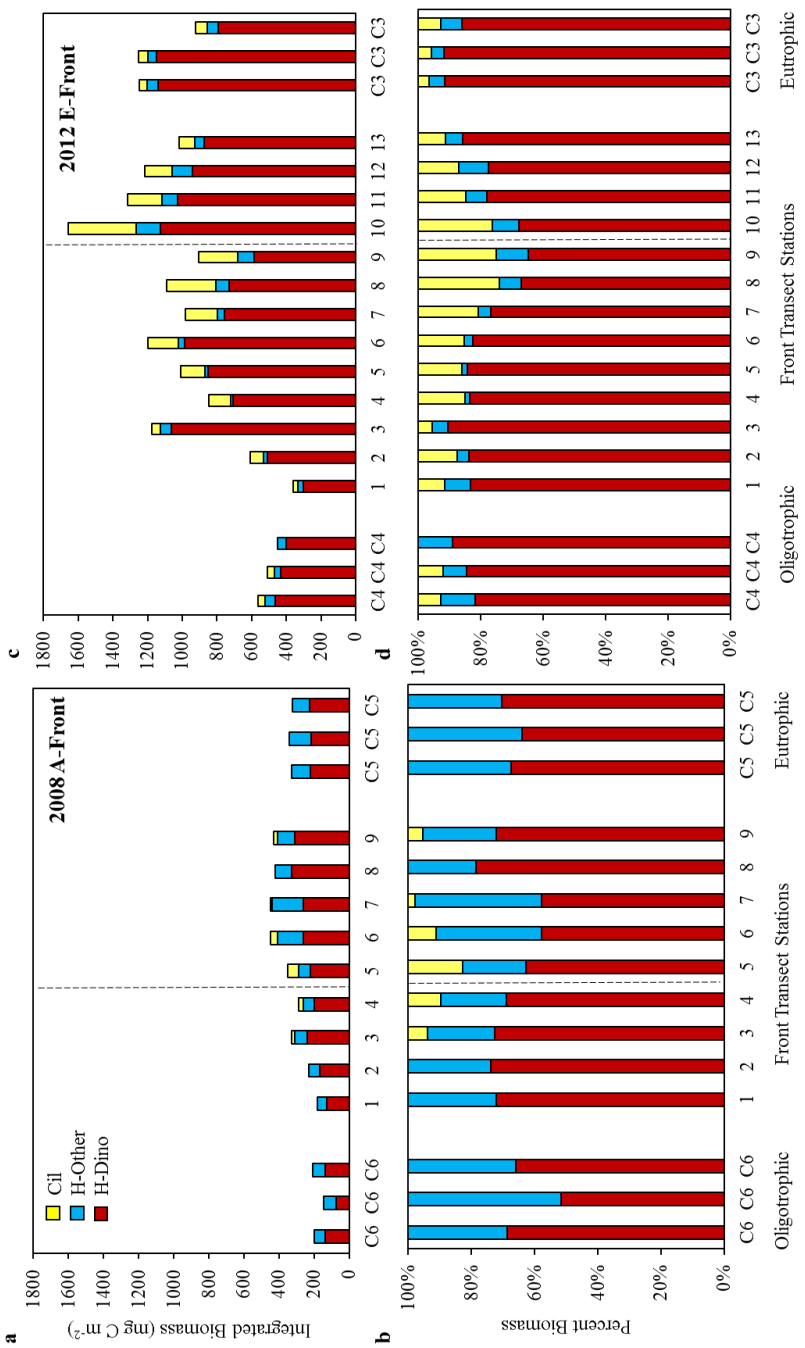

Figure 4.4 A-Front (a) heterotrophic depth-integrated biomass (mg C m^{-2}) and (b) percent biomass by type for the front transect stations and cycles on either side of the front (C5 and C6). The same is shown in panels (c) and (d), respectively, for the E-Front transect stations and cycles on either side of that front (C5 and C6). Dashed lines indicate the location of the fronts along the transects.

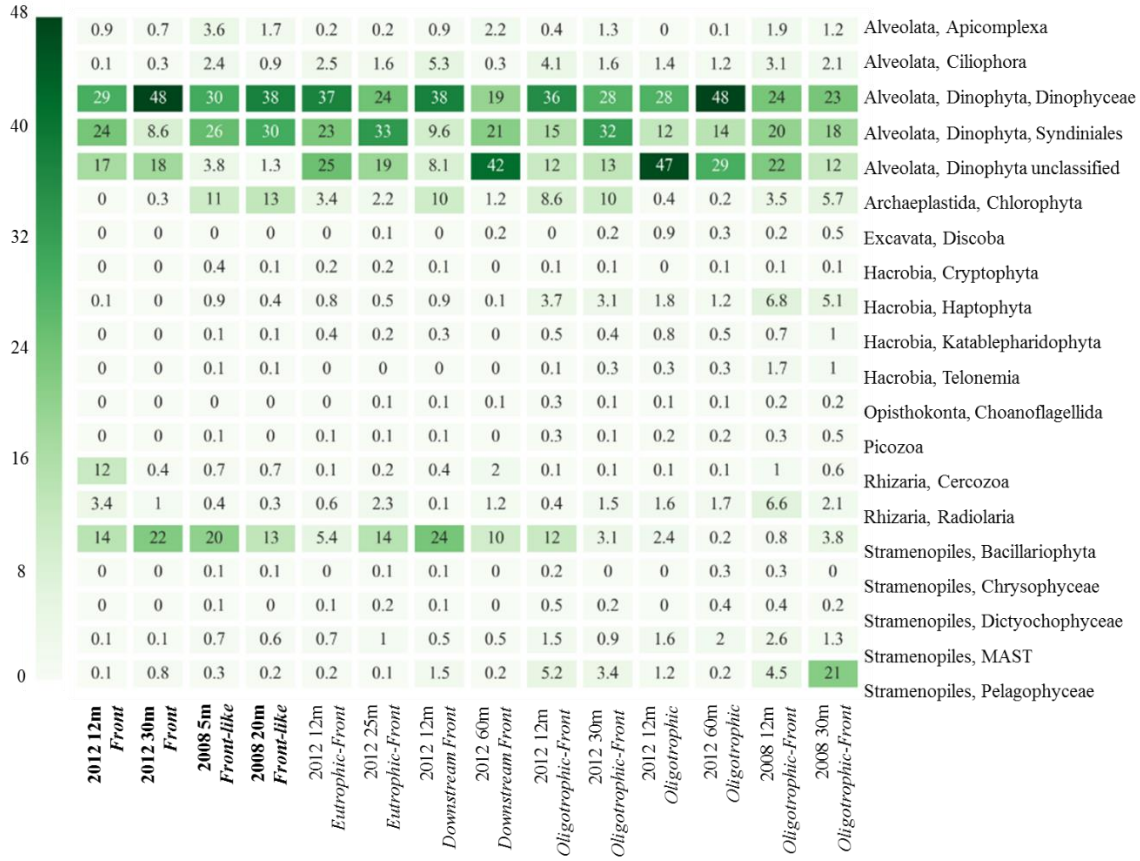

Figure 4.5 Percent abundance of 18S V9 rDNA reads from select samples in 2008 and 2012. Bold text indicates cycles that are on or closest to their respective fronts. Labels refer to samples from the following years and cycles: 2012 Front from 2012 Cycle 1, 2008 Front-like from 2008 Cycle 5, 2012 Eutrophic-Front from 2012 Cycle 3, 2012 Downstream Front from 2012 Cycle 5, 2012 Oligotrophic-Front from 2012 Cycle 2, 2012 Oligotrophic from 2012 Cycle 4, and 2008 Oligotrophic-Front from 2008 Cycle 6.

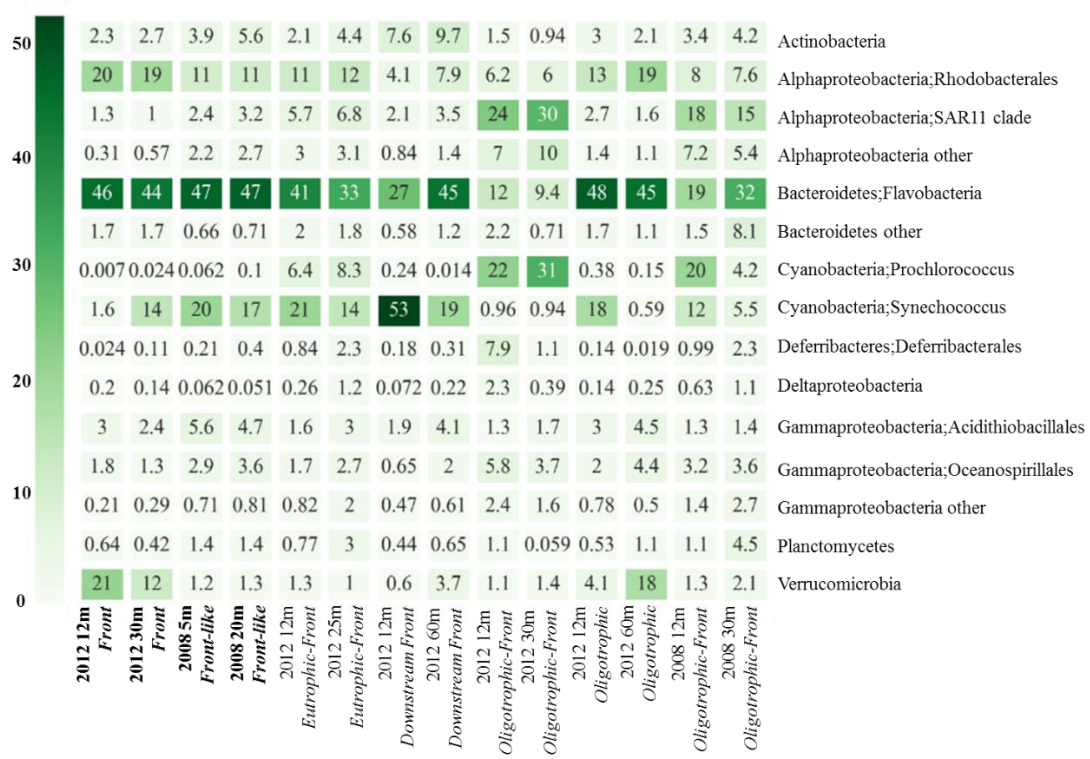

Figure 4.6 Relative percent abundance of 16S rDNA amplicons from select samples in 2008 and 2012. Bold text indicates cycles that are on or closest to their respective fronts. Labels refer to the same samples identified in the Figure 4.5 caption.

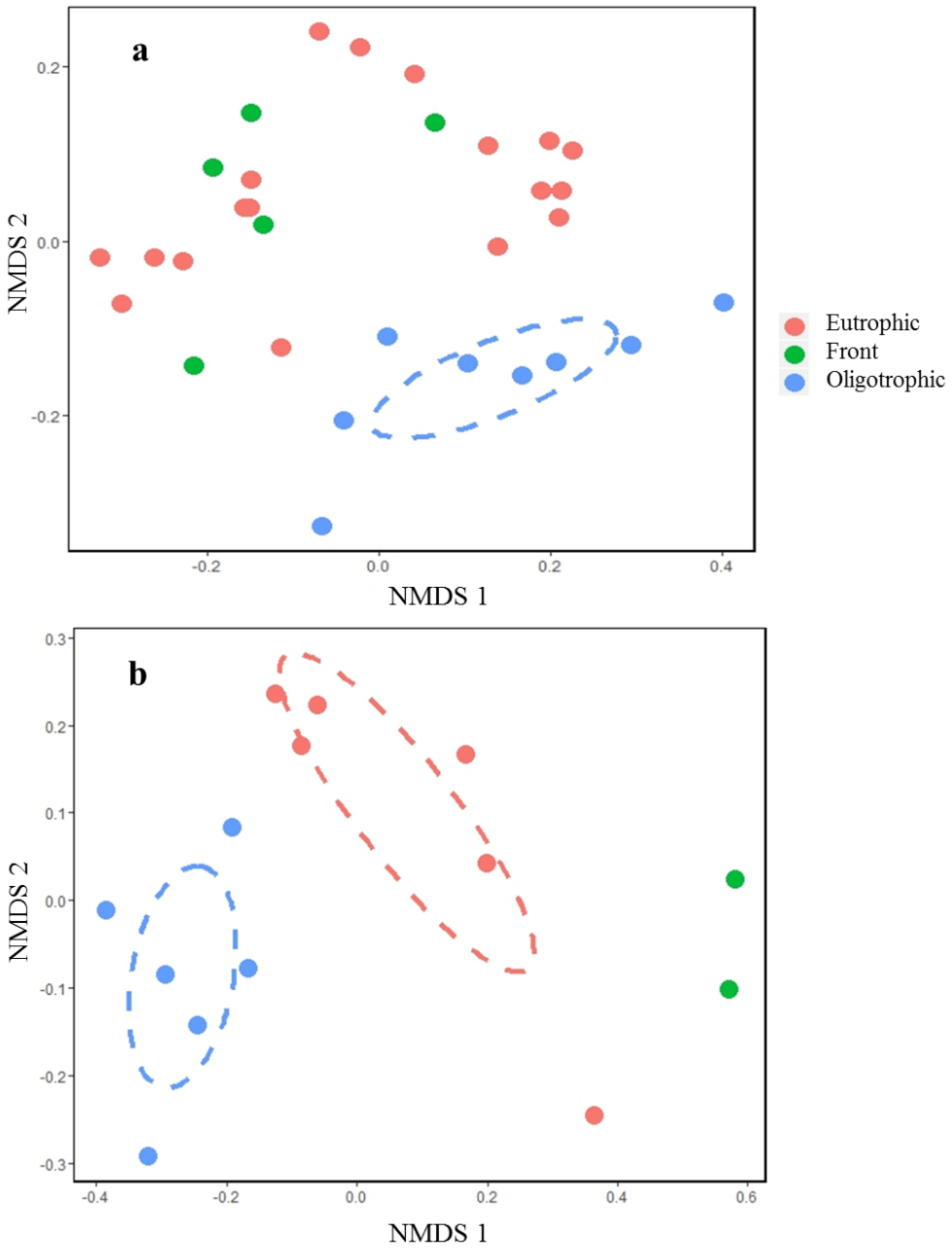

Figure 4.7 NMDS plots of Bray-Curtis dissimilarity for integrated sample biomass of all plankton groups measured by microscopy (a, n = 29) and molecular analyses of 18S V9 and 16S rDNA (b, n = 14). Ellipses show 95% confidence intervals around the weighted average means for each of the three groups: eutrophic, oligotrophic, and front. Frontal sites were identified as such by their location on or immediately adjacent to the identified front. Samples with integrated chlorophyll a levels ≥ 1 mg Chl a m^{-2} and/or ≥ 0.5 µM nitrate and nitrite concentrations were categorized as eutrophic and those < 1 mg Chl a m^{-2} and/or < 0.5 µM were categorized as oligotrophic.

Supplementary Table 4.1 2012 E-Front depth-integrated biomass (mg C m^{-2}) for autotrophic and heterotrophic groups identified using microscopy and flow cytometry data. Total autotrophic carbon includes Pro, Syn, Diatoms, AD, AF, and Prym, while total heterotrophic carbon includes only the protists HD, HF, and Cil. Dashes indicate where no data was available.

			INTEGRATED BIOMASS (mg C m^{-2})											
			AUTOTROPHS						HETEROTROPHS				TOTAL	
E-Front (stn)	Lat (°N)	Lon (°W)	PRO	SYN	Diat	A-Dino	A-Other	Prym	H-Bact	H-Dino	H-Other	Cil	Auto	Hetero
1	34.60	123.08	346	51	3	213	102	172	457	301	30	30	887	362
2	34.60	122.99	348	45	7	335	37	139	473	511	22	76	911	609
3	34.59	122.90	207	139	658	536	128	378	756	1064	60	51	2046	1175
4	34.59	122.88	228	215	583	489	117	293	823	707	12	126	1925	845
5	34.59	122.87	238	260	841	521	57	230	920	850	17	140	2148	1007
6	34.58	122.85	239	259	1730	221	120	230	914	987	34	175	2799	1196
7	34.58	122.83	197	210	820	365	90	293	881	755	40	188	1975	983
8	34.58	122.79	203	109	833	263	113	161	363	730	77	282	1682	1088
9	34.58	122.78	105	218	1374	282	108	213	1207	587	92	226	2299	905
10	34.58	122.74	69	195	2669	461	170	256	1904	1127	141	391	3820	1659
11	34.34	122.41	16	530	2406	527	96	212	1744	1028	88	199	3787	1315
12	34.57	122.39	14	866	1050	240	160	138	1799	943	115	158	2468	1216
13	34.57	122.34	14	1045	23	586	158	231	1230	872	56	87	2057	1016
Cycle 1 (day)														
1	34.57	122.76	16	234	2259	574	207	247	2353	1291	120	383	3537	1794
2	34.21	122.90	14	264	2901	927	202	181	2480	2503	112	235	4489	2850
3	33.86	122.96	31	612	2049	648	157	176	1917	794	204	184	3673	1182
4	33.54	122.86	35	856	787	486	212	335	1963	1116	76			
Cycle 2 (day)														
1	34.57	123.04	303	150	72	320	169	273	633	505	563	46	1287	1114
2	34.09	123.26	217	187	-	-	-	-	897	-	-	100	-	-
3	33.58	123.18	175	48	-	-	-	-	469	-	-	50	-	-
Cycle 3 (day)														
1	34.55	122.50	8	705	195	670	178	227	1460	1133	63	98	1983	1294
2	34.50	122.48	7	492	291	516	98	209	1373	1165	52	84	1613	1301
3	34.51	122.40	8	416	123	201	114	182	1121	794	64	63	1044	921
Cycle 4 (day)														
1	34.54	123.27	145	17	11	93	84	163	336	231	32	28	513	291
2	34.32	123.46	179	28	15	259	65	128	312	430	38	50	673	518
3	34.06	123.69	161	78	29	191	129	279	495	404	49	29	867	482
Cycle 5 (day)														
1	34.08	123.31	111	176	893	379	169	212	555	508	55	77	1940	640
2	33.78	123.62	112	267	-	-	-	-	866	-	-	71	-	-

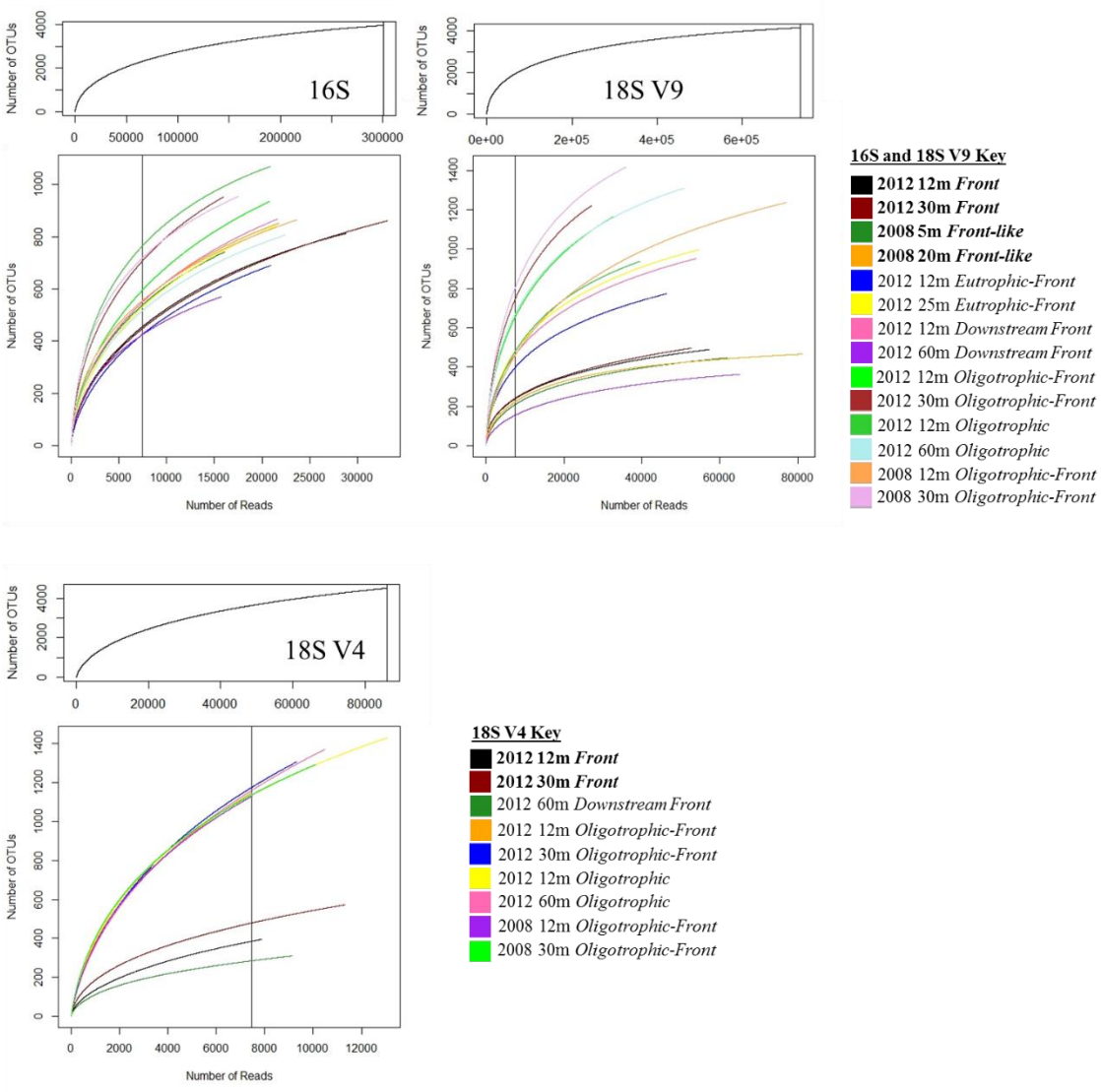

Supplementary Figure 4.1 Rarefaction curves for all OTUs by sample in the 16S, 18S V9, and 18S V9 datasets.

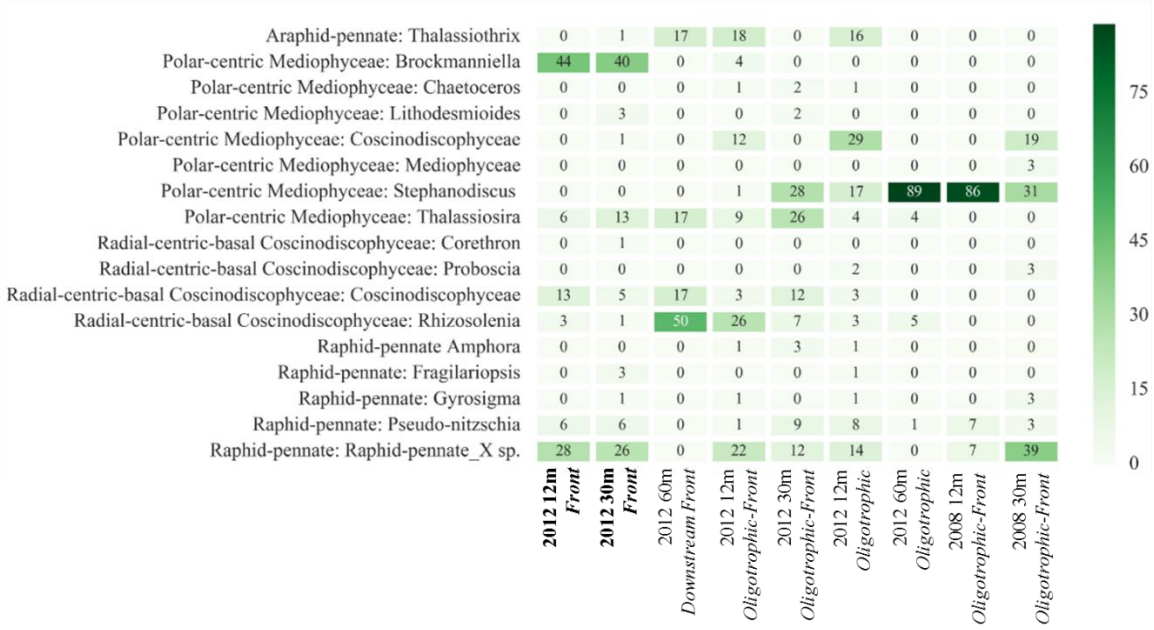

Supplementary Figure 4.2 Percent abundance of 18S V4 rDNA reads for diatoms (Bacillariophyta) from select samples in 2008 and 2012. Bold text indicates cycles that are on or closest to their respective fronts. Labels refer to the same samples identified in the Figure 4.5 caption.

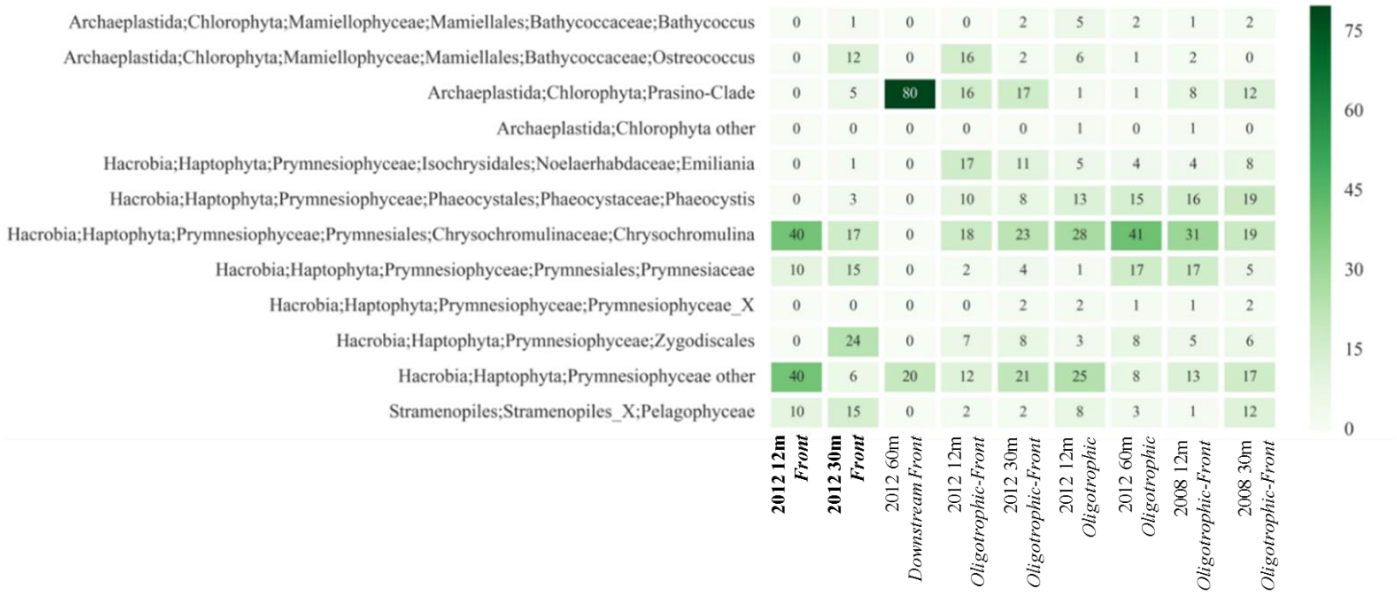

Supplementary Figure 4.3 Percent abundance of 18S V4 rDNA reads for picoeukaryote groups (Chlorophyta, Haptophyta, and Pelagophyceae) from select samples in 2008 and 2012. Bold text indicates cycles that are on or closest to their respective fronts. Labels refer to the same samples identified in the Figure 4.5 caption.

Supplementary Figure 4.4 Percent abundance of 16S rDNA reads identified as eukaryotic plastids in 2008 and 2012. Bold text indicates cycles that are on or closest to their respective fronts. Labels refer to the same samples identified in the Figure 4.5 caption.

References

Abell, G.C.J., and Bowman, J.P. (2005a) Ecological and biogeographic relationships of class Flavobacteria in the Southern Ocean. *FEMS Microbiology Ecology*, 51(2): 265–277.

Abell, G.C.J., and Bowman, J.P. (2005b) Colonization and community dynamics of class *Flavobacteria* on diatom detritus in experimental mesocosms based on Southern Ocean seawater. *FEMS Microbiology Ecology*, 53(3): 379–391.

Allen, J.T., Brown, L., Sanders, R., Moore, C.M., Mustard, A., Fielding, S., Lucas, M., Rixen, M., Savidge, G., Henson, S., and Mayor, D. (2005) Diatom carbon export enhanced by silicate upwelling in the northeast Atlantic. *Nature Letters*, 437:728-732.

Alonso, C., Warnecke, F., Amann, R., and Pernthaler, J. (2007), High local and global diversity of *Flavobacteria* in marine plankton. *Environmental Microbiology*, 9(5): 1253–1266.

Binder, B.J., Chisholm, S.W., Olson, R.J., Frankel, S.L., and Worden, A.Z. (1996) Dynamics of picophytoplankton, ultraphytoplankton and bacteria in the central equatorial Pacific. *Deep-Sea Research II*, 43(4-6):907-931.

Brzezinski, M.A., Krause, J.W., Bundy, R.M., Barbeau, K.A., Franks, P., Goericke, R., Landry, M.R., and Stukel, M.R. (2015) Enhanced silica ballasting from iron stress sustains carbon export in a frontal zone within the California Current. *Journal of Geophysical Research: Oceans*, 120:4654-4669.

Bruland, K.W., Donat, J.R., and Hutchins, D.A. (1991) Interactive influences of bioactive trace metals on biological production in oceanic waters. *Limnology and Oceanography*, 36(8):1555-1577.

Caron, D.A., and Countway, P.D. (2009) Hypotheses on the role of the protistan rare biosphere in a changing world. *Aquatic Microbial Ecology*, 57(3):227-238.

Checkley Jr., D.M., and Barth, J.A. (2009) Patterns and processes in the California Current System. *Progress in Oceanography*, 83(1):49-64.

Choi, J.W., and Stoecker, D.K. (1989) Effects of fixation on cell volume of marine planktonic protozoa. *Applied Environmental Microbiology*, 55(7):1761-1765.

Claustre, H., Kerhervé, P., Marty, J.C., Prieur, L., Videau, C., and Hecq, J.-H. (1994) Phytoplankton dynamics associated with a geostrophic front: Ecological and biogeochemical implications. *Journal of Marine Research*, 52(4):711-742(32).

Coale, K.H., Johnson, S.K., Fitzwater, S.E., Gordon, R.M., Tanner, S., Chavez, F.P., Ferioli, L., Sakamoto, C., Rogers, P., Millero, F., Steinberg, P., Nightingale, P., Cooper, D., Cochlan, W.P., Landry, M.R., Constantinou, J., Rollwagen, G., Trasvina, and A., Kudela, R. (1996) A massive phytoplankton bloom induced by an ecosystem-scale iron fertilization experiment in the equatorial Pacific Ocean. *Nature*, 383:495-501.

Cottrell, M.T., and Kirchman, D.L. (2000) Natural Assemblages of Marine Proteobacteria and Members of the *Cytophaga-Flavobacter* Cluster Consuming Low- and High-Molecular-Weight Dissolved Organic Matter. *Applied Environmental Microbiology*, 66(4): 1692-1697.

Decelle, J., Romac, S., Stern, R.F., Bendif, el M., Zingone, A., Audic, S., Guiry, M.D., Guillou, L., Tessier, D., Le Gall, F., Gourvil, P., Dos Santos, A.L., Probert, I., Vaulot, D., de Vargas, C., and Christen, R. (2015) PhytoREF: a reference database of the plastidial 16S rRNA gene of photosynthetic eukaryotes with curated taxonomy. *Molecular Ecology Resources*, 15(6):1435-45.

De Vargas, C., Audic, S., Henry, N., Decelle, J., Mahé, F., Logares, R., Lara, E., Berney, C., Le Bescot, N., Probert, I., and Carmichael, M. (2015) Eukaryotic plankton diversity in the sunlit ocean. *Science*, 348(6237):1261605-1-1261695-11.

Di Lorenzo, E. (2015) Climate science: The future of coastal ocean upwelling. *Nature*, 518:310-311.

Dupont, C.L., McCrow, J.P., Valas, R., Moustafa, A., Walworth, N., Goodenough, U., Roth, R., Hogle, S., Bai, J., Johnson, Z.I., Mann, E., Palenik, B., Barbea, K.A., Venter, J.C., and Allen, A.E. (2015) Genomes and gene expression across light and productivity gradients in eastern subtropical Pacific microbial communities. *ISME Journal,* 9:1076-1092.

Edgar, R.C. (2010) Search and clustering orders of magnitude faster than BLAST. *Bioinformatics*, 26(19):2460-1.

Fielding, S., Crisp, N., Allen, J.T., Hartman, M.C., Rabe, B., and Roe, H.S. (2001) Mesoscale subduction at the Almeria–Oran front: Part 2. Biophysical interactions. *Journal of Marine Systems*, 30(3):287-304.

Franks, P.J. (1992a) Sink or swim: Accumulation of biomass at fronts. *Marine Ecological Progress Series*, 82(1):1-2.

Franks, P.J. (1992b) Phytoplankton blooms at fronts: patterns, scales, and physical forcing mechanisms. *Reviews of Aquatic Science*, 6(2):121-37.

Franks, P.J., Di Lorenzo, E., Goebel, N.L., Chenillat, F., Rivière, P., Edwards, C.A., and Miller, A.F. (2013) Modeling physical-biological responses to climate change in the California Current System. *Oceanography*, 26(3):26-33.

Garrison, D.L., Gowing, M.M., Hughes, M.P., Campbell, L., Caron, D.A., Dennett, M.R., Shalapyonok, A., Olson, R.J., Landry, M.R., Brown, S.L., Liu, H., Azam, F., Steward, G.F., Ducklow, H.W., and Smith, D.C. (2000) Microbial food web structure in the Arabian Sea: a US JGOFS study. *Deep Sea Research II*, 47:1387-1422.

Irigoien, X., Flynn, K.J., and Harris, R.P. (2005) Phytoplankton blooms: a 'loophole' in microzooplankton grazing impact? *Journal of Plankton Research*, 27(4):313-321.

Johnson, Z.I., Zinser, E.R., Coe, A., McNulty, N.P., Woodward, E.M.S., and Chisholm, S.W. (2006) Niche partitioning among Prochlorococcus ecotypes along ocean-scale environmental gradients. *Science*, 311(5768):1737-1740.

Kahru, M., Di Lorenzo, E., Manzano-Sarabia, M., and Mitchell, B.G. (2012) Spatial and temporal statistics of sea surface temperature and chlorophyll fronts in the California Current. *Journal of Plankton Research*, 34(9):749-60.

King, A.L., and Barbeau, K. (2007) Evidence for phytoplankton iron limitation in the southern California Current System. *Marine Ecology Progress Series*, 342:91-103.

Kirchman, D.L. (2002) The ecology of *Cytophaga-Flavobacteria* in aquatic environments. *FEMS Microbiology Ecology*, 39:91-100.

Landry, M.R. (1981) Switching between herbivory and carnivory by the planktonic marine copepod Calanus pacificus. *Marine Biology*, 65(1):77-82.

Landry, M.R., Ohman, M.D., Goericke, R., Stukel, M.R., Barbeau, K.A., Bundy, R., and Kahru, M. (2012) Pelagic community responses to a deep-water front in the California Current Ecosystem: overview of the A-Front Study. *Journal of Plankton Research*, 24:1-10.

Laubscher, R.K., Perissinotto, R., and McQuaid, C.D. (1993) Phytoplankton production and biomass at frontal zones in the Atlantic sector of the Southern Ocean. *Polar Biology*, 13(7):471-81.

Leakey, R.J., Burkill, P.H., and Sleigh, M.A. (1994) A comparison of fixatives for the estimation of abundance and biovolume of marine planktonic ciliate populations. *Journal of Plankton Research*, 16(4):375-89.

Li, Q.P., Franks, P.J.S., Ohman, M.D., and Landry, M.R. (2012) Enhanced nitrate fluxes and biological processes at a frontal zone in the southern California current system. *Journal of Plankton Research*, 34(9):790-801.

Lynch, M.D.J., and Neufeld, J.D. (2015) Ecology and exploration of the rare biosphere. *Nature Reviews Microbiology*, 13(4):217-229.

Mahé, F., Rognes, T., Quince, C., de Vargas, C., and Dunthorn, M. (2014) Swarm: robust and fast clustering method for amplicon-based studies. *PeerJ*, 2.

Menden-Deuer, S., and Lessard, E.J. (2000) Carbon to volume relationships for dinoflagellates, diatoms, and other protist plankton. *Limnology and Oceanography*, 45:569-579.

Monger, B.C., and Landry, M.R. (1993) Flow cytometric analysis of marine bacteria with Hoechst 33342. *Applied Environmental Microbiology*, 59(3):905-911.

Moore, J.K., and Abbott, M.R. (2002) Surface chlorophyll concentrations in relation to the Antarctic Polar Front: seasonal and spatial patterns from satellite observations. *Journal of Marine Systems*, 37:69-86.

Nejstgaard, J.C., Hygum, B.H., Naustvoll, L.J., and Bmstedt, U. (2001) Zooplankton growth, diet and reproductive success compared in simultaneous diatom- and flagellate-microzooplankton-dominated plankton blooms. *Marine Ecology Progress Series*, 221:77-91.

Ohman, M.D., Powell, J.R., Picheral, M., and Jensen, D.W. (2012) Mesozooplankton and particulate matter responses to a deep-water frontal system in the southern California Current system. *Journal of Plankton Research*, 34(9):815-837.

Oksanen, J., Blanchet, F.G., Friendly, M., Kindt, R., Legendre, P., McGlinn, D., Minchin, P.R., O'Hara, R.B., Simpson, G.L., Solymos, P., Stevens, M.H.H., Szoecs, E., and Wagner, H. (2016) Vegan: Community Ecology Package. R package version 2.4-1. https://CRAN.R-project.org/package=vegan.

Partensky, F., Blanchot, J., and Vaulot, D. (1999) Differential distribution and ecology of Prochlorococcus and Synechococcus in oceanic waters: a review. *Bulletin de l'Institut Océanographique de Monaco*, 19:457-475.

Pearson, W.R., and Lipman, D.J. (1988) Improved tools for biological sequence comparison. *PNAS*, 85(5):2444-2448.

Putt, M., and Stoecker, D.K. (1989) An experimentally determined carbon:volume ratio for marine "Oligotrichous" ciliates from estuarine and coastal waters. *Limnology and Oceanography*, 34:1097-1103.

Quast, C., Pruesse, E., Yilmaz, P., Gerken, J., Schweer, T., Yarza, P., Peplies, J., and Glöckner, F.O. (2013) The SILVA ribosomal RNA gene database project: improved data processing and web-based tools. *Nucleic Acids Research*, 41(D1):D590-D596.

Reeder, J., and Knight, R. (2009) The 'rare biosphere': a reality check. *Nature Methods*, 6:636-637.

Rykaczewski, R.R., and Dunne, J.P. (2010) Enhanced nutrient supply to the California Current Ecosystem with global warming and increased stratification in an earth system model. *Geophysical Research Letters*, 37(21).

Sherr, E.B., and Sherr, B.F. (1993) Preservation and storage of samples for enumeration of heterotrophic protists. In: Kemp, P.K. (ed) *Handbook of methods in aquatic microbial ecology*. Lewis Publishers, Boca Raton, 207-212.

Sherr, E.B., and Sherr, B.F. (2007) Heterotrophic dinoflagellates: a significant component of microzooplankton biomass and major grazers of diatoms in the sea. *Marine Ecology Progress Series*, 352:187-197.

Stukel, M.R., Aluwihare, L.I., Barbeau, K.A., Chekalyuk, A.M., Georicke, R., Miller, A.J., Ohman, M.D., Ruacho, A., Song, H., Stephens, B.M., and Landry, M.R. (2017) Mesoscale ocean fronts enhance carbon export due to gravitational sinking and subduction. *PNAS*, doi:10.1073/pnas.1609435114.

Sudek, S., Everroad, R.C., Gehman, A.L.M., Smith, J.M., Poirier, C.L., Chavez, F.P., and Worden, A.Z. (2015) Cyanobacterial distribtions along a physico-chemical gradient in the Northeastern Pacific Ocean. *Environmental Microbiology*, 17(10):3692-3707.

Taylor, A.G., Goericke, R., Landry, M.R., Selph, K.E., Wick, D.A., and Roadman, M.J. (2012) Sharp gradients in phytoplankton community structure across a frontal zone in the California Current Ecosystem. *Journal of Plankton Research*, 34(9):778-89.

Venrick E.L. (2000) Summer in the Ensenada Front: the distribution of phytoplankton species, July 1985 and September 1998. *Journal of Plankton Research*, 22:812-841.

Zhang, J., Kobert, K., Flouri, T., and Stamatakis, A. (2014) PEAR: A fast and accurate Illumina Paired-End reAd mergeR. *Bioinformatics*, 30(5):614-620.

Chapter 4, in full, is currently being prepared for submission for publication of the material with the following co-authors: Freibott, A., Taylor, A.G., Rabines, A., McCrow, J.P., Beatty, J.L., Selph, K.E., Allen, A.E., Landry, M.R. The dissertation author was the primary investigator and author of this paper.

CHAPTER 5.

Impacts of the 2014 Blob on microbial community dynamics in the southern California Current

Abstract

We investigated the microbial community composition and plankton food web dynamics in the southern California Current during the anomalous environmental conditions of summer 2014. The so-called "Blob" was a large pool of anomalously warm water that enhanced stratification and reduced nutrient availability, leading to decreased plankton biomass and primary production. Using dilution experiments to assess impacts on phytoplankton growth and microzooplankton grazing rates, and 16S and 18S rDNA metabarcoding to characterize the microbial community, we compared our findings to similar data collected during typical environmental conditions in 2006 and 2007. We found that there were significant changes in plankton growth and grazing dynamics during the Blob, but not in microbial community composition. The coastal environment was dominated by chlorophytes (up to 43%), dinoflagellates (up to 86%), *Synechoccocus* (up to 44%), and Flavobacteria (up to 67%). Although chlorophyte dominance is uncommon in coastal upwelling areas of the CCE, which are usually associated with high biomass of diatoms, it is not unprecedented. Phytoplankton growth rates were slightly depressed compared to normal years (0.40 day^{-1} in 2014 vs. 0.44-0.54 day^{-1} in 2006-07) at coastal locations. Grazing rates were also higher at coastal sites during 2014 (0.39 day-

^{1} in 2014 vs. 0.21-0.29 day^{-1} in 2006-07), with the majority of daily phytoplankton growth consumed by micrograzers. The funneling of most, if not all, phytoplankton growth through micrograzers decreased food web energy efficiency by increasing the number of trophic steps, and may partially explain the decreased energy available to large marine organisms during the 2014 anomalous warm-water event.

Introduction

The southern California Current is a dynamic region that exhibits large-scale onshore-offshore trends in plankton diversity and biomass, as well as mesoscale variability due to fronts, jets and eddies (Checkley and Barth 2009). In 2014, the southern California Current region was directly affected by the Blob, a phenomenon of anomalously warm water (~2 °C anomaly) in the North Pacific that persisted for many months (Kintisch 2015, Peterson et al. 2015a). Initially appearing off of the Alaskan coast in fall 2013 as a result of a high atmospheric pressure ridge, the Blob entered a second phase in spring 2014 after the pressure ridge disappeared (Kintisch 2015, Peterson et al. 2015a). During this second phase, warm water along the west coast of North America eventually resolved into two distinct, warm water pools, one near Washington state in the U. S. and the other near Baja California in Mexico (Kintisch 2015, Peterson et al. 2015a). Climate models suggest that the Blob was the result of increasing variability in the Pacific Decadal Oscillation and the North Pacific Gyre Oscillation associated with climate change (Di Lorenzo and Mantua 2016). Thus, similarly intense environmental phenomena could become more common in the future ocean (Di Lorenzo and Mantua 2016).

The warm ocean temperatures during the Blob were associated with decreased westerly winds, weaker currents, and increased stratification of the water column (Petersen et al. 2015b). These temperature-stratified conditions resulted in decreased phytoplankton biomass (Gómez-Ocampo et al. 2017) and primary productivity (Whitney 2015), which impacted the ranges and health of many marine organisms. For example, many species of warm-water copepods, sardine, and anchovy larvae were found in the northern California Current far beyond their normal ranges (Peterson et al. 2016), while various tropical fish (Hendricks 2015) and crustaceans (Gorman 2016) were observed in the normally too-cold California Current (Leising et al. 2015). In addition, widespread starvation and death of Cassin's auklets in late 2014 (Opar 2015) and California sea lions during 2013-15 (NOAA 2017) have been attributed to the Blob's low productivity conditions.

Here, we characterized for the first time the impact of the Blob on microbial community composition and rates of phytoplankton growth and microzooplankton grazing in the southern California Current. Based on previously noted sightings of uncommon tropical marine organisms (Peterson et al. 2016, Hendricks 2015, Leising et al. 2015, Gorman 2016), low levels of phytoplankton biomass (Gómez-Ocampo et al. 2017) and primary productivity (Whitney 2015), and the harmful impact of these conditions on higher trophic levels (Opar 201, NOAA 2017), we expected a dramatic shift in the microbial community composition and food web dynamics compared to previous measurements in the southern California Current. Moreover, because of the warm, low-nutrient conditions across the southern California Current region during this time, we expected that small phytoplankton (i.e. *Synechococcus*, *Prochlorococcus*, and

picoeukaryotes) would dominate the plankton community at all sampled locations. Anticipating a less efficient food web with more trophic flow through micrograzers, we hypothesized that daily phytoplankton growth would be consumed by microzooplankton at rates significantly higher than previously observed in the California Current.

Methods

Study Site

Sampling and process studies were conducted in the California Current near Point Conception from 6 August to 4 September 2014 on the *R/V Melville*. Experiment locations were chosen to represent coastal and offshore regions, as well as the low-salinity core of the California Current located a few 100 km offshore (Fig. 1). Anomalously warm sea surface temperatures were measured at all locations during the cruise (Fig. 2a).

Semi-Lagrangian drift array and dilution experiments

We used a satellite-tracked drift array with a drogue anchored in the mixed layer to track individual water masses for periods of 3-4 days, called experimental cycles. At the start of each cycle, we collected seawater for experiments from a CTD cast, and once the experimental dilution bottles were prepared, they were attached to the drifter line with mesh bags at specific depths. The drift array was deployed for 24-h before being recovered and re-deployed with a new set of experiments. This process continued daily until the end of the experimental cycle, resulting in 3 consecutive, 24-h experiments in the same water mass.

Dilution experiments were deployed at multiple depths to determine the rates of phytoplankton growth and microzooplankton grazing in situ. Two sets of dilution experiments were run each day: regular two-treatment dilutions and size-fractioned dilutions. For the two-treatment experiments, a single diluted bottle (33% whole seawater with 0.1-μm filtered seawater) and an undiluted community bottle (Landry et al. 2009) was prepared with water from each of 6 depths in the euphotic zone. Size-fractioned experiments were replicated three-point dilutions with 2 bottles filled with 18% of 200-μm prefiltered seawater and 0.1-μm filtered seawater, 2 bottles filled with 47% of 200-μm filtered seawater, and 2 bottles filled with 200-μm prescreened undiluted seawater. These 6 bottle size-fractioned experiments were prepared from, and deployed at, a single depth in the mixed layer.

Samples for initial and final chlorophyll *a* (Chl *a*) concentration (250 ml seawater) were collected for each 2-treatment experiment, extracted in 8 ml 90% acetone for 24 h, and analyzed on shipboard with a Turner 10AU fluorometer according to the standard procedures of the California Cooperative Oceanic and Fisheries Investigations (CalCOFI, http://calcofi.org/ references/methods/8-chlorophyll-methods.html). Samples for flow cytometry (FCM) analysis (1 ml sample and 0.5% paraformaldehyde, v/v final concentration) were collected from every experimental bottle at the beginning and end of each experiment. Initial and final samples were also collected for molecular analysis of 18S and 16S rDNA in each dilution experiment (250 ml from the 2-treatment, 500 ml from the size-fractioned dilutions).

Water from the same Niskin bottles used to set up the dilution experiments was also analyzed for dissolved nutrient concentrations (nitrate, nitrite, phosphate, and silica; http://calcofi.org/ccpublications/calcofi-methods/422-nutrient-methods.html), primary production via ^{14}C uptake experiments, which were incubated simultaneously with dilution experiments (http://calcofi.org/references/methods/25-primary-productivity.html), and epifluorescence microscopy (Taylor et al. 2015). Data was obtained through the CCE Long-Term Ecological Research (LTER) Datazoo online database.

Flow cytometry analysis of bacterial communities

Seawater samples of 1 ml were preserved with 0.5% paraformaldehyde (v/v, final concentration), flash frozen in liquid nitrogen, and stored at -80 °C. Prior to analysis, samples were thawed and stained with Hoechst 34442 (1 mg ml^{-1}) for 1 h in the dark (Monger and Landry 1993). Aliquots of 100 ml were analyzed using a Beckman Coulter EPICS Altra flow cytometer with a Harvard Apparatus syringe pump for volumetric sample delivery and two argon lasers tuned to UV (200 mW) and 488 nm (1 W) excitation. Fluorescence signals were collected using filters for Hoechst-bound DNA (blue fluorescence, 450 nm), phycoerythrin (orange fluorescence, 575 nm) and Chl a (red fluorescence 680 nm), and normalized to external standards of 0.5 mm yellow-green and 0.5 mm UV polystyrene beads. Cell fluorescence and light-scatter properties were acquired with Expo32 software and subsequently analyzed with FlowJo software to define heterotrophic bacterial (H-Bact) populations based on DNA presence (all living cells), absence of photosynthetic pigment and light-scatter signals (forward and 90° light scatter, measures of relative size).

Cell abundance estimates for *Synechococcus* and *Prochlorococcus* from FCM analysis were converted to carbon biomass using carbon per cell conversions, with bead-normalized forward angle light scattering (FALS) as a relative size measure. Estimates of cell carbon content were made using mixed layer estimates of 32 and 101 fgC $cell^{-1}$ for *Synechococcus* and *Prochlorococcus*, respectively (Brown et al. 2008).

Molecular analysis of planktonic communities

Extraction and amplification. Seawater samples of 250-500 ml were collected directly from the CTD Niskin bottles for initial measurements and from each dilution bottle at the end of the 24-h incubations. Samples were filtered onto 0.2-µm Supor filters, flash frozen in liquid nitrogen, and stored at -80 °C until analysis. Filtered samples were extracted using the NucleoMag 96 Plant kit and amplified using polymerase chain reaction (PCR). Eukaryotes were amplified by targeting 18S rDNA in the hypervariable V9 (1389F-TTGTACACACCGCCC, 1510R-CCTTCYGCAGGTTCACCTAC) and V4 regions (F-CCAGCASCYGCGGTAATTCC, R-ACTTTCGTTCTTGATYR) and prokaryotes by targeting the V3-V4 regions of 16S rDNA (F-GTGYCAGCMGCCGCGGTAA, R-CCGYCAATTCMTTTRAGT). Amplified DNA was purified using the AMPure XP kit and all samples were pooled at concentrations of no more than 1 ng DNA before sequencing on an Illumina MiSeq.

Sequence processing and phylogenetic assignments. Illumina MiSeq paired sequencing reads from 18S V9 amplicons were quality trimmed to Phred score 30 (Q30, minimum average, in sliding window of size 2 bp). Paired reads were aligned using PEAR (Zhang et al. 2014) and then filtered to remove possible chimeras using

USEARCH (Edgar 2010) and a minimum length of 50 bp. Reads from 16S and 18S V4 were quality trimmed to Q20 due to the lower maximum quality scores of these sequences. Paired reads from 18S V4 were not aligned due to the poor quality of read 2, so only read 1 was used. Quality control measures resulted in a total of 523,266 reads (mean 47,569 ± 22,207 per sample) for 18S V9 samples (n=11), 217,777 reads (21,777 mean ± 7,243 per sample) for 18S V4 samples (n=10), 395,629 reads (mean 35,966 ± 13,380 per sample) for 16S samples (n=11), and 1,494 reads (mean 276 ± 421 per sample) from plastids (n=9) from both cruises. All metazoan sequences were removed from both 18S datasets to limit the impact of multicellular organisms, leaving a total of 89,324 (mean 14,887 ± 5,857 per sample) in the V9 dataset and 199,337 (19,933 ± 5,806 per sample) V4 dataset.

Reads from all three amplicons were clustered into operational taxonomic units (OTUs) using SWARM (Mahé et al. 2014), and custom python scripts were used to aggregate library specific OTU read counts (https://github.com/allenlab/rRNA_pipeline). Rarefaction curves for OTUs from all samples are available in Supp. Fig. 1. All operational taxonomic units (OTUs) from each sample were converted to Bray Curtis distances and visualized on an nMDS created using the vegan package in R (Oksanen et al. 2016) to assess community similarity. OTUs were classified by the best hit using FASTA36 GLSEARCH (Pearson and Libman 1988) against the appropriate database. For 16S, the SILVA v111 database was used (Quast et al. 2013), and any OTUs that were classified as potential plastid sequences were separated and re-classified using the PhtyoRef database (Decelle et al. 2015). For 18S, the PR2 database was used, with taxonomic updates from the Tara Oceans W2 (de Vargas et al. 2015). A total of 3,685

OTUS were identified in the 18S V9 samples, 5,574 in the 18S V4 samples, and 3,970 OTUs in the 16S samples.

Calculation of phytoplankton growth and mortality due to grazing rates

Growth and grazing rates were calculated with results from two analytical methods: flow cytometry and metabarcoding of 16S and 18S rDNA. Apparent growth rate (day^{-1}) in each experimental bottle was calculated using initial and final measurements of cell abundance (i.e. FCM) or percent abundance of sequence reads per OTU (i.e. metabarcoding). The apparent growth rate of each bottle at all dilution levels was graphed and a linear regression used to calculate the instantaneous phytoplankton growth (intercept of the line) and mortality due to grazing (slope of the line) for each experiment (Landry and Hassett 1982).

FCM data were used to calculate growth and grazing rates of *Synechococcus, Prochlorococcus,* and picoeukaryote cells using daily changes in cell abundances. For metabarcoding data, the percent abundances of OTUs per sample were used instead of raw sequence reads to account for the semi-quantitative nature of the amplification and sequencing techniques. Thus, the relative growth and grazing rates obtained using this type of data refer to changes in the abundance of reads per day recovered in the sample, but not to actual changes in cell abundance per day. A conversion factor for *Synechoccocus* was also estimated using the FCM-based biomass data and the corresponding metabarcoding percent abundances in the same samples.

Results

Microbial community composition

18S V9 data revealed that the eukaryotic community in the mixed layer of the southern California Current during the study period was largely dominated by either Dinophyceae (16-86%, mean 59%) or Chlorophyta (6-43%, mean 22%), depending on location (Fig. 3). With the exception of Cycle 1, which had more Dinophyceae (86%) than any other sampled location, Chlorophyta (42-43%) were relatively more abundant at coastal locations, while Dinophyceae (54-58%) comprised the majority of the reads in the California Current waters and offshore locations (Fig. 3). Even at the coastal sites where Chlorophyta were most abundant, Dinophyceae were still a significant portion of the community (16-24%). Dinoflagellate relative abundance should be interpreted with care, however, because they tend to have high and variable rDNA copy numbers. Nonetheless, dinoflagellates are known to be numerous in the CCE, often dominating community biomass based on microscopy so their importance in the molecular results is not unreasonable (Taylor et al. 2012, Taylor et al. 2015). Stramenopiles include the diatoms that normally dominate coastal upwelling zones in the California Current Ecosystem (CCE), but these were only relatively abundant at one coastal location (Cycle 2, 31%) during the Blob. For the most part, Stramenopiles were a small, but consistently present, minority in the plankton community at all locations (2-4%). Interestingly, neither chlorophytes nor dinoflagellates were significantly correlated with environmental conditions such as temperature or nutrients, but stramenopiles were significantly correlated with nutrient concentrations. Stramenopiles correlated with conditions associated with upwelling, including higher nitrate and nitrite concentrations ($r=0.54$, $p<0.05$) and silica concentration ($r=0.64$, $p<0.01$)

The results of the 18S V4 dataset, which identifies higher taxonomic resolution, indicated that taxa in the Prasino-Clades (i.e. prasinophytes) were the most numerous group of Chlorophyta (12-73%, mean 49%, Fig. 4). Cycle 2 was the lone exception to this pattern, with the tiny taxa in Mammiellales comprising the majority of chlorophytes (26%, with 18% likely *Ostreococcus* sp.). The V4 data also revealed high percentages of Prymnesiophyceae at all locations (22-55%, mean 39%), which were not apparent in the V9 dataset. In Cycle 2, prymnesiophytes were even more numerous than chlorophytes (40% vs. 55%), contrary to the V9 results. Cycles 2 and 3 appeared to be comparable coastal communities in the V9 dataset that were both dominated by chlorophytes (42% and 43%, respectively, Fig. 3), but the V4 data exposed the different composition of dominant picoeukaryote taxa in these coastal locations: prymnesiophytes in Cycle 2 and prasinophytes in Cycle 3 (Fig, 4).

The majority of Dinophyceae sequences in the V4 dataset were identified as uncultured taxa (81-97%, mean 92%) and are not shown here. However, 17% of Dinophyceae sequences in Cycle 2 were identified as Gymnodiniales, in stark contrast to the other cycles which had only ~2-3% Gymnodiniales. Cycle 2, the only cycle with a notable percentage of Stramenopiles in the V9 dataset (31%, Fig. 3), had very different types of Stramenopiles than the other cycles (Fig. 5). Cycle 2 included raphid-pennate diatoms such as *Pseudo-nitzschia* (22%), unidentified Stramenopiles (21%), and polar-centric Mediophyceae diatoms (15%), while Cycle 3 was dominated by Pelagophyceae (64%) and Cycles 4 and 5 by a different type of polar-centric Mediophyceae (52% and 71%, respectively, Fig. 5). Unfortunately, no V4 samples from Cycle 1 were successfully

amplified and sequenced, so there are no further details on the community composition at that location.

Plastid sequences from the 16S dataset further highlighted the patterns seen in the V9 and V4 datasets: prasinophytes and prymnesiophytes dominant across all locations (Fig. 6). In this dataset, Prasinophyceae ranged from 32-69% of the assemblage (mean 45%) and were the most abundant group in Cycles 2-4 (Fig. 6). Here, Prymnesiophyceae were not as abundant in the coastal locations (~12%) as they were in the California Current (30%) and offshore (35%, Fig. 6). The presence of Bacillariophyceae (4%), Coscinodiscophyceae (12%), and other Bacillariophyta (10%) in Cycle 2 reaffirmed the significant presence of diatoms at this single location (Fig. 6). Finally, the plastid data revealed more details of the Chrysophyceae and Dictyophyceae groups, which were nearly absent from the V4 dataset. Both Chrysophyceae (11-15%) and Dictyophyceae (~7%) were most abundant at offshore locations.

Bacterial community composition showed a clear pattern across all sampled locations (Fig. 7) pointing to three distinct communities: coastal communities in Cycles 2 and 3, offshore communities in Cycles 4 and 5, and a unique community in Cycle 1. Coastal and offshore locations exhibited the expected switch in dominance between *Synechoccocus* and *Prochlorococcus*, with *Synechococcus* dominant in coastal waters (40-44%) and *Prochloroccocus* dominant in offshore waters (~34%). This was further highlighted by the significant, negative correlation between *Prochlorococcus* and primary production ($r=-0.53$, $p<0.05$), which is lower offshore where *Prochlorococcus* are most abundant. Moreover, *Synechococcus* was significantly correlated with nitrate and nitrite

concentrations ($r=-0.55$, $p<0.05$), while *Prochlorococcus* was significantly correlated with phosphate instead ($r=-0.74$, $p<0.01$). Both offshore and coastal locations had high percentages of Alphaproteobacteria (18-19% coastal, 24-32% offshore) and Flavobacteria (24-25% coastal, 21-28% offshore). Cycle 1 was dominated by Flavobacteria (75%) and had only small percentages of *Synechococcus* (9%), Alphaproteobacteria (8%), and Verrucomicrobia (7%), making it unique from the other sites sampled. Flavobacteria was also significantly correlated with conditions common in productive, upwelling waters, including lower temperatures ($r=-0.54$, $p<0.05$) and higher nitrate and nitrite concentrations ($r=0.55$, $p<0.05$), Chl *a* ($r=0.59$, $p<0.05$), and primary production ($r=-0.53$, $p<0.70$).

Finally, some taxa co-occurred with others across the 16S and 18S datasets, possibly pointing to similar environmental preferences among organisms and/or grazing pressures. Stramenopiles and Planctomycetes were significantly positively related ($r=0.57$, $p<0.05$), as indicated previously (Morris et al. 2006, Pizzetti et al. 2011, Allen et al. 2012). Dinoflagellates were significantly positively correlated with *Synechococcus* ($r=-0.61$, $p<0.05$), haptophytes ($r=0.58$, $p<0.05$), and cryptophytes ($r=0.83$, $p<0.001$). Chlorophytes were significantly correlated with picozoans ($r=0.73$, $p<0.01$, choanoflagellates ($r=0.64$, $p<0.05$), Katablepharidophyta (a clade within the Hacrobia, $r=0.85$, $p<0.0001$), all of which are small (<20 μm) phagotrophic or heterotrophic flagellates (Marchant and Scott 1993, Boenigk and Arndt 2000, Okamoto et al. 2009, Seenivasan et al. 2013).

Comparison between the Blob and normal years in the CCE

The microbial communities in 2014 were similar to those in samples collected from the mixed layer in the CCE at various coastal and offshore locations during previous years (Fig. 8, 9). Samples from three days in offshore 2014 Cycle 5 clustered very closely with other oligotrophic samples, and 2014 Cycle 2 was most similar to other eutrophic locations that also had a significant portion of Stramenopiles. Although 2014 Cycle 3 was close to the coast and considered coastal based on its location, it was categorized as oligotrophic based on total integrated chlorophyll *a* and nitrate and nitrite concentrations, and the 16S community did not cluster closely with either the eutrophic or oligotrophic groups. This is interesting considering that Cycle 3 appeared similar to Cycle 2 16S communities based on the percent taxonomic composition of broad taxonomic categories (Fig. 7). The 18S V9 data tells a slightly different story, with one day of Cycle 3 grouping closely with the oligotrophic cluster and another day separated from the cluster, suggesting that there were fairly significant changes in the eukaryotic assemblage over a short period of time. Similarly, both datasets show significant separation between two days of 2014 Cycle 2, suggesting that the community shifted dramatically over just a few days in that cycle as well. These results show that the community composition in these two coastal cycles was dynamic, changing rapidly as the water parcels advected offshore (Fig 1).

Epifluorescence microscopy and flow cytometry data available from the California Current Oceanographic and Fisheries Investigations (CalCOFI) program from 2005-2013, offers further insight into the seasonal trends in the CCE, which must be taken into account when comparing the “normal” years of spring 2006 and 2007 with the Blob of summer 2014. Direct comparison of the CalCOFI plankton biomass data from

spring and summer 2005-2013 at a representative coastal station (CalCOFI station 80.55) with spring and summer 2014 shows substantially higher total biomass of autotrophs and heterotrophs during spring (Fig. 10c, 2005-2013: 50 ± 9 μg C L^{-1}, 2014: 99 μg C L^{-1}), and a much lower total biomass during summer (Fig. 10c, 2005-2013: 85 ± 11 μg C L^{-1}, 2014: 29 μg C L^{-1}). Diatoms comprised a much smaller percentage of the spring and summer 2014 phytoplankton communities (Fig. 11c, spring and summer 2014: 24% and 17%, spring and summer 2005-2013: 50% and 53%), while pico-sized taxa increased, including *Synechococcus* (spring: mean 4% vs. 24% in 2014, summer: mean 9% vs. 43% in 2014) and autotrophic flagellates (spring: mean 12% vs. 35% in 2014, summer: mean 12% vs. 21% in 2014). When both autotrophs and heterotrophs are considered, the percentage of picoplankton is even greater during the Blob (Fig. 11b, 2014: 48% and 70%, 2005-2013: 24% and 30%) because of the disproportionate increase in heterotrophic bacteria (Fig. 10d, 2014: 26% and 31%, 2005-2013: 21% and 20%). Prymnesiophytes increased slightly during summer 2014 compared to the 9-year mean (Fig. 11b, 11% vs. 6%); however, the microscopy category A-Flag, which did increase during the Blob, is composed of small eukaryotes that may have been indistinguishable as prymnesiophytes specifically.

Phytoplankton growth rates

Chlorophyll a *results.* Phytoplankton community growth rates in the mixed layer, as determined from the 2-treatment experiments, ranged from a minimum of 0.26 d^{-1} offshore to a maximum of 0.58 d^{-1} at the coast (Table 1). Growth rates at coastal locations (Cycles 1-3) were 0.40 d^{-1} on average, slightly higher than the offshore average

growth rate (0.30 d^{-1}). Compared to previous measurements in the same study region during May 2006 and April 2007, years that exhibited typical conditions in the CA Current, coastal growth rates during the Blob were slightly lower (2014: mean 0.40 d^{-1}, 2006-07: mean 0.52 d^{-1}), as were offshore growth rates (2014: mean 0.30 d^{-1}, 2006-07: mean 0.40 d^{-1}, Table 1).

Flow cytometry results. Taxon-specific growth rates were determined from both the 2-treatment and the size-fractioned dilution experiments in the mixed layer. Growth rates from the former calculated from FCM cell abundances ranged from 0.35-1.20 d^{-1} for *Synechococcus,* 0.21-0.97 d^{-1} for *Prochlorococcus,* and 0.58-1.95 d^{-1} for picoeukaryotes. The growth rates of *Synechococcus*, *Prochloroccus,* and picoeukaryotes in the size-fractioned experiments, which were filtered through 200-μm mesh to leave only micrograzers, had narrower ranges (*Synechococcus:* 0.10-0.52 d^{-1}, *Prochlorococcus:* 0.53-0.64 d^{-1}, picoeukaryotes: 0.18-0.51 d^{-1}). Despite this difference, however, the mean growth rates of each taxa per cycle were not significantly different between the standard 2-treatment and size-fractioned experiments. Furthermore, the differences that were observed between growth rates in each experiment did not exhibit a consistent pattern (e.g. higher or lower growth rates for taxa at all locations).

Molecular data results. Potential growth rates were calculated for *Synechococcus* and *Prochlorococcus* using the change in percent abundance of *Prochlorococcus* and *Synechococcus* 16S sequence reads in initial and final size-fractioned dilution experiment bottles. Based on this data, *Synechococcus* ranged from 0.37-1.14 d^{-1} and *Prochlorococcus* from 0.47-0.81 d^{-1}. While the magnitudes of the growth rates

determined using FCM and molecular data are not directly comparable because one measures actual changes in cell abundances and the other relative change in sequence numbers, the trend was the same for both methods. Ordering the cycles from highest to lowest growth rates using both methods returned the same results for *Synechocccocus*: Cycle 4, Cycle 2, Cycle 5 and Cycle 3. This was not true for *Prochlorococcus;* however, and the less robust results for *Prochlorococcus* likely contributed to the mismatch in trends.

To further characterize the relationship between these two measurements of *Synechoccocus* growth, cell abundance (ml^{-1}) and sequence reads (ml^{-1}) were plotted against each other (Fig. 12). There was a positive linear relationship between *Synechoccocus* cell and sequence abundances ($y = 3702.6x + 1210.1$, $R^2 = 0.60$), which supports the use of metabarcoding sequence data to calculate relative growth rates, at least for this group.

Assuming that the relative growth rates from molecular data more broadly reflect the trends in growth from cell abundance, we applied the same technique to the full 18S V9, 18S V4, and 16S datasets. Mean relative growth rates for the most dominant taxa, calculated as the change in percent abundance of sequences, were compared to the mean Chl *a* ($\mu g\ L^{-1}$) at each sampled location to determine which taxa grew fastest under conditions of low to high trophic richness (Fig. 13a). In the 16S dataset, Alphaproteobacteria and Gammaproteobacteria were the fastest growing bacterioplankton at low Chl *a* (Fig. 13a). With the exception of two experiments where *Synechococcus* grew the fastest, they generally maintained low growth rates (Fig. 13a).

This pattern suggests that trophic conditions had less impact on *Synechococcus* growth than other factors, such as grazing pressure. In the 18S V9 dataset, Dinophyceae, Haptophyta, which included prymnesiophytes, and Stramenopiles, achieved the highest growth rates at all Chl *a* concentrations (Fig. 13b). Interestingly, although chlorophytes were the most abundant sequence at most locations, they did not have the highest relative growth or exhibit the largest changes in relative growth rates across locations. Examining the growth rates of the picoeukaryote taxa with the 18S V4 data, revealed that Mammielles grew fastest at low Chl *a*, while pelagophytes and prasinophytes grew fastest at higher Chl *a* (Fig. 13c).

Rates of phytoplankton mortality due to microzooplankton grazing

Chlorophyll a *results.* Microzoolankton grazing rates on the phytoplankton community in the mixed layer ranged from 0.27 d^{-1} offshore to 0.55 d^{-1} near the coast, as determined from the 2-treatment experiments (Table 1). Grazing rates at coastal locations (Cycles 1-3) were 0.38 d^{-1} on average, slightly higher than the offshore average growth (0.30 d^{-1}). The highest grazing rates were recorded in Cycle 3 (0.55 d^{-1}), along with the highest growth rates (0.58 d^{-1}). This cycle was dominated by small chlorophytes, which are suitable prey for micrograzers. Compared to grazing rates measured during 2006 and 2007 when conditions in the CCE were considered normal, coastal grazing rates were elevated (2014: mean 0.39 d^{-1}, 2006-07: 0.28 d^{-1}) and offshore grazing rates were similar (2014: mean 0.30 d^{-1}, 2006-7: mean 0.35 d^{-1}, Table 1).

Flow cytometry results. Taxa-specific growth rates from 2-treatment experiments ranged from 0.57-1.53 d^{-1} for *Synechococcus*, 0.06-0.73 d^{-1} for *Prochlorococcus*, and

0.55-2.01 day^{-1} for picoeukaryotes. In the size-fractioned experiments, the growth rates of *Synechococcus*, *Prochloroccus*, and picoeukaryotes were 0.00-0.53 d^{-1}, 0.48-1.09 d^{-1}, and 0.26-0.43 d^{-1}. Overall, the grazing rates in the size-fractioned experiments had narrower ranges and lower maxima, suggesting that some larger micrograzers may have been removed or damaged during the prefiltration process. The percentage of daily growth grazed for *Synechoccocus* and *Prochlorococcus* at coastal sites was higher on average in the size-fractioned experiments (114% *Synechoccocus* and 134% *Prochlorococcus* vs. 69% *Synechococcus* and 79% *Prochlorococcus*, Table 2), and lower on average offshore (63% *Synechococcus* and 81% *Prochlorococcus* vs. 146% *Synechococcus* and 91% *Prochlorococcus*).

Molecular data results. Mean grazing rates for the most dominant taxa in the 16S, 18S V9, and 18S V4 datasets, calculated as the change in percent abundance of sequences, were graphed against the mean Chl *a* (μg L^{-1}) at each sampled location (Fig. 14). Grazing on *Synechoccocus* were highest at locations with the lowest and highest Chl *a* concentrations (Fig. 14a). Flavobacteria experienced higher grazing rates at the offshore, low Chl *a* locations, while other taxa did not exhibit any clear patterns in grazing rate with Chl *a* concentration (Fig. 14a). In the V9 data, Dinophyceae were heavily grazed at both low and high Chl *a* (Fig. 14b). Chlorophyta were grazed heavily in at least one low Chl *a* location (Fig. 14b), and the V4 results suggest these were likely prasinophytes (Fig. 14c).

The percentage of daily growth grazed, which takes into account both the growth and grazing rates of each group, are presented in Figure 15. This clarifies some of the

complex patterns in the growth and grazing rates presented in Figures 9 and 10, highlighting the phytoplankton that experience the highest grazing pressure relative to their growth. With the exception of a single location where *Prochlorococcus* were heavily grazed at low Chl *a* conditions offshore, *Synechococcus* experienced the heaviest grazing pressures of any bacterioplankton at all locations (Fig. 15a). Chlorophytes, specifically prasinophytes, experienced the highest grazing pressure at locations with low Chl *a* (Fig. 15b, c), while the grazing pressures appeared relatively comparable among taxa at locations with high Chl *a*.

Discussion

Although the Blob created relatively homogenous conditions of elevated temperature and low nutrient availability during summer 2014, changes in the microbial community composition based on the molecular information was not unprecedented for the CCE region when compared to 2006 and 2007. Concurrent data available from the California Current Oceanographic and Fisheries Investigations (CalCOFI) program from 2005-2013, however, offers further insight into the seasonal biomass trends in the CCE, which must be taken into account when comparing the "normal" years of spring 2006 and 2007 with the Blob of summer 2014. The CalCOFI data showed a marked decrease in the total plankton biomass during summer 2014 compared to the mean biomass during 2005-2013 (85 ± 11 μg C L^{-1} vs. 29 μg C L^{-1} in 2014), in agreement with other published findings (Gómez-Ocampo et al. 2017). Diatom percent biomass decreased in both spring and summer 2014 (spring: 14% in 2014 vs. 33% mean, summer: 10% in 2014 vs. 36%

mean), which was also apparent in the molecular data, while multiple pico-sized taxa increased in biomass contributions (*Synechococcus,* autotrophic flagellates, heterotrophic bacteria in Fig. 11). Together with the molecular data, we know that the specific picoautotrophs that increased during summer 2014 were chlorophytes (Fig. 3) and that they have been dominant before in coastal samples from 2006 and 2007 (Fig. 8). Essentially, the molecular data alone shows a Blob microbial assemblage that is unusual, but not unprecedented for the CCE, while the biomass data determined via microscopy compared to the 9-year mean for the area makes the significant impacts of the Blob on the community clearer. Taken together, these results confirm our hypothesis that there was a significant shift beyond the normal seasonal changes in the CCE microbial community during the Blob.

The dominance of both chlorophytes and dinoflagellates across all locations is unsurprising given the stratified, low-nutrient conditions created by the Blob, which are an extreme version of normal, stratified summer conditions in the CCE. Dinoflagellates have a variety of trophic strategies to survive in warm, low-nutrient conditions, such as mixotrophy (Stoecker 1999), while small size gives the chlorophytes an advantage as competitors for nutrient uptake. Moreover, not all of the dinoflagellate types identified by molecular analyses were functionally photosynthetic. Prymnesiophytes, whose presence was indicated in the V4 data, can also be mixotrophic (Unrein et al. 2014), enabling them to better compete in these environmental conditions.

We also hypothesized that the Blob would result in picoplankton-dominated communities, which was clearly supported by both the molecular results from our cruise

in August, which found abundant chlorophytes and *Synechococcus* at coastal sites, and microscopy biomass data available from the spring and summer 2014 CalCOFI cruises in the same area (Figs. 10b, 11c). In fact, picoplankton dominance during the Blob was quite striking, with the percent biomass nearly double in spring 2014 (48% vs. 24%) and more than double in summer 2014 (70% vs. 30%), compared to the 9-year means (Fig. 10b). This pattern of picoplankton dominance holds true for both auto- and heterotrophs (Figs. 10b, 11c), and directly contrasts with previous analyses in the CCE that did not find picoautotrophs dominant at any coastal or offshore location during multiple seasons over a 6-year period (Taylor et al. 2015). Thus, the shift in the size structure of the microbial community was highly unusual for the CCE and likely had a significant impact on the trophic dynamics of the food web.

In that regard, we found that phytoplankton growth rates were slightly lower at coastal sites in 2014 (mean 0.40 ± 0.10 d^{-1}) compared to rates reported for 2006 (mean 0.44 ± 0.12 d^{-1}) and 2007 (0.54 ± 0.11 d^{-1}, Table 1) in Landry et al. (2009). Chlorophytes dominated these regions in 2014, instead of the rapidly growing diatoms common in 2006-07, which likely explains this finding. However, grazing rates were significantly higher at coastal sites in 2014 (mean 0.39 ± 0.03 d^{-1}) compared to 2006 and 2007 (mean 0.29 ± 0.02 and 0.21 ± 0.09 d^{-1}, respectively), confirming our hypothesis of higher microzooplankton grazing impact during the Blob as a percentage of phytoplankton productivity. This is widely predicted to be a consequence of enhanced thermal stratification and temperature-related effects on grazer metabolism associated with global change (Behrenfeld 2006, Rose and Caron 2007, Chen et al. 2012). Our data indicate significant positive correlations between chlorophytes and multiple heterotrophic pico-

and nanoflagellate taxa (e.g. picozoans, choanoflagellates, and katablepharidophytes), who likely contributed to the overall increase in microzooplankton grazing rates.

The combination of reduced growth rates and higher microbial grazing pressure translated into overall elevated grazing pressure on phytoplankton during the Blob. At 2014 coastal sites, the mean percentage of daily growth grazed was 97%, compared to 68% in 2006 and 35% in 2007. This result is indicative of an enhanced coupling between phytoplankton growth and microherbivore consumption, which increases the mean trophic position of higher-level consumers and decreases the overall efficiency of energy transfer in the food web. This finding is further supported by the dominance of picoplankton during the Blob, which has not previously been documented to dominate the microbial community biomass in this region, and would shift the majority of grazing to the nano- and microzooplankton who are able to consume these small producers. The shift in community size structure to picophytoplankton dominance resulted in lower total biomass, and combined with the effects of temperature on grazer metabolism, altered the balance of growth-grazing dynamics in the food web. This would act to decrease the total energy available to higher trophic levels and may explain many of the negative effects observed on fish, seabirds and marine mammals during the Blob (Opar 2015, NOAA 2017).

Conclusions

The patterns observed in the current study, which includes multiple years and locations within the CCE, suggest two phytoplankton community modes in this region: diatom- and chlorophyte-dominated. This dichotomy may even override the often

dominant dinoflagellates, which were numerous in nearly all communities sampled in the CCE, but did not appear to have any significant correlations that would alter the growth-grazing dynamics of the food web as clearly as the diatoms and chlorophytes. Diatoms were significantly positively associated with high nutrient concentrations similar to those at upwelling regions, while chlorophytes were not associated with any specific environmental conditions measured here, suggesting they will rise in importance under conditions do not favor diatoms out-growing them. Furthermore, chlorophytes were strongly associated with the presence of small, heterotrophic flagellates and were found at coastal sites with much lower growth rates and higher microzooplankton grazing rates in 2014, suggesting that chlorophyte-dominated communities are both less productive and less efficient in transferring energy than diatom-dominated ones. If upwelling decreases in the future CCE as events like the Blob increase, it would be reasonable to expect more chlorophyte-dominated communities, with similar productivity and transfer characteristics, across the region.

The impacts of the 2014 Blob on the microbial community of the southern CCE was most apparent in the altered size structure. Pico-sized chlorophytes and *Synechococcus* have previously been observed to be important contributors to biomass at times in the CCE, but it was the extent to which these picoplankton dominated the community that significantly lowered the total biomass, altered growth-grazing dynamics at the base of the food web, and led to deleterious effects on higher organisms in the food web (Hendricks 2015, Gorman 2016, Peterson et al. 2016). Decreased energy available to higher organisms via this microbial assemblage not only highlights the importance of microzooplankton grazers in the food web of this region, but also points to other possible

implications of the Blob that were not investigated in this study. If phytoplankton were of lower nutritional quality for grazers during these conditions (Christaki et al. 1999, Jones et al. 2002, Jones and Flynn 2005), this would impact energy availability in ways undetectable by community composition and rate analysis. Alternatively, the impact of parasites and viral lysis on plankton mortality can be significant (Cottrell and Suttle 1995, Fuhrman and Noble 1995, Evans et al. 2003) and viral-phytoplankton dynamics are likely to be altered by changes in temperature and nutrient concentrations such as those in the Blob (Nagasaki and Yamaguchi 1998, Gachon et al. 2010, Danovaro et al. 2011). Such alternative sources of phytoplankton mortality would also shunt primary production away from higher trophic levels, converting it directly into dissolved and small particulate matter (Fuhrman 1999, Brussaard 2004, Haaber and Middelboe 2009). As unusual climate events such as the Blob become more common with climate variability in the future, it is imperative to further document the implications of altered community composition and growth-grazing dynamics on the multiple pathways of energy transfer in the marine food web.

Acknowledgements

Thank you to the captain and crew of the *R/V Melville*. Special thanks to Ralf Goericke and Megan Roadman for collecting and analyzing many of the samples during this cruise and for providing the chlorophyll, nutrient, and primary production data. Thanks to Karen Beeri for her expertise with sequencing, Hong Zheng for her support while processing molecular samples, and Andrés Gutiérrez-Rodríguez for his advice on data analysis. The 2014 cruise was supported by the U.S. National Science Foundation

grant OCE 10-26607 to the CCE LTER Program and molecular sample analyses was supported through the Mullin Fellowship from the Scripps Institution of Oceanography to A. Freibott.

Table 5.1 Community phytoplankton growth (day^{-1}) and grazing rates (day^{-1}) from 2-treatment dilution experiments conducted in the southern California Current during May 2006, April 2007 and August 2014. Mean rates ± 1 standard deviation are shown for each location.

	2006			2007			2014		
Location	**Cycle**	**Growth (d^{-1})**	**Grazing (d^{-1})**	**Cycle**	**Growth (d^{-1})**	**Grazing (d^{-1})**	**Cycle**	**Growth (d^{-1})**	**Grazing (d^{-1})**
Coastal	1	0.56 ± 0.10	0.32 ± 0.17	1	0.54 ± 0.11	0.21 ± 0.09	1	0.24 ± 0.09	0.34 ± 0.05
	3	0.32 ± 0.07	0.28 ± 0.10				2	0.39 ± 0.08	0.28 ± 0.09
	4	0.51 ± 0.04	0.23 ± 0.04	4	0.65 ± 0.05	0.33 ± 0.04	3	0.58 ± 0.07	0.55 ± 0.13
CA Current	2	0.54 ± 0.08	0.43 ± 0.22				4	0.35 ± 0.07	0.32 ± 0.06
Offshore	5	0.36 ± 0.04	0.32 ± 0.05	2	0.28 ± 0.04	0.30 ± 0.04	5	0.39 ± 0.03	0.27 ± 0.04

Table 5.2 Percent daily phytoplankton growth grazed (%) determined via flow cytometry results for *Synechococcus* (*Syn*), *Prochlorococcus* (*Pro*), and picoeukaryotes (Peuk). Means ± 1 standard deviation are shown for cycles that had multiple days of dilution experiments in the same water parcel.

		Mean Daily Growth Grazed (%)					
		Size Fractioned 200-µm			2-treatment		
Location	**Cycle**	***Syn***	***Pro***	**Peuk**	***Syn***	***Pro***	**Peuk**
Coastal	1	-	-	-	76 ± 25	63 ± 28	111 ± 15
	2	128 ± 80	134	126 ± 44	53 ± 31	94 ± 23	95 ± 25
	3	101 ± 73	71 ± 30	66 ± 3	161 ± 108	79 ± 11	111 ± 17
	(Mean)	*(114 ± 5)*	*(134 ± 30)*	*(96 ± 29)*	*(96 ± 57)*	*(79 ± 8)*	*(105 ± 9)*
CA Current	4	67 ± 36	232	96	271 ± 302	121 ± 80	91 ± 30
Offshore	5	63 ± 12	81 ± 16	46 ± 39	146 ± 77	91 ± 27	175 ± 144

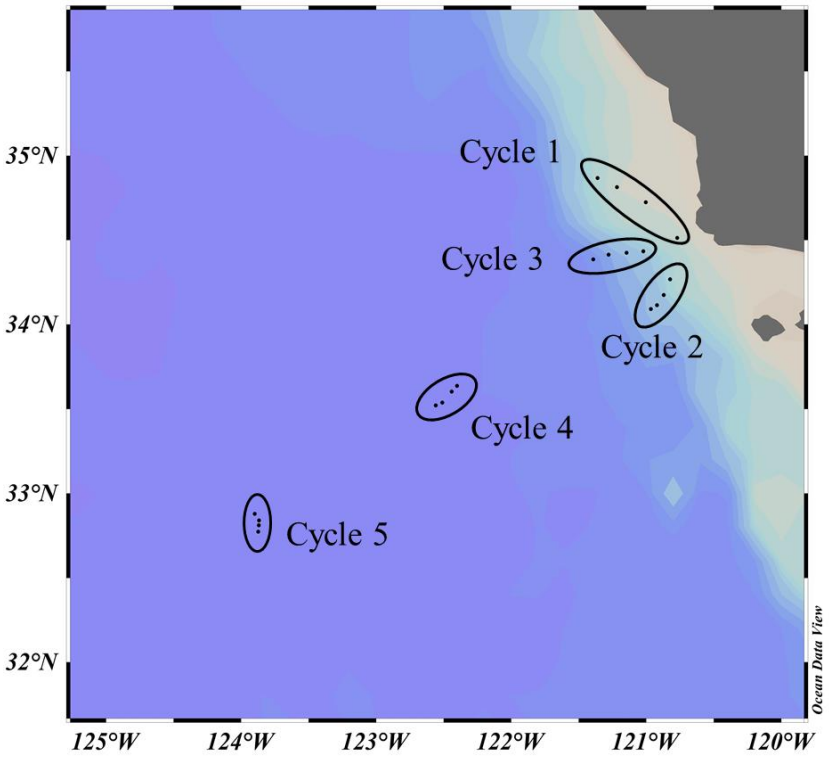

Figure 5.1 Daily sample locations for each of the five experimental cycles conducted during the spring 2014 cruise.

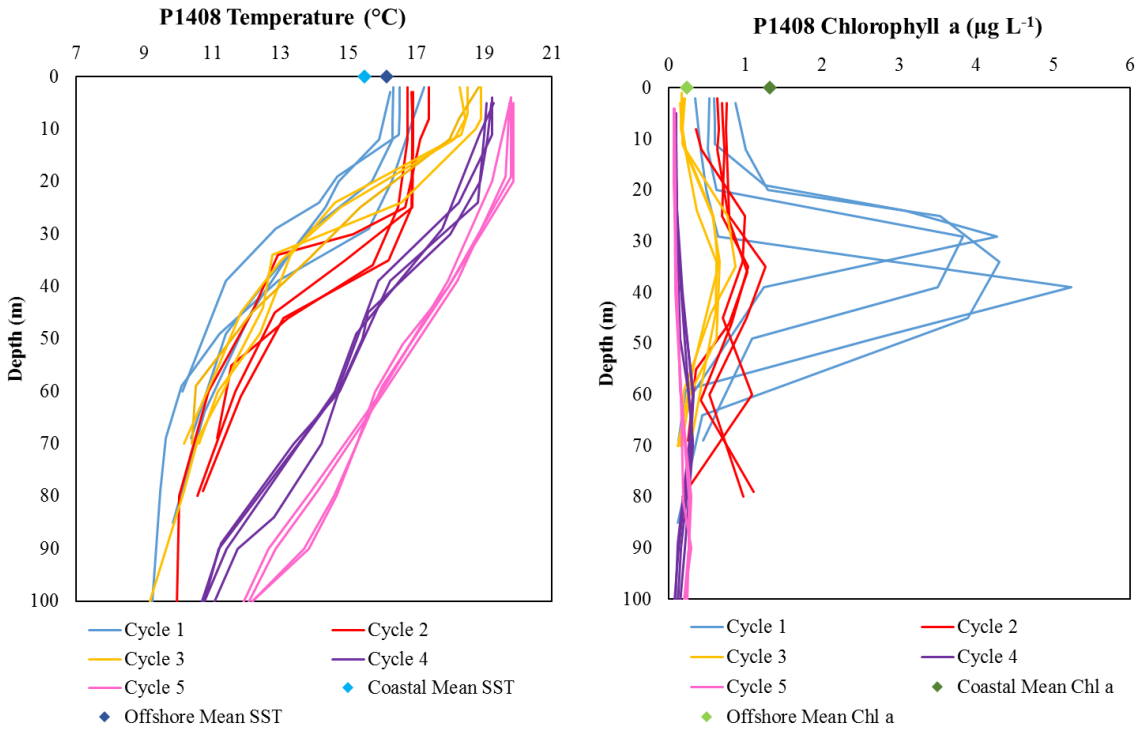

Figure 5.2 Vertical profiles of (a) temperature and chlorophyll a fluorescence from the daily casts that were used to collect water for the minidiultion and size-fractioned dilution experiments in all cycles. The diamonds on the x-axis indicate the average surface values of stations on lines 80 and 90 of the California Cooperative Oceanic Fisheries Investigations (CalCOFI) between 2004-2013 for comparison.

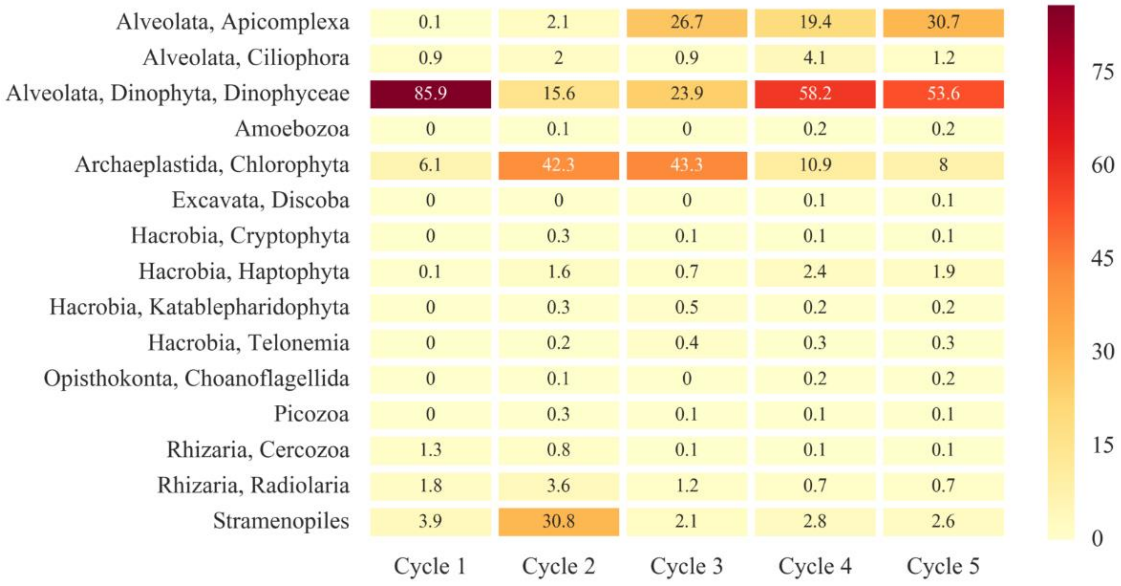

Figure 5.3 Percent abundance of sequences from 18S V9 analyses of seawater samples averaged across multiple days in the same cycle.

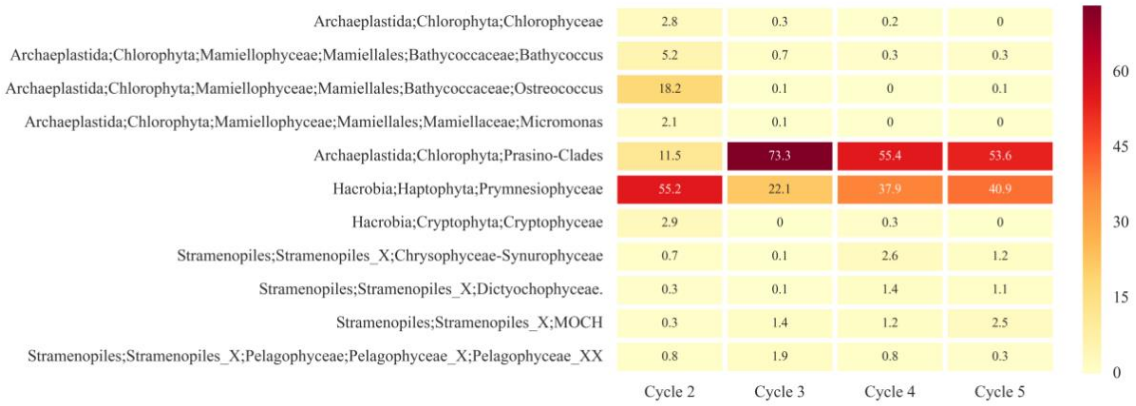

Figure 5.4 Percent abundance of sequences from 18S V4 analyses of seawater samples for known picoeukaryote taxa, averaged across multiple days in the same cycle.

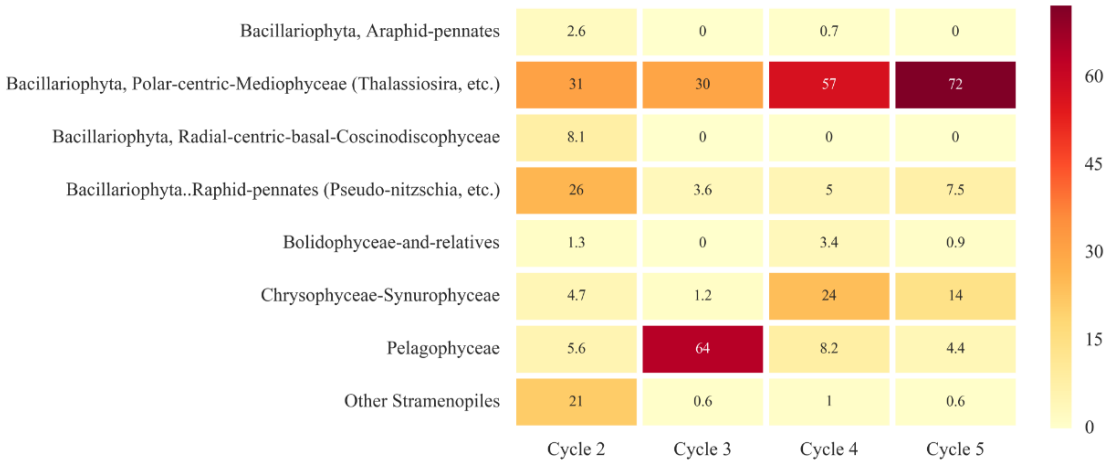

Figure 5.5 Percent abundance of sequences from 18S V4 analyses of seawater samples for Stramenopile taxa, averaged across multiple days in the same cycle.

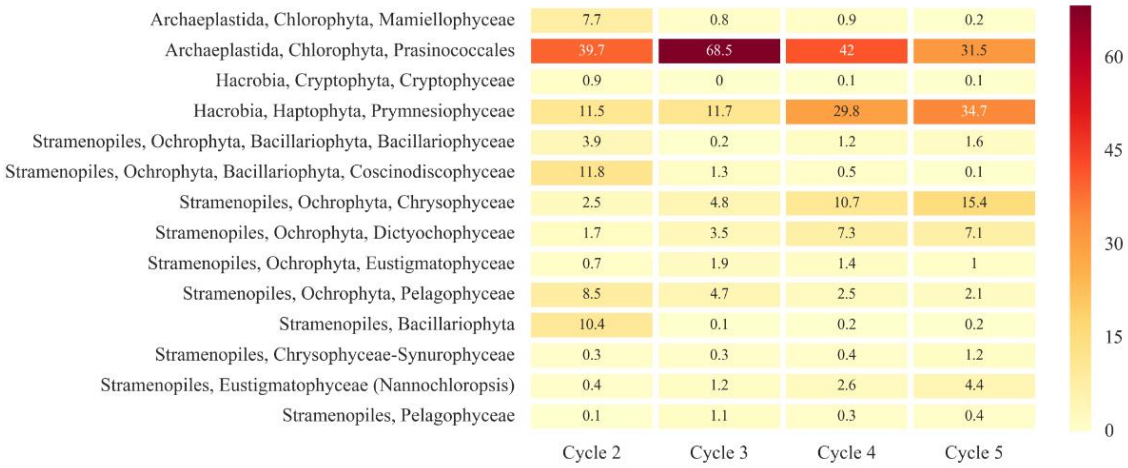

Figure 5.6 Percent abundance of sequences identified as plastids from 16S analyses of seawater samples, averaged across multiple days in the same cycle.

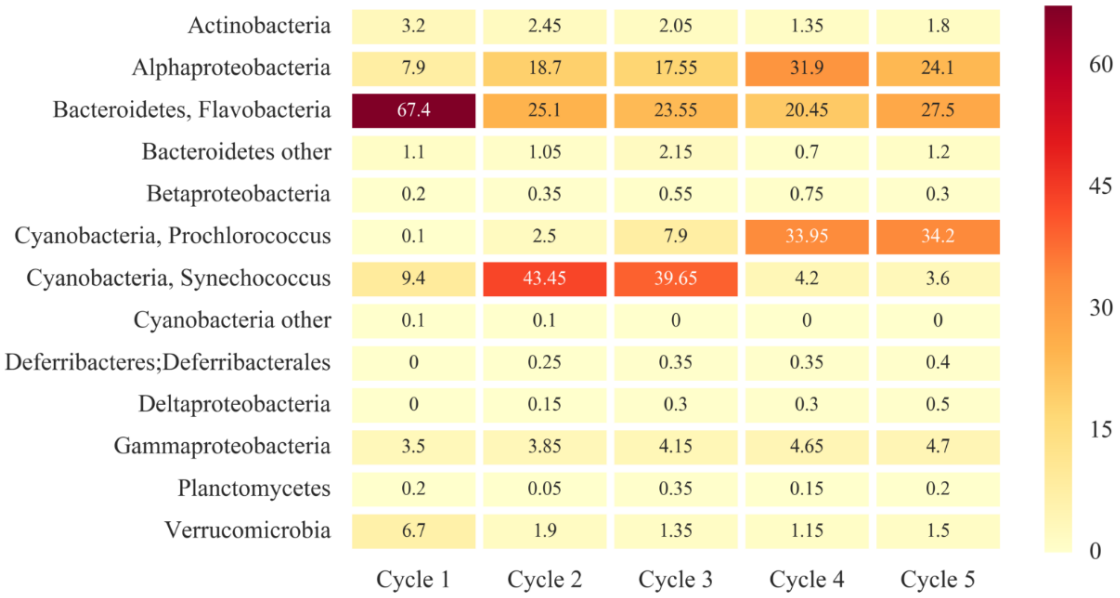

Figure 5.7 Percent abundance of sequences from 16S analyses of seawater samples, averaged across multiple days in the same cycle.

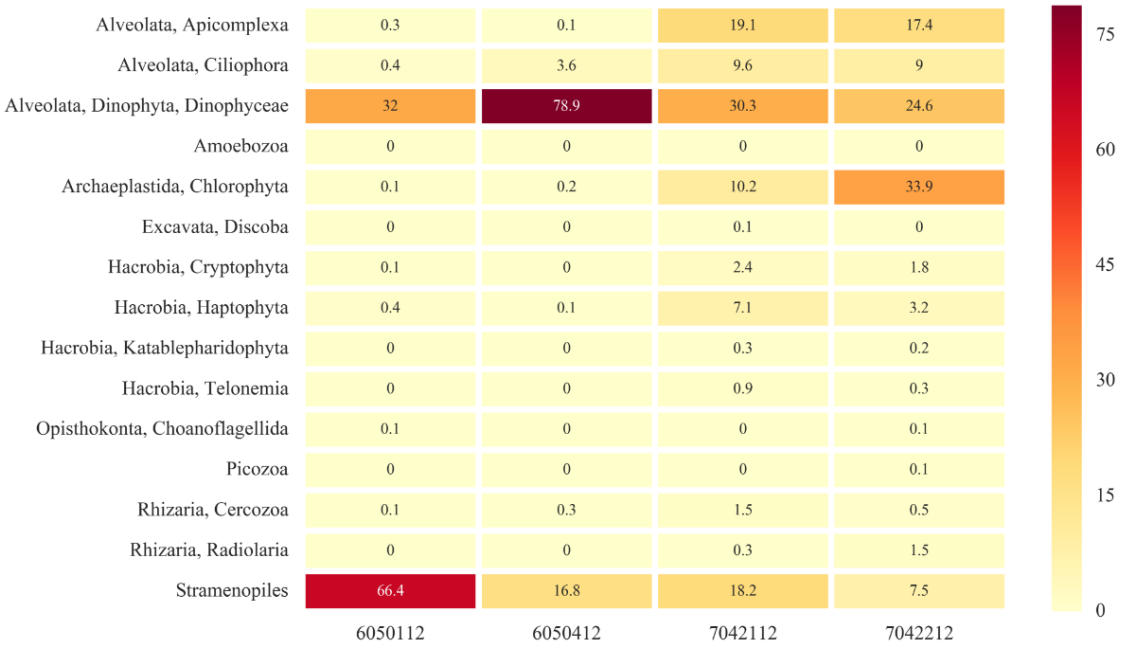

Figure 5.8 Percent abundance of sequences from 18S V9 analyses of seawater samples from 4 coastal locations in the southern California Current during May 2006 and April 2007.

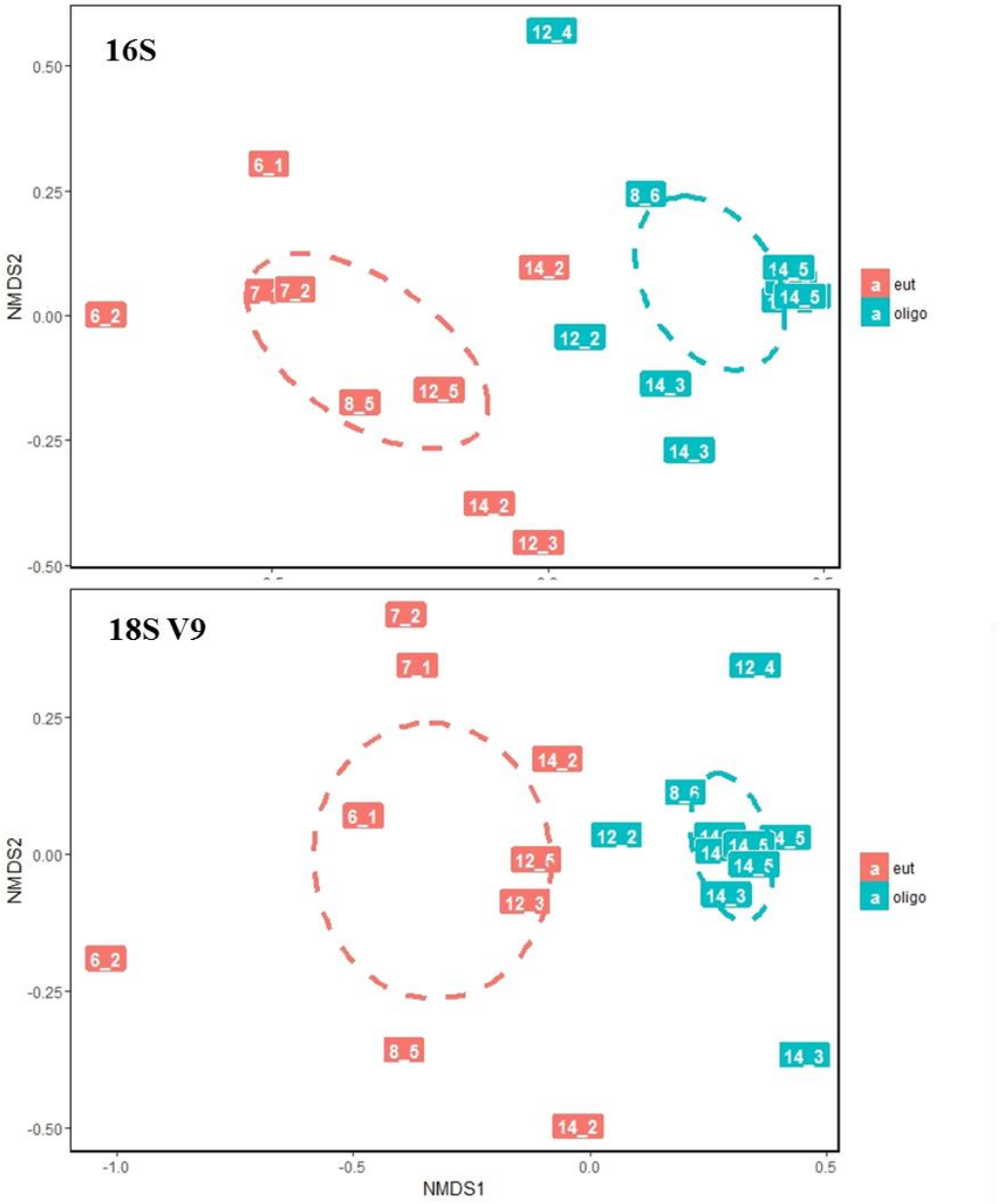

Figure 5.9 NMDS plots of Bray-Curtis dissimilarity for molecular analyses of 18S V9 and 16S rDNA (b, n=17). Included in the analysis with 2014 data are all available samples from the CCE for comparison, including: coastal samples from 2006, 2 coastal samples from 2007, and non-front samples from 2008 and 2012, previously reported in Chapter 4. Ellipses show 95% confidence intervals around the weighted average means for each of the two groups: eutrophic and oligotrophic. Samples with integrated chlorophyll a levels ≥ 1 mg Chl a m^{-2} and/or ≥ 0.5 µM nitrate and nitrite concentrations were categorized as eutrophic (eut) and those < 1 mg Chl a m^{-2} and/or < 0.5 µM nitrate and nitrite concentrations were categorized as oligotrophic (oligo). Labels inside the symbols indicate the year and cycle location of each sample: 6_1 = Cycle 1 in 2006, 7_1 = Cycle 1 in 2007, 8_5 = Cycle 5 in 2008, etc.

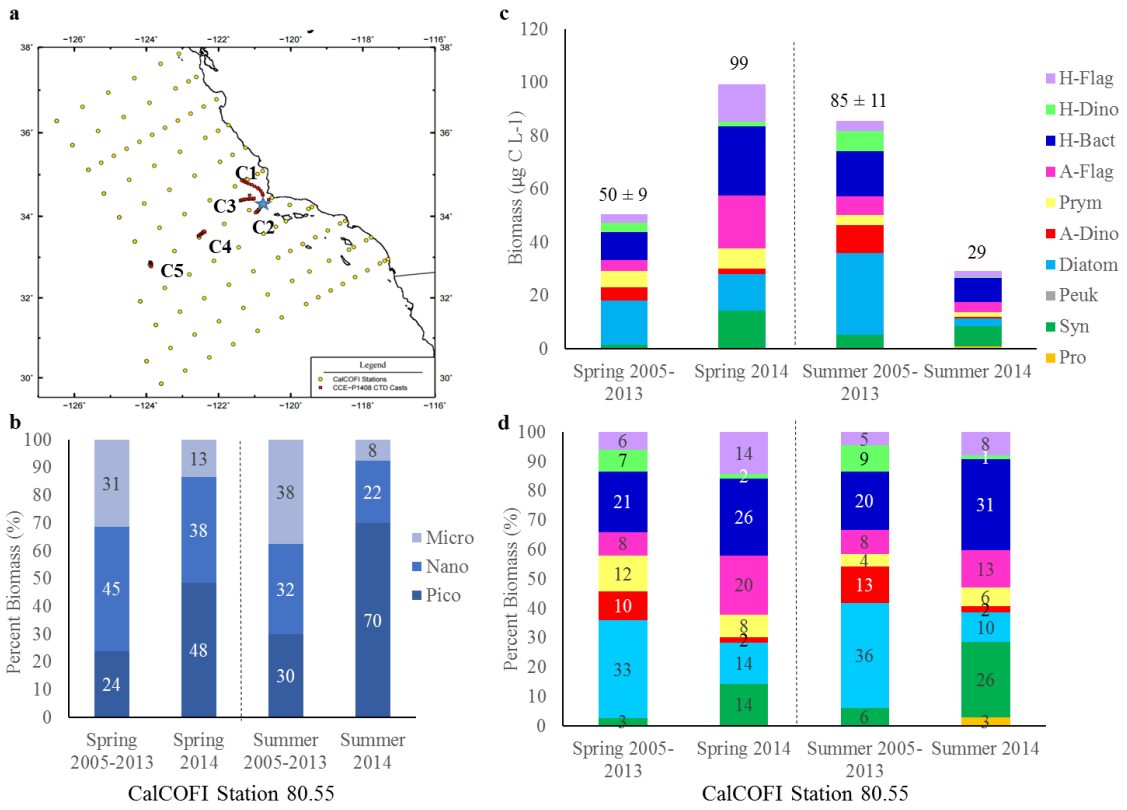

Figure 5.10 Map of the (a) CalCOFI station grid (yellow circles) with CCE 2014 cruise cycle locations (C1-C5) overlaid (red squares). Blue star indicates CalCOFI station 80.55. (b) Mean percent biomass (%) of each size class for all the taxa at coastal CalCOFI station 80.55 during spring and summer 2005-2013 compared to spring and summer 2014. Dotted line separates spring and summer data. (c) Mean biomass (µg C L^{-1}) for the same station and same years and (d) percent biomass (%). Captions above the bars in (c) indicate mean total biomass ± standard error for 2005-2013. Abbreviations used for taxa are: Pro for *Prochlorococcus*, Syn for *Synechococcus*, A-Dino for autotrophic dinoflagellate, Prym for prymnesiophyte, A-Flag for autotrophic flagellate, H-Bact for heterotrophic bacteria, H-Dino for heterotrophic dinoflagellate, and H-Flag for heterotrophic flagellate.

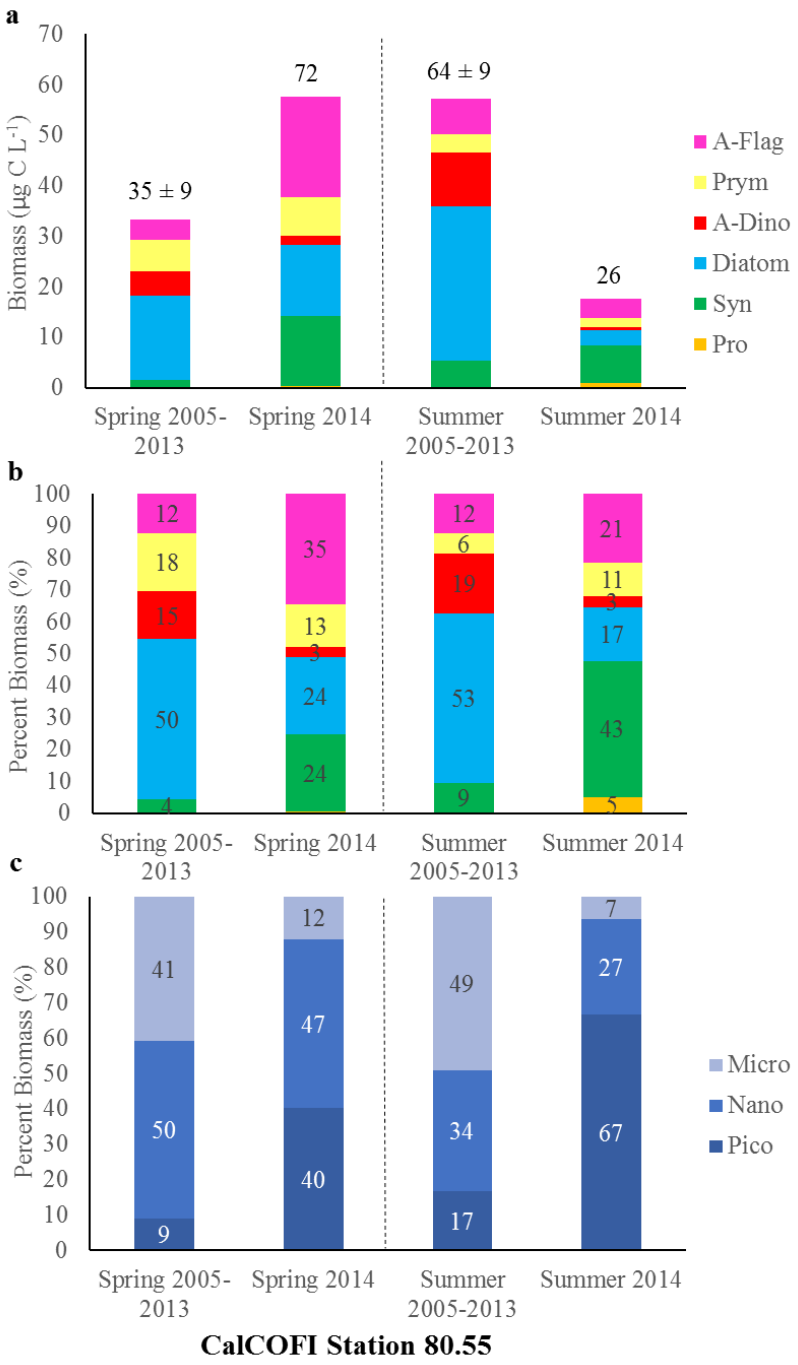

Figure 5.11 (a) Mean biomass (µg C L^{-1}) of autotrophic taxa at coastal CalCOFI station 80.55 during spring and summer 2005-2013 compared to spring and summer 2014. Percent biomass (%) is shown for each autotrophic taxa (b) and size class (c) for the same locations and years. Captions above the bars in (a) indicate mean total biomass ± standard error for 2005-2013. Dotted line separates spring and summer data.

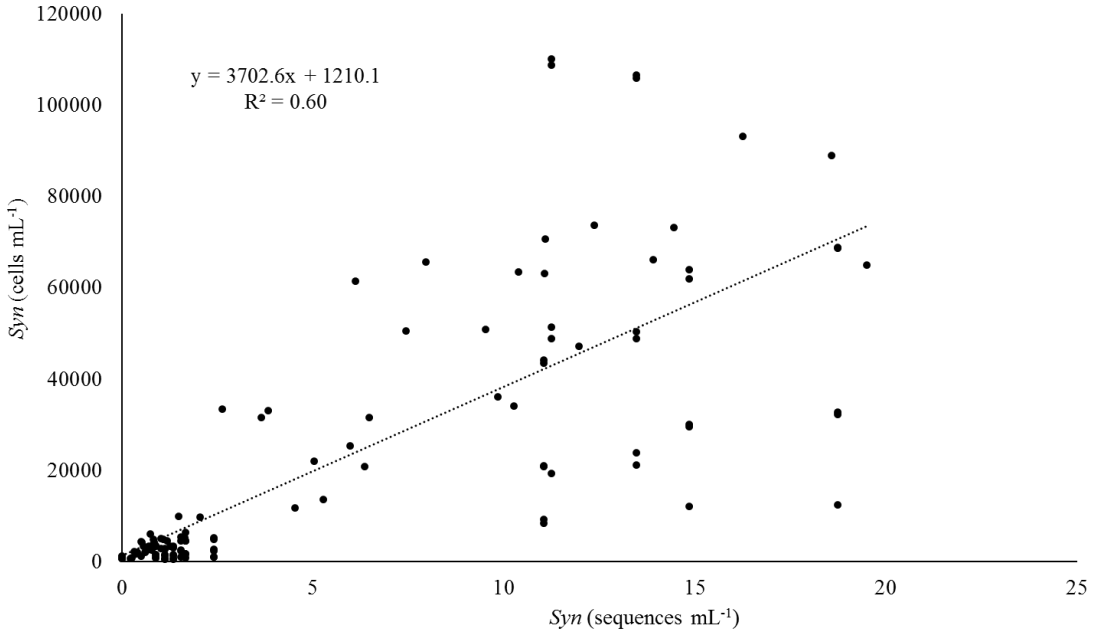

Figure 5.12 Relationship between the abundance of *Synechococcus* sequences (ml^{-1}) determined via 16S analyses and the abundance of *Synechococcus* cells (ml^{-1}) determined via flow cytometry ($y = 3702.6x + 1201.1$, $R^2 = 0.60$).

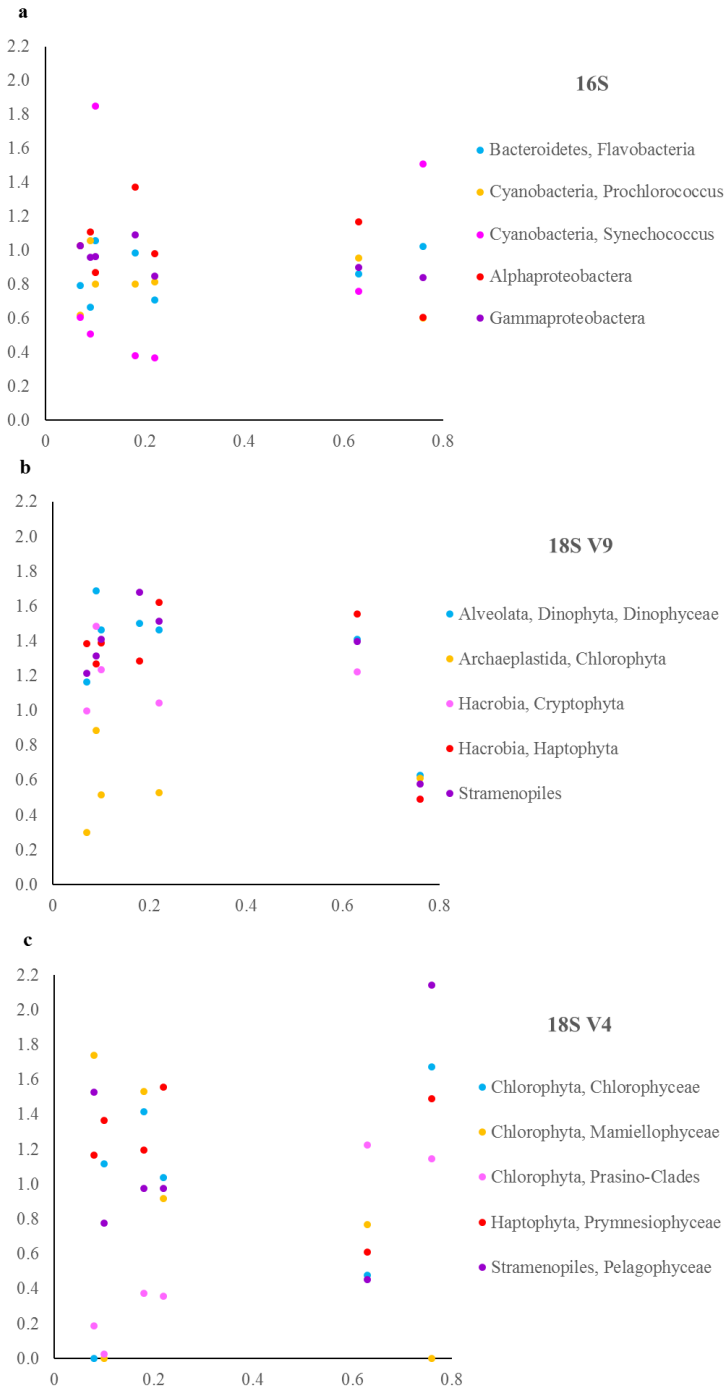

Figure 5.13 Growth rates (day^{-1}) of 5 selected taxa of interest from (a) 16S, (b) 18S V9, and (c) 18S V4 datasets versus chlorophyll *a* (µg L^{-1}) in the mixed layer of each sample location.

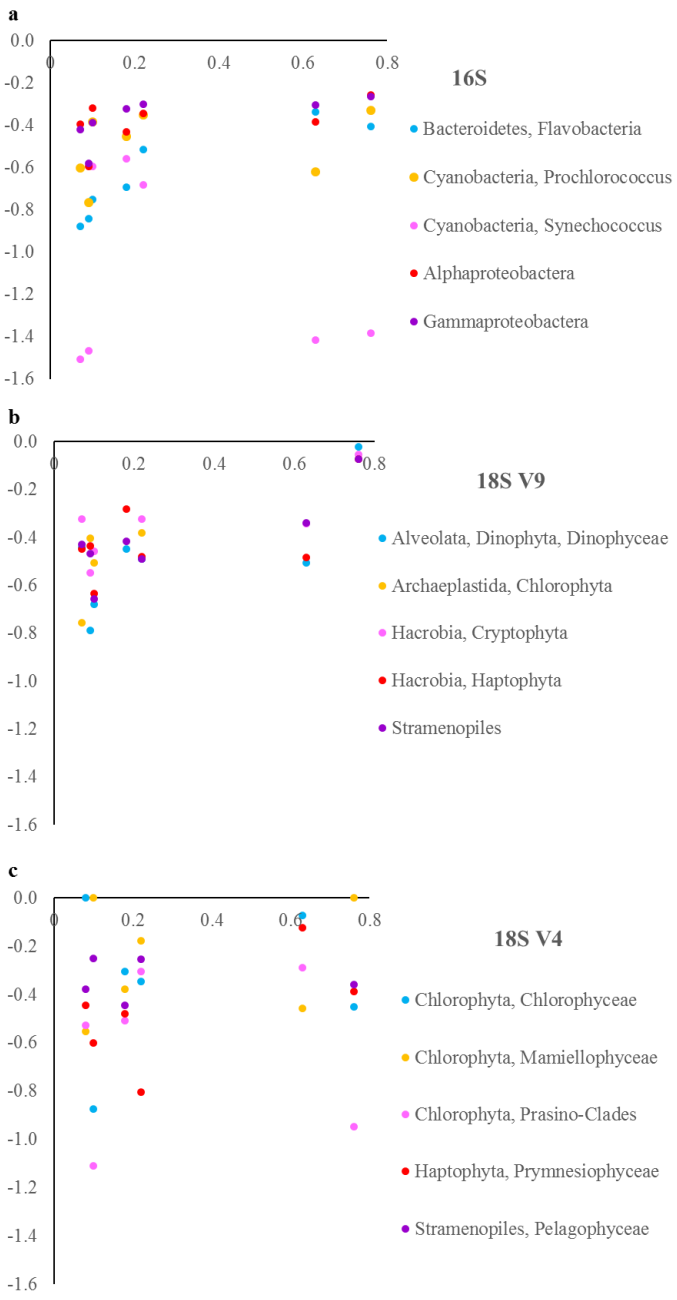

Figure 5.14 Rates of mortality due to microzooplankton grazing (day^{-1}) for 5 selected taxa of interest from (a) 16S, (b) 18S V9, and (c) 18S V4 versus chlorophyll *a* ($\mu g\ L^{-1}$) in the mixed layer of each sample location.

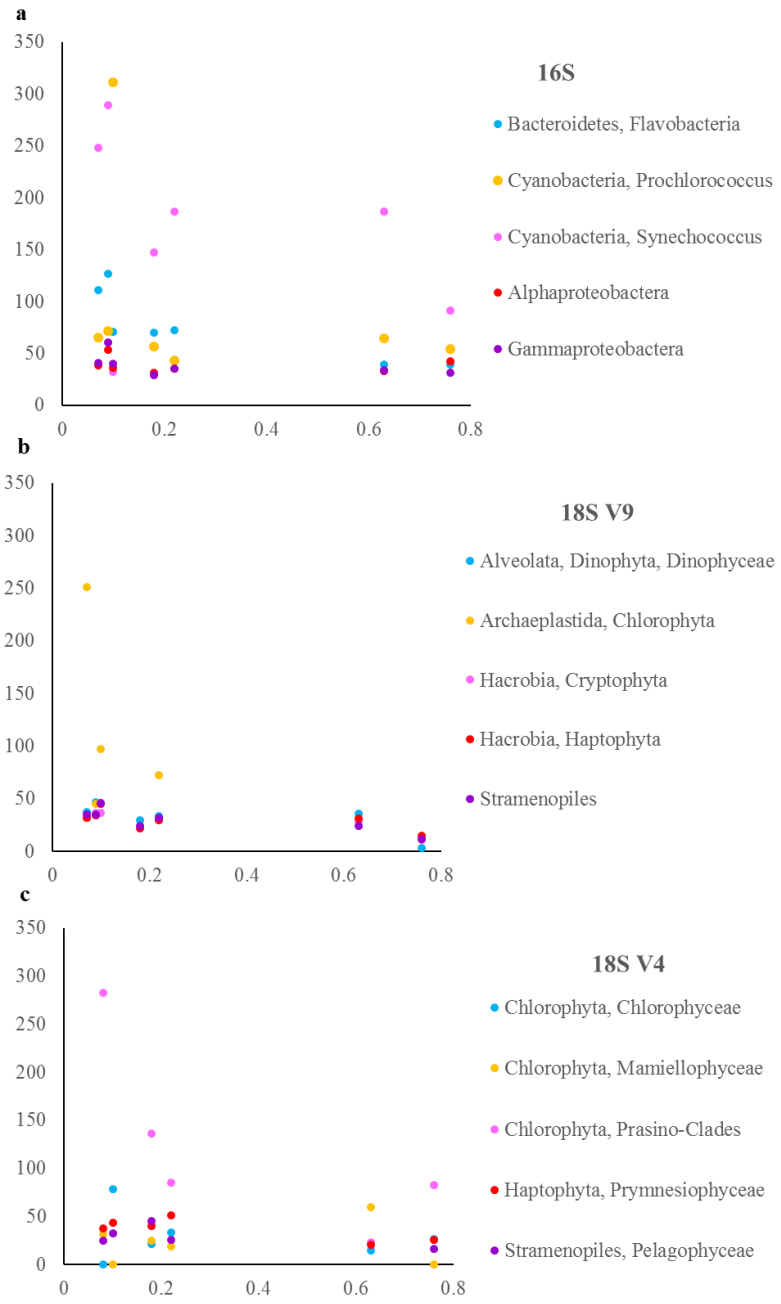

Figure 5.15 Percent of the daily phytoplankton growth grazed (%) for 5 selected taxa of interest from (a) 16S, (b) 18S V9, and (c) 18S V4 versus chlorophyll *a* (µg L^{-1}) in the mixed layer of each sample location.

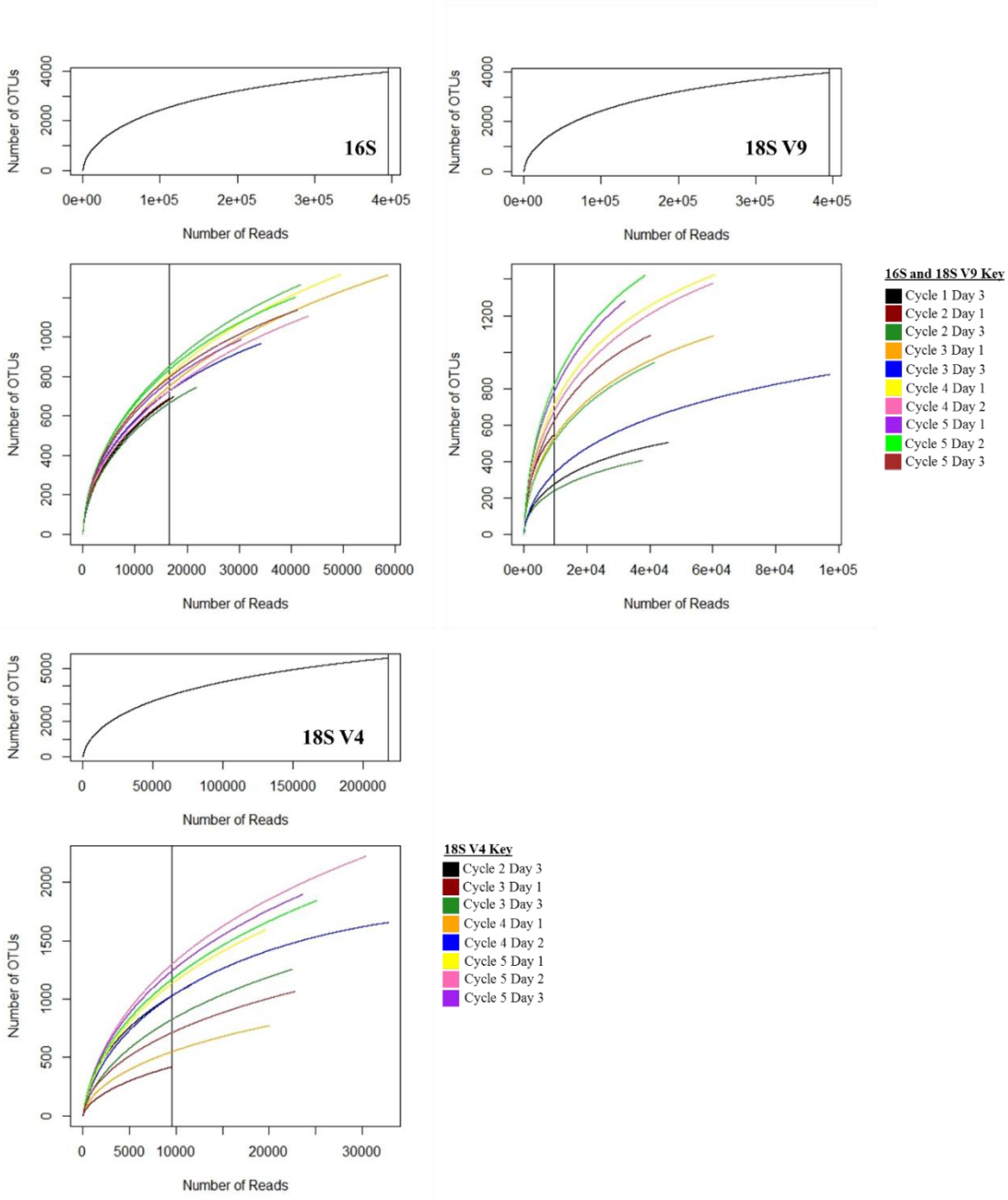

Supplementary Figure 5.1 Rarefaction curves for all OTUs by sample in the 16S, 18S V9, and 18S V9 datasets.

References

Allen, L. Z., Allen, E. E., Badger, J. H., McCrow, J. P., Paulsen, I. T., Elbourne, L. D. H., Thiagarajan, M., Rusch, D. B., Nealson, K. H., Williamson, S. J. Venter, J. C., and Allen, A. E. (2012) Influence of nutrients and current on the genomic composition of microbes across an upwelling mosaic. *ISME Journal*, 6:1402-1414.

Behrenfeld, M. J. (2006) Climate-driven trends in contemporary ocean productivity. Nature, 444:752-755.

Binder, B. J., Chisholm, S. W., Olson, R. J., Frankel, S. L., and Worden, A. Z. (1996) Dynamics of picophytoplankton, ultraphytoplankton and bacteria in the central equatorial Pacific. *Deep-Sea Research II*, 43(4-6):907-931.

Boenigk, J., and Arndt, H. (2000) Comparative studies on the feeding behavior of two heterotrophic nanoflagellates: the filter-feeding choanoflagellate *Monosiga ovata* and the raptorial-feeding kinetoplastid *Rhynchomonas nasuta*. *Aquatic Microbial Ecology*, 22:243-249.

Brown, J. H., et al. (2004) Toward a metabolic theory of ecology. *Ecology*, 85:1771-1789.

Brown, S. L., Landry, M. R., Yang, E. J., Rii, Y. M., and Bidigare, R. R. (2008) Diatoms in the desert: Plankton community response to a mesoscale eddy in the subtropical North Pacific. *Deep Sea Research II*, 55:1321–1333.

Brussaard, C. P. D. (2004) Viral control of phytoplankton populations – a review. *Eukaryotic Microbiology,* 51(2):125-138.

Checkley, D. M., and Barth, J. A. (2009) Patterns and processes in the California Current System. *Progress in Oceanography*, *83*(1):49-64.

Chen, B., et al. (2012) Does warming enhance the effect of microzooplankton grazing on marine phytoplankton in the ocean? *Limnology and Oceanography*, 57:519-526.

Christaki, U., Jacquet, S., Dolan, J. R., Valuot, D., and Rassoulzadegan, F. (1999) Growth and grazing on *Prochlorococcus* and *Synechococcus* by two marine ciliates. *Limnology and Oceaongraphy*, 44(1):52-61.

Cottrell, M. T., and Suttle, C. A. (1995) Dynamics of lytic virus infecting the photosynthetic marine picoflagellate *Micromonas pusilla*. *Limnology and Oceanography,* 40(4):730-739.

Danovaro, R., Corinaldesi, C., Dell'Anno, A., Fuhrman, J. A., Middelburg, J. J., Noble, R. T., and Suttle, C. A. (2011) Marine viruses and global climate change. *FEMS Microbiology Reviews,* 35(6): 993-1034.

Decelle, J., Romac, S., Stern, R. F., Bendif, el M., Zingone, A., Audic, S., Guiry, M. D., Guillou, L., Tessier, D., Le Gall, F., Gourvil, P., Dos Santos, A. L., Probert, I., Vaulot, D., de Vargas, C., Christen, R. (2015) PhytoREF: a reference database of the plastidial 16S rRNA gene of photosynthetic eukaryotes with curated taxonomy. *Molecular Ecological Resources,* 15(6):1435-45.

De Vargas, C., Audic, S., Henry, N., Decelle, J., Mahé, F., Logares, R., Lara, E., Berney, C., Le Bescot, N., Probert, I., and Carmichael, M. (2015) Eukaryotic plankton diversity in the sunlit ocean. *Science,* 348(6237):1261605-1-1261695-11.

Di Lorenzo, E., and Mantua, N. (2016) Multi-year persistence of the 2014/15 North Pacific marine heatwave. *Nature Climate Change,* 6:1042-1048.

Edgar, R. C. (2010) Search and clustering orders of magnitude faster than BLAST. *Bioinformatics,* 26(19):2460-2461.

Evans, C., Archer, S. D., Jacquet, S., and Wilson, W. H. (2003) Direct estimates of the contribution of viral lysis and microzooplankton grazing to the decline of a *Micromonas* spp. Population. *Aquatic Microbial Ecology*, 30:207-219.

Fuhrman, J. A., and Noble, R. T. (1995) Viruses and protists cause similar bacterial mortality in coastal seawater. *Limnology and Oceanography*, 40(7);1236-1242.

Fuhrman, J. A. (1999) Marine viruses and their biogeochemical and ecological effects. *Nature*, 399:541-548.

Gachon, C. M. M., Sime-Ngando, T., Strittmatter, M., Chambouvet, A., and Kim, H. K. (2010) Algal diseases: spotlight on a black box. *Trends in Plant Science,* 15(11):633-640.

Garrison, D. L., Gowing, M. M., Hughes, M. P., Campbell, L., Caron, D. A., Dennett, M. R., Shalapyonok, A., Olson, R. J., Landry, M. R., Brown, S. L., Liu, H., Azam, F., Steward, G. F., Ducklow, H. W., and Smith, D. C. (2000) Microbial food web structure in the Arabian Sea: a US JGOFS study. *Deep Sea Research II,* 47:1387-1422.

Gómez-Ocampo, E., Gaxiola-Castro, G., Durazo, R., and Beier, E. (2017) Effects of the 2013-16 warm anomalies on the California Current phytoplankton. *Deep-Sea Research II,* http://dx.doi.org/10.1016/j.dsr2.2017.01.005

Gorman, S. (May 17, 2016) Red tuna crabs carpet southern California beaches again. *Rueters.*

Haaber, J., and Middelboe, M. (2009) Viral lysis of *Phaeocystis poughetii:* Implications for algal population dynamics and heterotrophic C, N, and P cycling. *ISME Journal,* 3:420-441.

Hendricks, J. (June 1, 2015) Bluefin tuna invade southern California waters. *Sport Fishing*.

Jones, R. J., Flynn, K. J., and Anderson, T. R. (2002) Effect of food quality on carbon and nitrogen growth efficiencies in the copepod *Acartia tonsa. Marine Ecology Progress Series,* 235:147-156.

Jones, R. H., and Flynn, K. J. (2005) Nutritional status and diet composition affect the value of diatoms as copepod prey. *Science,* 307(5714):1457-1459.

Kintish, E. (2015) 'The Blob' invades Pacific, flummoxing climate experts. *Science,* 348(6230):17-18.

Landry, M. R., & Hassett, R. (1982) Estimating the grazing impact of marine micro-zooplankton. *Marine Biology,* 67(3):283-288.

Landry, M. R., Ohman, M. D, Georicke, R., Stukel, M. R., and Tsyrklevich, K. (2009) Lagrangian studies of phytoplankton growth and grazing relationships in a coastal upwelling ecosystem off Southern California. *Progress in Oceanography,* 83:208-216.

Leising, A. W., Schroeder, I. D., Bograd, S.J., Abell, J., Durazo, R., Gaxiola-Castro, G., Bjorkstedt, E. P., Field, J., Sakuma, K., Robertson, R. R., Goericke, R., Peterson, W. T., Brodeur, R., Barceló, C., Auth, T. D., Daly, E. A., Suryan, R. M., Gladics, A. J., Porquez, J. M., McClatchie, S., Weber, E. D., Watson, W., Santora, J. A., Sydeman, W. J., Melin, S. R., Chavez, F. P., Golightly, R. T., Schneider, S. R., Fisher, J., Morgan, C., Bradley, R., Warybok, P. (2015) State of the California Current 2014-15: Impacts of the warm-water "Blob."

Lürling, M., Eshetu, F., Faassen, E. J., Kosten, S., and Huszar, V. L. M. (2012) Comparison of cyanobacterial and green algal growth rates at different temperatures. *Freshwater Biology,* 58(3):552-559.

Mahé, F., Rognes, T., Quince, C., de Vargas, C., and Dunthorn, M. (2014) Swarm: robust and fast clustering method for amplicon-based studies. *PeerJ,* 2.

Marchant, H. J., and Scott, F. J. (1993) Uptake of sub-micrometre particles and dissolved organic material by Antarctic choanoflagellates. *Marine Ecology Progress Series*, 92:59-64.

Monger, B. C., and Landry, M. R. (1993) Flow cytometric analysis of marine bacteria with Hoechst 33342. *Applied and Environmental Microbiology*, 59(3):905-911.

Morris, R. M., Longnecker, K., and Giovannoni, S. J. (2006) *Pirellula* and OM43 are among the dominant lineages identified in an Oregon coast diatom bloom. *Environmental Microbiology*, 8(8):1361-1370.

Nagasaki, K., and Yamaguchi, M. (1998) Effect of temperature on the algicidal activity and the stability of HaV (*Heterosigma akashiwo* virus). *Aquatic Microbial Ecology*, 15(3):211-216.

National Oceanic and Atmospheric Administration Fisheries (2017) 2013-2017 California Sea Lion unusual mortality event in California.

Opar, A. (March-April 2015) Lost at sea: Starving birds in a warming world. *Audobon Magazine.*

Pearson, W. R., Lipman, D. J. (1988) Improved tools for biological sequence comparison. *Proceedings of the National Academy of Science*, 85(5):2444-2448.

Peterson, W., Robert, M., and Bond, N. (2015a) The warm blob – Conditions in the northeastern Pacific Ocean. *PICES Press*, 23(1):37-38.

Peterson, W., Robert, M., and Bond, N. (2015b) The warm Blob continues to dominate the ecosystem of the northern California Current. *PICES Press*, 23(2):44-46.

Peterson, W., Bond, N., and Robert, M. (2016) The Blob (Part Three): Going, going, gone? *PICES Press*, 24 (1):46-48.

Pizetti, I., Ruchs, B. M., Gerdts, G., Wichels, A., Wiltshire, K. H., and Amann, R. (2011) Temporal variability of coastal *Planctomycetes* clades at Kabeltonne Station, North Sea. *Applied and Environmental Microbiology*, 77(14):5009-5017.

Oksanen J, Blanchet FG, Friendly M, Kindt R, Legendre P, McGlinn D, Minchin PR, O'Hara RB, Simpson GL, Solymos P, Stevens MHH, Szoecs E, Wagner H (2016) Vegan: Community Ecology Package. R package version 2.4-1. https://CRAN.R-project.org/package=vegan

Okamoto, N., Chantangsi, C., Hork, A., Leander, B. S., and Keeling, P. J. (2009) Molecular phylogeny and description of the novel katablepharid *Roombia truncta*

gen. et sp. Nov., and establishment of the Hacrobia taxon nov. *PLoS ONE*, 4(9):e7080.

Quast, C., Pruesse, E., Yilmaz, P., Gerken, J., Schweer, T., Yarza, P., Peplies, J., and Glöckner, F. O. (2013) The SILVA ribosomal RNA gene database project: improved data processing and web-based tools. *Nucleic Acids Research*, 41(D1):D590-D596.

Rose, J. M., and Caron, D. A. (2007) Does low temperature constrain the growth rates of heterotrophic protists? Evidence and implications for algal blooms in cold waters. Limnology and Oceanography, 52: 886-895.

Seenivasan, R., Sausen, N., Medlin, L. K., Melkonian, M. (2013) *Picomonas judraskeda* Gen. Et. Sp. Nov.: The first identified member of the Picozoa phylum nov., a Widespread group of picoeukaryotes, formerly known as 'picobiliphytes.' *PLoS ONE*, 8(3): e59565.

Stoecker, D. K. (1999) Mixotrophy among dinoflagellates. *Journal of Eukaryotic Microbiology*, 46(4):397-401.

Taylor, A. G., Landry, M. R., Selph, K. E., and Wokuluk, J. J. (2015) Temporal and spatial patterns of microbial community biomass and composition in the Southern California Current Ecosystem. *Deep Sea Research II*, 112:117-128.

Taylor, A. G., Goericke, R., Landry, M. R., Selph, K. E., Wick, D. A., and Roadman, M. J. (2012) Sharp gradients in phytoplankton community structure across a frontal zone in the California Current Ecosystem. *Journal of Plankton Research*, 34(9):778-789.

Unrein, F., Gasol, J. M., Not, F., Forn, I., and Massana, R. (2014) Mixotrophic haptophytes are key bacterial grazers in oligotrophic coastal waters. *ISME Journal*, 8:164-176.

Whitney, F. A. (2015) Anomalous winter winds decrease 2014 transition zone productivity in the NE Pacific. *Geophysical Research Letters*, 42:428-431.

Worden, A. Z., Nolan, J. K., and Palenik, B. (2004) Assessing the dynamics and ecology of marine picophytoplankton: The importance of the eukaryotic component. *Limnology & Oceanography*, 49(1):168-179.

Zhang, J., Kobert, K., Flouri, T., and Stamatakis, A. (2014) PEAR: A fast and accurate Illumina Paired-End reAd mergeR. *Bioinformatics*, 30(5):614-620.

Chapter 5, in full, is currently being prepared for submission for publication of the material with the following co-authors: Freibott, A., Rabines, A., McCrow, K.E., Allen, A.E., Landry, M.R. The dissertation author was the primary investigator and author of this paper.

CHAPTER 6.

Conclusions

As presented in the introduction, and seen in the results of my thesis chapters, microzooplankton play critical and complex roles in the marine food web. To highlight the important results found during my research, I will discuss the findings relevant to the guiding research questions stated previously: What is the range in diversity and grazing rates seen in microzooplankton communities across trophic gradients in the eastern Pacific? How are microzooplankton composition and grazing activities shaped by the plankton communities they feed on? What insights can molecular analyses provide about the taxa-specific grazing impacts of microzooplankton on their phytoplankton prey?

Major findings

In order to accurately assess the major groups that comprised the microzooplankton assemblages in my study areas, I needed to develop a time-efficient method for enumerating the ciliates that had previously been underestimated by epifluorescence microscopy. I developed a microscopy technique that can be used to filter ciliates preserved in traditional acid Lugol's fixative onto polycarbonate membranes. Many microscopy preparations (i.e., epifluorescence microscopy, filter-transfer-freeze) that required additional fixatives or heating/cooling techniques were too

destructive to fragile ciliates and resulted in significant underestimates of their abundance and biomass in plankton communities. Furthermore, the long-established settling chamber method for counting ciliates is very time consuming, and does not maintain a sample preparation for additional or repeated analysis, and does not allow imaging by automated microscopy techniques because the cells are suspended in liquid. The method I presented in Chapter 2 addressed these issues and provided a convenient alternative for obtaining accurate counts of ciliates in natural communities. I used this method to characterize the composition of microzooplankton assemblages in both the Costa Rica Dome (CRD, Chapter 3) and the California Current Ecosystem (CCE, Chapter 4).

My analysis of the heterotrophs in the picoplankton-dominated Costa Rica Dome (CRD) upwelling region revealed the importance of the smallest grazers, nanozooplankton, and the impact of top-down pressure from larger mesozooplankton grazers. Nanozooplankton comprised the majority of heterotrophic biomass and were significantly positively associated with picoplankton biomass, pointing to their dominance as grazers in this region. Despite clear changes in autotrophic biomass across multiple locations in the CRD, total heterotrophic biomass changed very little. This, combined with the high biomass and grazing impact of mesozooplankton in the region (Décima et al. 2015), highlighted the strong top-down control of mesozooplankton predation on micrograzers in the CRD, which limits their population response to changes in their phytoplankton prey. These findings illustrated both the bottom-up (e.g., picoplankton and their nanozooplankton grazers) and top-down (e.g., microzooplankton and their mesozooplankton predators) forcing in the CRD food web.

In the California Current Ecosystem (CCE), a large coastal upwelling system, microzooplankton grazing has previously been estimated to consume on average 70% of the daily phytoplankton growth, with top-down mesozooplankton predation causing this percentage to drop to as little as 40% in certain locations (Landry et al. 2009). It was not surprising, therefore, that I found high average microzooplankton grazing pressures during the warm Blob of 2014 (72-141%). However, as hypothesized based on the dominance of picoautotrophs during the Blob event, grazing pressures were much higher in 2014 than in previous studies during normal years, particularly at the coast (103% in 2014 vs. 63% in 2006 and 45% in 2007). Furthermore, pico-sized chlorophytes, which dominated 2 out of 3 coastal locations in 2014, were significantly positively correlated with multiple groups of known heterotrophic nanoflagellates, suggesting their role as major prey for these small nanograzers.

I also found that frontal features in the CCE, which have been observed to be more common in the last decade (Kahru et al. 2012), were sites with distinct microbial communities and dynamics dominated by diatoms. This, combined with their impact on local primary production (Landry et al. 2012) and carbon export (Stukel et al. 2017), highlight the importance of frontal features to the overall function of the region.

Synthesis of results and future directions

Both the CCE and the CRD are upwelling systems, but they are characterized by very different plankton assemblages. CCE upwelling areas are largely dominated by diatoms (Taylor 2014), while the CRD is dominated by *Synechococcus* and other picoplankton (Taylor et al. 2016). Despite these important differences in community

composition, microzooplankton are major grazers of phytoplankton growth in both regions (Landry et al. 2009, Landry et al. 2015, Chapter 5), agreeing with the previously determined global average microzooplankton grazing pressure of 67% (Calbet and Landry 2004).

Upon closer inspection, however, I found that the phytoplankton composition appears to shift the majority of the grazing pressure within the broader microzooplankton category between nano- (2-20 μm) and micrograzers (20-200 μm). Nano-sized grazers, the presumptive major consumers of picoplankton prey, dominated heterotrophic protistan biomass in the CRD, reflecting a strong bottom-up size relationship. In addition, however, micro-sized grazers appeared to be held at relatively low and consistent concentrations by top-down predation pressure from mesozooplankton. This combination of effects created an atypical biomass structure in which nanoflagellates were the primary consumers. In the CCE, molecular analysis revealed that multiple heterotrophic nanoflagellate taxa were significantly correlated with chlorophytes, suggesting nanozooplankton were actively grazing on these picophytoplankton. Future work should focus on clarifying the role of nanozooplankton in upwelling regions, in combination with data on mesozooplankton grazing pressure, to fully understand the bottom-up and top-down pressures acting on the microzooplankton assemblage as a whole.

Across the CRD and CCE regions, dinoflagellates are very common. They dominate microzooplankton biomass in microscopical analyses and often the entire plankton community in molecular datasets, including autotrophic, mixotrophic and heterotrophic forms. While their important role as grazers is readily apparent by virtue of

their high biomass, their overall role in the upwelling plankton community was less clear in my research. Due to the wide variety of functional types included in the Dinophyceae, their diverse ecological niches, and their highly variable copy numbers, interpretation of their community roles from 18S rDNA analyses is a major challenge to be addressed in the future. Moreover, dinoflagellate counts did not demonstrate any significant correlations with the environmental factors tested in Chapter 5 (e.g., temperature, nutrient concentration) that might hint at their specific functional relationships in this region. Clearly, they play major roles in the food web of upwelling areas, both as producers and consumers; however, the data presented here do not illuminate exactly what those roles are. Targeted analysis of dinoflagellates, using highly quantitative, taxon-specific molecular methods in combination with dilution experiments or other experimental designs, is needed to tease apart the different functions of this complex group.

A second area to requires further research is the balance of microzooplankton grazing and viral lysis on phytoplankton mortality in the CCE. Previous results of experiments that directly compared rates of mortality due to viral lysis and grazing in the CCE found only a few instances where viral lysis was a significant source of phytoplankton mortality (Pasulka et al. 2015). However, in light of the large percentage of 18S rDNA sequences in samples across the CCE that belong to known parasitic taxa (e.g., Syndiniales, Apicomplexa) and the clear impact of the Blob on the balance of growth-grazing dynamics in the CCE, it is possible that viral lysis was more significant during the unusual environmental conditions. Changes to the relative balance of viral lysis and microzooplankton grazing rates would have significant impacts on the marine

food web, because viral lysis shunts energy away from higher trophic levels while grazing acts as a link between producers and larger consumers.

Finally, if upwelling in the CCE increases in the future (Rykaczewski and Dunne 2010, Di Lorenzo 2015) along with fronts (Kahru et al. 2012), diatoms could dominate the region, decreasing the role of microzooplankton grazers, and creating a more energy-efficient food web. However, phenomena such as the Blob in 2014, which was unprecedented for this region, are predicted to occur more frequently in the future (Di Lorenzo and Mantua 2016). This outcome would greatly increase the role of microzooplankton as trophic links in the food web. To establish a stronger baseline for analyzing shifts in plankton communities in the CCE, additional studies from "normal" years in the CCE should be analyzed to create a larger baseline dataset for comparison. The impact of mesozooplankton grazing as a top-down control on microzooplankton assemblages also needs to be further clarified through grazing experiments. In particular, the impact of gelatinous zooplankton, which have been observed in large numbers at times in the CCE (Lavaniegos and Ohman 2003), needs to be considered in light of the fact that these organisms circumvent the microzooplankton trophic link and compete directly for small phytoplankton. Finally, the creation of an interactome using the vast data available as part of the CCE Long-Term Ecological Research program and the California Current Oceanographic and Fisheries Investigations (CalCOFI) would be invaluable for identifying the key plankton taxa in the region and their specific impacts on food web dynamics.

References

Calbet, A., and Landry, M. R. (2004) Phytoplankton growth, microzooplankton grazing, and carbon cycling in marine systems. *Limnology and Oceanography,* 49:51-57.

Décima, M., Landry, M. R., Stukel, M. R., Lopez-Lopez, L., Krause, J. W. (2016) Mesozooplankton biomass and grazing in the Costa Rica Dome: amplifying variability through the plankton food web. *Journal of Plankton Research,* 38(2): 317-330. doi: 10.1093/plankt/fbv091

Kahru, M., Kudela, R. M., Manzano-Sarabia, M., and Mitchell, B. G. (2012) Trends in the surface chlorophyll of the California Current: Merging data from multiple ocean color satellites. *Deep Sea Research II,* **77**:89-98.

Landry, M. R., Decima, M., Simmons, M. P., Hannides, C. C., and Daniels, E. (2008) Mesozooplankton biomass and grazing responses to Cyclone *Opal*, a subtropical mesoscale eddy. *Deep Sea Research II,* 55:1378-1388.

Landry, M. R., Ohman, M. D., Goericke, R., Stukel, M. R., Barbeau, K. A., Bundy, R., and Kahru, M. (2012). Pelagic community responses to a deep-water front in the California Current Ecosystem: overview of the A-Front Study. *Journal of Plankton Research*, 34(9):739-748.

Landry, M. R., Selph, K. E., Décima, M., Gutiérrez-Rodríguez, A., Stukel, M. R., Taylor, A. G., Pasulka, A. L., (2016) Phytoplankton production and grazing balances in the Costa Rica Dome. *Journal of Plankton Research,* 38(2): 366-379. doi: 10.1093/plankt/fbv089

Stukel, M. R., Aluwihare, L.I., Barbeau, K.A., Chekalyuk, A.M., Goericke, R., Miller, A.J., Ohman, M.D., Ruacho, A., Song, H., Stephens, B.M., and Landry, M.R. (2017) Mesoscale ocean fronts enhance carbon export due to gravitational sinking and subduction. *PNAS*, 114(6):1252-1257.

Taylor, A. G. (2014) Biomass structure and environmental relationships for phytoplankton communities in the southern California Current and adjacent ocean ecosystems, PhD dissertation. UC San Diego: Oceanography, b8170131.

Taylor, A. G., Landry, M. R., Selph, K. E., and Wokuluk, J. J. (2015) Temporal and spatial patterns of microbial community biomass and composition in the Southern California Current Ecosystem. *Deep Sea Research II,* 112:117-128.